NASA Technical Memorandum 84328

Numerical Simulation of Separated Flows

Philippe R. Spalart, Anthony Leonard and Donald Baganoff

February 1983

National Aeronautics and Space Administration

NASA Technical Memorandum 84328

Numerical Simulation of Separated Flows

Philippe R. Spalart,
Anthony Leonard, Ames Research Center, Moffett Field, California
Donald Baganoff, Stanford University, Stanford, California

National Aeronautics and
Space Administration

Ames Research Center

Table of contents.

ABSTRACT

A new numerical method, based on the Vortex Method, for the simulation of two-dimensional separated flows, has been developed and tested on a wide range of cases. The fluid is incompressible and the Reynolds number is high.

A rigorous analytical basis for the representation of the Navier-Stokes equations in terms of the vorticity is used. It includes an equation for the control of circulation around each body, which has sometimes been overlooked.

In the Vortex Method the vorticity transport equation is solved numerically in a Lagrangian reference frame, by following elementary vortices. The resulting method is grid-free and concentrates its points in the regions of steep gradients; it also allows a simple and exact treatment of the far-field conditions. It is well adapted to the modeling of transport phenomena.

The Vortex Method has been criticized for its handling of the viscous effects. In this study most of the effort has been devoted to understanding and controlling the parasitic numerical effects, and to reproducing the true physical effects. This was achieved by coupling an inviscid outer flow (computed by the Vortex Method), with a viscous boundary layer flow (computed by an Eulerian method).

Two significant advantages of this new version of the Vortex Method are the capacity to treat bodies of arbitrary shape, and the ability to accurately compute the pressure and shear stress at the solid boundary. These two quantities reflect the structure of the boundary layer.

Several versions of the method are presented and applied to various problems, most of which had massive separation. The comparison of its results with other results, generally experimental, demonstrates the reliability and the general accuracy of the new method, with little dependence on empirical parameters. Many of the complex features of the flow past a circular cylinder, over a wide range of Reynolds numbers, are correctly reproduced.

The method appears to incorporate many of the physical mechanisms of separated flows, and the dependence on Reynolds number has been obtained. Its accuracy, when experimental results are taken as a reference, is limited mostly by difficulties in modeling turbulence, and by the two-dimensional assumption.

List of figures.

Nomenclature.

Roman symbols.

(a, b) A set of Lagrangian coordinates.

A_m Area of solid region S_m

B_f Intensity of the buffer vortex sheet.

c Chord of airfoil.

C_d Drag coefficient: $C_d = drag/(.5\rho c^2 {U_\infty}^2)$

C_l Lift coefficient.

C_n Normal force coefficient.

C_m Moment coefficient: $C_m = moment/(.5\rho c^3 {U_\infty}^2)$

C_p Pressure coefficient: $C_p = (p - p_\infty)/(.5\rho {U_\infty}^2)$

C_{p0}, C_{p1s}, C_{p1c} Fourier coefficients of the pressure during the dynamic stall.

D_0 Parameter in merging device.

D_i Distance from i^{th} vortex to the wall.

d/dt Eulerian time derivative (fixed point in space).

D/Dt Lagrangian time derivative (particle).

F Fluid region.

i Imaginary complex number: $i^2 = -1$

i, j Indices of two vortices.

k Reduced frequency of the dynamic stall pitching.

l Side of the square cells used for the taylor expansions.

K, L Indices of two cells for Taylor expansions.

L Length scale associated with the solid body.

m Index of a solid.

M Number of solids.

n Coordinate normal to the wall in inner region.

$\mathbf{n}$ Unit vector normal to ∂S.

n Number of cells for approximating the vortex interactions.

N_g Number of grid points in a Finite Difference simulation.

N_v Number of vortices.

N_w Number of points along the wall.

p Pressure (divided by the density).

$\mathbf{r}$ Vector representation of (x,y):

$$\mathbf{r} = \begin{pmatrix} x \\ y \end{pmatrix}$$

R (large) distance from the origin in an asymptotic expansion.

Re Reynolds number. $Re = |U_\infty| L/\nu$

R_0 Distance from the creation points to the wall.

s Coordinate parallel to the wall in inner region.

Δs Size of intervals along the wall.

S Solid region (union of the S_m's)

∂S Boundary of S (union of the ∂S_m's).

S_m Interior of the m^{th} solid.

∂S_m Boundary of S_m

$\mathbf{t}$ Unit vector tangent to the boundary ∂S

t Time.

u, v Velocity in x and y directions.

$\mathbf{U}$ Velocity vector:

$$\mathbf{U} = \begin{pmatrix} u \\ v \end{pmatrix}$$

$\mathbf{U}_m(x, y)$ Velocity of the solid material in the m^{th} body at (x, y).

$\mathbf{U}_{m0}$ Reference velocity of the m^{th} body (at $x = y = 0$)

$\mathbf{U}_\infty$ Velocity at large distances (in general aligned with x axis).

V_0 Tolerance in the merging device.

x, y Coordinates.

z Complex representation of (x, y): $z = (x + iy)$

Z Complex variable, used in model equations.

Greek symbols.

α incidence of the airfoil.

α_0, α_1 mean and amplitude of α during the dynamic stall.

β intermittency factor for the turbulence model.

γ normalized core vorticity distribution.

Γ Circulation: closed line integral of the velocity.

Γ_i Circulation of i_{th} vortex.

δ thickness of the numerical viscous region.

δ^* centroid of the inner region vorticity in the n direction.

$\hat{\delta}$ filtered version of δ^*.

Δ Laplace's operator: $\Delta = \partial_{x^2} + \partial_{y^2}$

Δt Time step of the numerical integration.

ϵ Amount of artificial dissipation.

η Function of regularization of the velocity, associated with γ.

∇ Gradient operator:

$$\nabla = \begin{pmatrix} \partial_x \\ \partial_y \end{pmatrix}$$

μ Coefficient of viscosity.

ν Coefficient of kinematic viscosity: $\nu = \mu/\rho$.

ρ Density of the fluid (ρ is constant and omitted in general)

ω Vorticity.

Ω_m Angular velocity of m^{th} solid.

Ψ Stream function.

σ Core radius.

τ Viscous shear stress at the solid wall.

Subscripts and superscripts.

∞ value at large distances (freestream).

$\overline{z}$ complex conjugate of z.

I) INTRODUCTION.

1) Description of the problem.

Separated flows, in which the fluid fails to smoothly follow the solid surface, in contrast with attached flows, are generally more complex and more challenging to measure or predict. It was shown by Prandtl that, for the same conditions, the viscous equations and the inviscid equations can have very different solutions even if viscosity is extremely weak, precisely because the viscous flow might separate while the inviscid flow does not [1] . Flows at high Reynolds numbers (low viscosity) are thus very sensitive and, by and large, we only have a qualitative and sometimes simplistic knowledge of their behavior.

In most designs, separation is undesirable since it results in inefficient operation, with high drag or loss of pressure, or even it leads to a dangerous situation like stall. However many devices, like wings or diffusers, often operate on the verge of separation. In other cases separation is present in the design conditions, where it is undesirable but unavoidable, like on aircraft tails or cars, or a normal feature of the flow, like on a three dimensional wing.

A relevant example is the flow around the retreating blade of a helicopter in translation [2] , [3] . The blade experiences large and rapid changes of incidence and velocity, sufficient to cause stall with strong unsteady effects. The blade may even move with the trailing edge forward for part of the cycle, which always causes separation. The dynamic stability of the system

strongly depends on the aerodynamic loads, especially the pitching moment, and these exhibit very significant non-linear and hysteretic effects. Figure 1 illustrates how much the loads can differ during dynamic stall from static loads at the same incidence (Fig. 1 is a personal communication by W. J. McCroskey. The data appeared in [60]). Accurately predicting dynamic stall would thus be very useful, and should be possible in the near future (at least for two-dimensional flow), thanks to improvements in numerical methods and computers.

Experimental results demonstrate the strong sensitivity of separated flows to details of body geometry, for instance surface roughness [4] , and of course to the Reynolds number [1] . The best known example is the circular cylinder: this flow still exhibits dramatic changes at Reynolds numbers of one million (Fig. 2 and 3). Wind tunnel tests are less reliable when fine viscous effects are involved than when the compressibility effects dominate, because the Reynolds number depends on model size, while the Mach number does not, and because separation is influenced by wind-tunnel turbulence. Analysis alone has not been able to produce many results, mainly because separated flows can rarely be treated as slightly perturbed from a known exact solution: they are not very accessible to small disturbance theories. Free streamline theory made use of the observation that, in many cases, drag depends mostly on the forebody shape (upstream of the separation point) and very little on the part of the body which is inside the wake [5] . Pressure also appears to be almost constant in that region. The idea developed was to treat the wake as a "dead-water" region and to assume a constant pressure in that region; in general the value of the base pressure is determined empirically. This theory did produce some good results [6] , but a method that ignores the unsteady character of the flow cannot be expected to be very accurate; it relies very much on empiricism. Thus there is an existing need for the development of numerical methods capable of solving either the full Navier-Stokes equations

or a high level approximation to them without relying on much empirical input. Once these methods have reached an acceptable level of accuracy, they are expected to be much faster and less expensive than large scale wind tunnel tests, and may be more accurate if they are carefully validated against flight tests.

Whereas accurate and practical numerical methods are available to compute attached flows [7] , similar methods do not exist for separated flows, which are vortical. The slowly-varying, attached, irrotational flows are very amenable to finite difference or finite element methods, and to an Eulerian formulation. Some of these methods can also treat separated flows, but obtaining accurate results becomes extremely costly at moderate or high Reynolds numbers [8] . One alternative is the Lagrangian "Vortex Method" [9] . This method provides a description which is better adapted to high-Reynolds number, vorticity-dominated, unsteady flows, and should result in a greater accuracy for a given level of computing resources.

The first objective of this work was to study the capabilities of the Vortex Method, review its inherent strengths and weaknesses, especially in the context of two-dimensional separated flows, and remedy some of the weaknesses. The other objective was to develop a reliable and accurate computer program, based on the Vortex Method, for the simulation of a general class of separated flows. This program has been validated by systematic comparison with known results, and is beginning to be used as an active research tool to investigate some candidate designs, in parallel with wind tunnel tests.

The flows to be considered are viscous flows past two-dimensional solid bodies in a uniform stream. Only incompressible flows are considered. The incompressibility limitation is associated with the Vortex Method. The two-dimensional restriction is not, but simulating two dimensional flows is a first step and reflects the "state of the art". (The extension to three dimensions

would not be straightforward, but it is certainly possible [9].) We consider here one or more bodies and they may be in non-uniform motion. Even if the motion is uniform, the flow is likely to be unsteady with a possible periodic character. Frequently separation of the boundary layer will occur as a result of the body being bluff or at high angles of attack. Large vortical structures will appear and form a wake having a turbulent character, and these structures will strongly influence the loads on the body. Their subsequent decay in the wake far downstream is of less interest because of their small influence on the loads. Again, typical examples are the flow past a circular cylinder, and the static or dynamic stall of an airfoil.

2) Equations.

The behavior of isotropic viscous fluids is described by the Navier-Stokes system of partial differential equations. The independent variables are the cartesian coordinates x and y and the time t. In the conventional formulation the dependent variables are the velocity vector $\mathbf{U} = (u, v)$ and the pressure p. The density ρ is constant since the fluid is incompressible; the symbol p will actually be taken to represent the ratio p/ρ, and ρ will be omitted in the writing. Similarly, the coefficient of viscosity μ is divided by ρ to yield the kinematic viscosity ν. The dependent variables are defined in the fluid region, that is the region of the plane exterior to the solid. Since the fluid is incompressible the problem involves only $\mathbf{U}$ and p, and the following system of equations prevails:

$$\text{(continuity)} \qquad \nabla.\mathbf{U} = 0 \tag{1}$$

$$\text{(momentum)} \quad \frac{\partial \mathbf{U}}{\partial t} + \mathbf{U}.\nabla\mathbf{U} = -\nabla p + \nu\Delta\mathbf{U} \tag{2}$$

where ∇ is the gradient operator and Δ is Laplace's operator.

The boundary conditions are as follows. At large distances from the body U tends to the "freestream velocity" U_∞. At the boundary with a solid the velocity U of the fluid equals the velocity of the solid material. No boundary conditions are needed for the pressure. Initial conditions for U at time 0 are also considered given.

Instead of the conventional "(u, v, p)" formulation, the vorticity formulation is sometimes useful. The role of vorticity in the dynamics of the problem considered here is crucial, and a more efficient method is likely to result if the vorticity is treated directly. It is defined by:

$$\omega = \frac{\partial v}{\partial x} - \frac{\partial u}{\partial y} \tag{3}$$

In two dimensions ω is a scalar quantity and is interpreted as the local angular velocity of the fluid (multiplied by 2).

We will show that, owing to the boundary conditions imposed on U, there is a one-to-one correspondence between an incompressible velocity field U and a vorticity field ω. This allows one to develop a solution by focusing on the vorticity.

The vorticity obeys a well-known conservation law. Taking the curl of Equation 2 and using Equation 1 we obtain:

$$\frac{D\omega}{Dt} = \frac{\partial \omega}{\partial t} + \mathbf{U}.\nabla\omega = \nu\Delta\omega \tag{4}$$

Equation 4 describes how vorticity is convected by the velocity field and diffused by viscosity. In two dimensions there is no term corresponding to "vortex stretching". Thus Equation 4 is of the same type as the equation governing dye concentration. If dye is released by the solid it stays in streaks that trail the solid and are confined to the wake. So will vorticity. The difference between dye and vorticity is that dye concentration does not interact with the velocity (it is a "passive" scalar) while vorticity and velocity are related by Eq. 3.

The incompressibility condition is now implicit and the pressure term drops from the equations. And as a result the number of unknowns is reduced from three to one. The main difficulty is in deriving appropriate boundary conditions (or conditions of another type) to form a complete system with Eq. 4. Many approaches exist in the literature and the one taken for this study will be described in detail later.

We can now turn our attention to the principal numerical methods that have been proposed to solve either Eqs. (1,2) or Eqs. (1,3,4).

3) Related investigations.

The finite difference method is the prevailing method in Computational Fluid Dynamics, as opposed to finite element methods, spectral methods, vortex methods, etc, and will be reviewed first. The finite element methods will not be described. They are quite similar to the finite difference methods and are receiving more and more attention because they are formally more accurate. They are probably less mature and certainly less widespread, at least in the English literature on fluid mechanics. Spectral methods can be extremely accurate, but are still much less versatile than the other methods; they have been used only with very simple geometries (periodic flows, or channels) and not for flows around solids. For that reason, they too will not be described. Finally, the Vortex Method is a promising although not very mature alternative to finite differences for the simulation of incompressible vortical flows. The method will be introduced and its literature reviewed after the finite difference methods have been considered. Then the relative advantages of the two methods will be assessed.

a) Finite difference methods.

The finite difference method is very well known [10] . Out of the large

number of finite difference publications, we shall describe only a few outstanding studies, which seem to be capable of treating two-dimensional flows, with large separation, at Reynolds numbers of at least 10^3. As a rule, the difficulty increases with the Reynolds number.

All of these studies used the Eulerian frame of reference and solved either Eqs. (1,2) or Eqs. (1,3,4) by finite difference approximations on a grid that does not evolve in time. With either formulation there is a variety of finite difference schemes available, time advance schemes, boundary condition procedures, and turbulence models if applicable.

In 1961 Thoman and Szewczyk treated the flow over a circular cylinder for Reynolds numbers ranging from 1 to $3. \times 10^5$ [11]. They used two overlapping grids: one near the surface and an outer grid, extending to only 5 diameters. Freestream conditions were imposed over most of the outer boundary. It is difficult to estimate a priori how much this affects the solution, compared to a situation in which the disturbances are allowed to extend much farther than 5 diameters. Thoman and Szewczyk used an upwind difference scheme to stabilize the computation. They recognize the important fact that this scheme is dissipative, in the sense that its stability comes from a numerical dissipation of the energy, not the physical dissipation. (The elementary form of upwind differencing introduces enough diffusion to bring the effective cell Reynolds number down to 2.) Thoman and Szewczyk carried their computations up to the onset of the drag crisis and the average drag they found was very accurate. They did not report results at higher Reynolds numbers. The pressure distribution was accurate up to a Reynolds number of 400 and quite inaccurate at $3. \times 10^5$, although fortuitously the drag did not reflect it. The Strouhal number was too low by about 30%. The results were quite good, but the accuracy of the upwind scheme was a subject of controversy.

Ten years later Jordan and Fromm treated the circular cylinder for

Reynolds numbers ranging from 100 to 1000 [12] . They used a log-polar grid of large extent (187 diameters) and an outer edge condition devised to allow the solution to oscillate freely. The time history of lift, drag, and torque clearly showed that a limit cycle was reached. The drag and shedding frequency were accurate but again the pressure distribution was not as satisfactory. The authors estimated that their computations should be considered as accurate up to $Re = 400$.

In 1977 Mehta computed the dynamic stall of an airfoil [8] . He used the vorticity formulation, Eqs. (1,3,4), a conformal mapping from the airfoil to a circle, and finite difference approximations. The numerical boundary conditions imposed at the outer edge were chosen to constraint the solution as little as possible. A very elaborate implicit program was used, to obtain high order accuracy and reasonable running times. Implicit time marching schemes are more stable, numerically, than explicit ones. The flow was incompressible and the simulation "direct" (no turbulence model) with Reynolds numbers up to 10^4 considered. Good agreement with flow visualizations was obtained. All the qualitative features of the flow were reproduced, but quantitative comparisons were not reported.

Wu treated the flow around a circular cylinder and around a stalled airfoil by an original method [13] . Wu presented a very good description and justification of his vorticity formulation in [14] . For the numerical method, he computed the vorticity on a grid, but only the cells that contained vorticity were active. This helped reduce the number of points, like in the Vortex Method, except that here an active cell could never be passive again: the computational domain could only grow with time. Also, while the vortical domain is formally infinite (because of viscosity), Wu kept it finite by activating a cell only if it contained more than an arbitrary "low" level of vorticity. The irregular domain is expected to make the vectorization of the program difficult. The velocity at the grid points was computed by Biot-Savart in-

tegration and the vorticity equation was solved in Eulerian coordinates by an explicit method. In a recent paper Wu and Gulcat treat separately the wake, the irrotational region and the attached boundary layer [15] . By adopting the simplest possible level of description for each region, they save significant computer time. Wu obtained very accurate results for the cylinder at low Reynolds numbers. At a Reynolds number of $4. \times 10^4$ Wu and Gulcat obtain what appears to be a very good pressure distribution and a good drag coefficient. However they compare the experimental pressure, averaged over a long time, with the computed instantaneous pressure at time 4.8 (based on velocity and radius). After such a short time the flow surely has not reached its limit cycle. Thus the agreement might be fortuitous. In general, Wu produced some very good ideas but did not always support them with sufficient numerical evidence.

In 1981 Tassa and Sankar treated dynamic stall in compressible turbulent flow [16] . They used an implicit finite difference program and an algebraic turbulence model. The overall quality of their results was comparable to the quality of the results to be reported in the present work. The agreement between different simulations or different experiments, for this difficult problem, is only qualitative. Shocks were not mentioned although the Mach number was 0.6 and high incidence angles were reached. It also seems that the downstream boundary condition used would not allow circulation to leave the computational domain; this is a problem with any method that solves the equations on a finite domain.

The study by Shang, in 1982, treated compressible flow around a circular cylinder [17] . Shang plans to extend it to three dimensions. Accordingly, he used the primitive variables (density, velocity, pressure, energy) and the compressible equivalent of the system of equations (1,2). The computational domain extended to 30 diameters; "non reflecting" boundary conditions were applied at the outer edge to minimize the constraint introduced by the finite

domain. The explicit McCormack scheme was used. The program was fully vectorized on the CRAY computer. The Mach number was 0.6 and the Reynolds number 1.67×10^5, which is quite high, but no turbulence model was implemented. This suggests that the computation was stabilized by the numerical dissipation of the McCormack scheme, which might be much stronger than the molecular dissipation, depending on the grid. The drag and shedding frequency agreed very well with experiments. The average pressures were not reported. The lift exhibited a markedly non-harmonic behavior; this is not mentioned in textbooks, but is consistently observed in experiments and in computations, both finite difference and vortex.

In 1982 Davis and Moore treated the incompressible flow past rectangles at Reynolds numbers between 100 and 2800 [18] . In that range, the molecular viscosity still has a significant effect and the flow characteristics depend on the Reynolds number. The finite difference scheme was chosen to provide a smooth solution with a minimum of numerical dissipation. The freestream conditions were imposed at the outer boundary, except on the downstream face where the numerical boundary condition was chosen to allow vortices to cross the boundary. The grid was adapted to the rectangular shape and it might be difficult to extend the program to other shapes. Satisfying agreement with experiments was obtained, especially at low Reynolds numbers. They estimated that the upper limit for good accuracy was about 1000. Computations at a higher Reynolds number will require a very fine grid, or a turbulence model, or both. A remarkable feature was that, while the flow at $Re = 250$ was very regular, with the lift signal almost a pure sinusoidal function of time, at $Re = 1000$ the shedding was much more irregular.

b) Vortex methods.

Before a discussion of the literature is presented, the basic idea of the Vortex Method will be introduced and its most salient features discussed.

The Vortex Method was designed in an attempt to provide a more natural and efficient description of the eddies and of the vorticity they carry. The method represents the vorticity field as the sum of a large number N_v of mobile functions with small supports:

$$\omega(\mathbf{r}) = \sum_{i=1}^{N_v} \Gamma_i \quad \gamma(|\mathbf{r} - \mathbf{r}_i|) \tag{5}$$

where $\mathbf{r}_i = (x_i, y_i)$ is the center and Γ_i is the circulation of the i^{th} vortex, and γ is the function of regularization or "core shape". γ is smooth, has a small support, and an integral of 1. Typically, γ is a Gaussian. This provides a very convenient description of the vorticity. The main advantage, when external flows are treated, is that in the large irrotational region no vortices will be needed. This saves large amounts of memory and allows vortices to be concentrated in the wake, where resolution is needed.

Dynamically, these blobs follow the fluid, like particles. This is a Lagrangian description. They retain their circulation in time, so that total vorticity is conserved; this corresponds to the inviscid fluid equations

$$\frac{d\Gamma_i}{dt} = 0 \tag{6}$$

$$\frac{d\mathbf{r}_i}{dt} = \mathbf{U}(\mathbf{r}_i, t) \tag{7}$$

Equations (5,6,7) give a closed problem involving only the $\mathbf{r}_i$'s and Γ_i's, provided that U can be calculated from ω. U needs to be known only at the vortex locations and not in the irrotational region; with incompressible fluid, this can be achieved by application of the Biot-Savart law. On the other hand, the main disadvantage with using the Biot-Savart law is that it makes each vortex interact with all the other vortices at every time step, which is very costly.

The advantage of a Lagrangian description for the solution of the inviscid version of Eq. 4 is obvious: in Lagrangian coordinates ω is constant in time. The transport of any quantity is always treated better by having the quantity travel across the domain rather than by transferring the quantity from a fixed grid point to the neighboring points. As a result, the Vortex Method has no obvious numerical dispersion and possibly less numerical diffusion than an Eulerian method (this last point will be discussed in more detail). The Vortex Method also turns out to be much more stable than most Eulerian methods. Large time steps can be taken as long as the accuracy is sufficient.

The efficiency of the Vortex Method, compared to a "u, v, p" formulation, arises in particular from the exploitation of two assumptions: the fluid is incompressible and inviscid.

The incompressibility restriction is clearly necessary to the Vortex Method in its present form (the Biot-Savart law depends on it). With air, it means that only flows at low Mach numbers can be treated, such as the flow around a landing airplane, or around the retreating blade of a helicopter. Even then, high subsonic Mach numbers can appear locally for freestream Mach numbers as low as 0.2. So far these effects have had to be neglected. For flows of liquids, incompressibility is obviously a good assumption.

The inviscid restriction is more controversial. The convergence of the algorithm to the solution of the inviscid equation has been mathematically demonstrated (in the absence of boundaries) [19] . Explicitely adding the viscous term $\nu\Delta\omega$ is not convenient in a Lagrangian reference frame because it involves derivatives with respect to the Eulerian coordinates. On the other hand the method often reproduces viscous behavior, especially around solids, even though it is based on the inviscid equation. For years this feature has been used to simulate viscous flows with an "inviscid" method. This will be made clearer by use of some theoretical arguments and some numerical experiments described in this report.

The method has been studied and refined for decades, without becoming operational and widely used. This is partly true because of the viscosity issue and partly because the problems it is applied to are very difficult for any method. We shall limit our review to papers treating flows past solids. Good research has been done on flows without boundaries, but the difficulties these simulations raise are quite different: in these cases viscosity actually plays a negligible role.

Bryson, in 1959, used a very simple model to represent the flow around a circular cylinder, with one pair of symmetrically placed vortices which moved away from the cylinder and gathered circulation with time [20] (Fig. 4a) (Bryson did not use Eqs. 6 and 7). Thus, flow separation was assumed but viscosity was not accounted for otherwise. This rather empirical model served well for a short time after a rapid start. It was intended for use in a slender body analogy: the steady three dimensional flow past a slender cone at angle of attack is analogous, cross-section by cross-section, to the two dimensional time-developing flow past an expanding circle in translation. The two flows have many common features, including the formation of two symmetric vortices, followed by a loss of stability and an asymmetric state with a side force. This side force can affect the control of airplanes with long noses.

At the next level of complexity, a large number of vortices are used and follow the fluid (Eqs. 6 and 7 are applied) and symmetry is not imposed [21] , [22] , [23] . New vortices are added at the separation points, which are either obvious (a corner on the body) or known empirically (the leading edge of an airfoil or an assumed separation point on its top surface, the 84° point on a circular cylinder in the subcritical range, etc). The strength and exact position of the new vortices are chosen in accordance with Prandtl's rule and a so-called "Kutta condition". Prandtl's rule states that the flux of

separating vorticity is $u^2/2$, where u is the velocity at the outer edge of the boundary layer. The "Kutta condition" is applied even though the wall is smooth; it states that the velocity at the wall, under the separating boundary layer, is zero. It would be described better as a selective application of the no-slip condition. Thus the boundary conditions are neither truly inviscid nor truly viscous. The distinction that is made between "under" and "over" the boundary layer is not very clear, especially when the upstream part of this boundary layer is not represented. This is a major source of uncertainty; the exact points where the velocity is sampled are quite arbitrary and have a strong influence on the results [24] . A mapping from the body shape to a circle is used, in conjunction with image vortices, so that the tangency condition is satisfied. This is the traditional way to treat inviscid flows. It is not as well adapted to viscous flows, and the method to be described in this report actually does not use images. In addition to degrading the accuracy (the interaction of a vortex with its image becomes very inaccurate when they are close to the wall), the use of mappings and images is extremely unwieldy: accurate conformal mappings for arbitrary shapes are not readily available. The viscous "no-slip" condition is satisfied only where the Kutta condition is applied.

Some authors allow the vortices to emanate from a fixed point on an ordered shear layer (Fig. 4b). In general this requires a redistribution of the vortices at each step to keep the curve smooth [25] . From time to time, the shear layer is cut on an empirical basis to allow the formation of the Karman street [22] . Other authors do not link the vortices and let them become a "jungle" (Fig. 4c).

In most of the papers of this period, the flow is called "inviscid" and the question of how any vorticity can leave the wall is not addressed. The value of the coefficient of viscosity is irrelevant. The method tends to overpredict the drag and an empirical suppression of vorticity is often used to decrease

the drag to the desired value [22] ,[26] , [27] . This suppression of vorticity, which violates the two-dimensional vorticity conservation law, is sometimes presented as a way to account for three-dimensional effects.

Deffenbaugh and Marshall attempted to couple the Vortex Method to a boundary layer, using an integral method for the boundary layer [28] . They encountered difficulties in locating the separation point , possibly because of the inaccuracies associated with the release of a single vortex at separation, and because of the questionable validity of Bernoulli's equation in a vortical flow. They used a merging device for adjacent vortices. They treated the circular cylinder at subcritical Reynolds numbers and concluded that the coupling algorithm still had to be refined. They also found that they had to destroy some of the vorticity, otherwise the drag came out too large. Deffenbaugh and Shivananda proposed a method to treat compressible flow at low Mach numbers [26] . Apparently their first attempt was not carried further.

A more ambitious approach was taken by Chorin [29] . A random walk displacement is added to the motion of the vortices. This random walk reproduces the effects of viscous diffusion statistically. This algorithm treats the whole flow as viscous, the Reynolds number is well defined and finite. The no-slip boundary condition is used, vortices are present all along the wall and the separation of the boundary layer is spontaneous (Fig. 4d). No empirical input is needed and the method can now solve problems on its own, provided that the resolution is fine enough for the statistical argument to hold. Unfortunately, it seems that this would require a huge number of vortices and an extremely accurate integration of the transport term, so that the scattering it creates does not dominate the random walk [30] , [31] ; the random walk idea is attractive but not so practical.

Chorin treated the boundary condition at the wall in two stages, using both sources and vortices. He applied the boundary conditions in collocation form,

which is not optimal. The integral form is more costly, since it requires the evaluation of logarithms (or arctangents), but it is much more accurate and less sensitive to the non-physical parameters, for example the core radius. Chorin treated the circular cylinder; his results for drag are accurate at $Re = 100$, but then seem to decrease monotonically above 100, which is not correct physically. With use of the sources Chorin did not need to employ a conformal mapping. However both he and his student, Cheer, later returned to the image-and-mapping method (probably so that the normal velocity would be identically zero at the wall, instead of oscillating near zero).

Chorin subsequently introduced the "Vortex Sheet Method" in order to take into account the widely different scales in the s and n directions of the boundary layer and to reduce the scattering in the direction normal to the wall [32] . The region exterior to the boundary layer is treated by the "isotropic" Vortex Blob Method with an exchange of vortex elements, sheets becoming blobs and vice versa. The circular cylinder and a Joukovsky airfoil were treated by Cheer with this hybrid method [33] . She reports good values for the drag of the cylinder (at subcritical Reynolds numbers), but the results were not very detailed and the runs seemed to be very short. Chorin and Cheer did not use a merging device and had to stop their simulations after a fairly short time to keep computer cost under control. In this case, like in Wu and Gulcat's case, such short simulations are questionable as they clearly do not reach a true asymptotic state. Although his work left room for many improvements it is clear that Chorin showed the way towards a method which is powerful and mathematical in spirit, rather than empirical.

More recently, Lewis independently introduced an image-free form of the Vortex Method which is similar to the one that will be presented here [34] . It is not clear whether Lewis correctly applied Eq. 10.5 (see below) or an equivalent condition. Lewis made use of the advantage of not needing a mapping to treat various shapes. Using a modest computer, Lewis introduced

only a small number of vortices, at only two separation points. The boundary layer was not treated separately. He applied Prandtl's rule, although he recognized that it is very delicate to apply. Porthouse and Lewis subsequently published results using a random walk model to account for viscosity [35]; these results seem to confirm that very many vortices and very short steps would be needed for the random walk effect to be meaningful at practical values of the Reynolds number.

c) Finite difference versus Vortex methods.

It appears that presently neither method alone can treat high Reynolds number flows with the level of accuracy that is needed for engineering. For example, reliable quantitative predictions have not been obtained for dynamic stall and computing these flows is a matter of research, not of production. In some cases, only qualitative agreement is obtained, for instance agreement with visualizations. In other cases, the quantitative agreement is good but limited to a few numbers like drag or shedding frequency. One reason is that quantitative and verified experimental data are often not available for separated flows; these seem to be as hard to measure as they are to compute. In addition, the numerical method is still two-dimensional and the experiments, even when the geometry is two-dimensional, often have significant three dimensional effects. The comparison with exact solutions would be a more rigorous test of the accuracy of the numerical results; unfortunately, almost no exact solutions are known for separated flows.

If the Reynolds number is quite low, less than 10^3, the finite difference methods work well, because the solution is very smooth. At the Reynolds numbers of aeronautical interest, which are of 10^6 or more, the vortical structures in the wake become so small that a very fine grid is needed, which requires a very large memory and very short time steps. If the grid is too coarse numerical diffusion and dispersion can easily dominate physical

diffusion. If this happens the simulation is not truly viscous; such a situation is often considered acceptable far from the walls, but not close to the wall. Reaching higher Reynolds numbers will mostly be a matter of computer power, both in terms of memory and speed, and of turbulence modeling.

The Vortex methods suffer from their imperfect viscous modeling and a certain lack of credibility, independent of the Reynolds number. Nearly all the studies treated the same shapes: cylinders, ellipses, Joukovsky airfoils. Also, too much empirical input was needed. On the other hand, the vortex programs needed relatively little memory and some of them ran very fast. Improving them is more a matter of improving the algorithm.

A basic advantage of the finite difference methods is that they rest on a well established theory of stability and convergence (at least for bounded or periodic geometries; infinite domains are not treated in a fully satisfying manner). The same cannot be said of the Vortex methods when viscosity and boundaries are involved.

Another advantage of finite difference methods over Vortex methods is that they can be extended to compressible flows without major changes. Treating compressible flows, with a Mach number above about 0.1, is even easier in some cases because it makes the celerity of the signals smaller. The extension to three dimensions is also simpler, conceptually, than for the Vortex Method.

The most significant difference is that the finite difference methods include the viscous terms, while the Vortex Method is essentially inviscid. However, the finite difference grid often is too coarse to resolve these viscous terms except close to the wall [35] . This effectively removes the laminar viscosity, and the energy is controlled by some form of numerical dissipation instead. The true advantages of the finite difference method, even over a Vortex Method coupled to a boundary layer, are that boundary layer assumptions are not involved (therefore no singularities are expected) and that the transition

from a viscous treatment (fine grid, near the wall) to an effectively inviscid treatment (coarse grid, away from the wall) is smooth.

Another issue is the modeling of the turbulent stresses in the wake. Whereas modeling these stresses is reasonably easy in the boundary layer, modeling them in the wake is extremely difficult. Thus, some finite difference methods include turbulent stresses, but these are evaluated with so much uncertainty that the benefit is not obvious in terms of accuracy. The turbulent stresses conveniently improve the stability of the finite difference computations; this is not an issue with the Vortex Method which is very stable.

The Vortex Method has only treated bodies in a uniform freestream flow. It is planned to extend it to bodies in a uniform shear flow, which will be quite simple. On the other hand it would be much more difficult to treat non-uniform incoming shear flow. In that domain the finite difference methods are still more versatile.

The main advantages of the Vortex Method are its accuracy in treating the convection terms, and the absence of a grid. Generating grids around complex shapes is not easy [36] , and unless the grid is very smooth the accuracy suffers. Furthermore, for many finite difference programs the computational efficiency depends on mapping the physical domain to a rectangular computational domain. Thus, treating several bodies either involves the use of a highly distorted grid, or a rather delicate zonal approach [37] ,[38] . These difficulties are totally absent in the Vortex Method, at least in its most recent versions, which makes it especially attractive for multiple bodies.

Another advantage is that the Vortex Method effectively includes the infinite domain whereas the finite difference methods include only a finite domain and require artificial boundary conditions at a finite distance from the body. Choosing these conditions is delicate: there is a danger of constraining the solution in a hidden way. The Vortex methods need less empiricism in this regard. It is also possible to add wind-tunnel wall effects to the Vortex

Method (this is quite simple if the flow does not separate from the tunnel walls).

The Vortex Method previously lacked versatility: with the use of conformal mappings it was awkward to treat shapes other than ellipses or Joukovsky airfoils. The situation has now reversed itself since, as we shall see, recent versions of the Vortex Method easily treat arbitrary shapes while avoiding grid generation [34] , [39] ,[40] .

It is not easy to assess the relative computer costs for the two methods. In the Vortex Method, N_v^2 interactions have to be computed at each time step, where N_v is the number of vortices. In contrast, many finite difference methods require only of the order of N_g operations, where N_g is the number of grid points. This is true for most explicit methods and for the implicit methods that have a suitable ordering of the grid. Since both methods, in their widely used forms, are second order accurate, the finite difference method seems to have the advantage. However in practical situations N_v and N_g are limited and the relevant question is: which values of N_v and N_g would achieve the desired level of accuracy? Then the memory requirements and the running times could be compared.

Only experience can answer the question, but two general rules apply. First, the Vortex Method will be more competitive if the vortical region is small, which makes N_v much smaller than N_g. Typically, the Vortex Method works well with an external flow, but not as well with an internal flow which might be filled with vorticity, and thus make N_v and N_g about equal. Second, the Vortex Method nearly always requires less memory, while the running times can differ greatly in one sense or the other. Many researchers reported extremely short running times for Vortex computations, but their resolution was very coarse and their accuracy questionable. Other Vortex computations required hundreds of hours of computer time.

To allow an evaluation of the method used in this study, the run time used

by the computations will be reported in the "Results" section.

4) Summary of the evolution of the present method.

The starting point of this study was an algorithm written by R. Rogallo (NASA Ames C. F. D. Branch, unpublished work). It was similar to Chorin's 1973 method [29] , but it included a merging device and made use of the integral form of the boundary condition, which is more efficient. It also had images. During the present study, which was also done at NASA Ames, the algorithm underwent three mutations, resulting in the versions $KPD1$, $KPD2$ and $KPD3$.

$KPD1$ makes use of the new boundary condition (without sources, images or conformal mapping), but does not employ a boundary layer. It is versatile, robust, and accurate for flows that are not sensitive to viscous effects, for example the flow past a square body at Reynolds numbers between 10^4 and 10^7. $KPD1$ has been successfully used for the "Vortex Flowmeter" study with Dr. Couet [40] . This configuration involves several interacting bluff bodies.

$KPD2$ is directly based on $KPD1$; it treats the boundary layer, from the attachment point to the first separation point, with an integral method and treats the rest of the domain with the Vortex Method. This removes the problems with premature separation experienced with $KPD1$. The integral method is designed for boundary layers imbedded in an irrotational flow; moreover, it exhibits a singularity at the separation point. This is why it cannot be applied beyond the separation point. The boundary layer is also considered as quasi-steady. $KPD2$ is suited to problems with a single streamlined body, and can capture the major viscous and turbulent effects to which $KPD1$ is insensitive. It has been used mostly for airfoil flows, including dynamic stall [39] and the tilt-rotor configuration (work to be published in

cooperation with W. J. McCroskey).

$KPD3$ is quite different from $KPD1$ or $KPD2$; it is the latest version of the program and possesses the most potential. It treats the viscous region along the wall with a truly unsteady implicit finite difference boundary layer method, in a manner that is valid even inside a vortical outer flow (like the wake of the body itself or the wake of another body). The boundary layer solver is not classical. It allows for separation and reattachment of vorticity; intuitive arguments are invoked to couple it as strongly as possible with the outer solution. $KPD3$ has been validated on the circular cylinder at moderate and high Reynolds numbers, using the Baldwin-Lomax algebraic turbulence model. It can treat several bodies without special precautions, and in general is more accurate and provides more information than $KPD1$ or $KPD2$. It is not quite as robust in its present version; in particular it can have difficulties near sharp edges.

1) Vorticity formulation.

The incompressible Navier-Stokes equations are formulated in terms of the vorticity, and the resulting system of equations will be solved numerically. It will be shown that the initial-value problem used for the vorticity is mathematically equivalent to the usual initial-value problem used for (u, v, p). Since the "(u, v, p)" system is well posed, the "ω" system will also be well posed. The vorticity formulation is considered to be more efficient numerically.

The first subsection will introduce the necessary definitions and present the formal proof of equivalence of the two systems. The procedure follows closely the work of J. Wu, described in [14]. The second subsection will contain some comments about the aspects of the procedure that do not follow the traditional train of thought and sometimes become misunderstood.

a) Definitions and proof of equivalence.

The domain is the (x, y) plane. It contains M solid regions called S_m; each S_m is an open and bounded domain with a boundary ∂S_m. Let S be the union of the S_m's and F be the fluid domain. Thus the plane is partitioned into the two open domains S and F and the boundary ∂S. In general, the solids move and therefore S and F depend on the time, t.

The momentum equation, Eq. 2, contains a parabolic diffusion term, $\nu \Delta \mathbf{U}$, and therefore the function $\mathbf{U}$ is expected to be smooth. $\mathbf{U}$ is considered as

being at least of class C_3 in F, that is three times continuously differentiable, at all times $t > 0$. The pressure is at least of class C_1.

The velocity of a point (x, y) belonging to the solid S_m is given by the function $\mathbf{U}_m$:

$$\mathbf{U}_m(x, y) = \mathbf{U}_{m0} + \Omega_m \begin{pmatrix} -y \\ x \end{pmatrix} \tag{8}$$

where $\mathbf{U}_{m0}$ and Ω_m are known functions of time. In this study the motion of the solid bodies will always be prescribed, but the theory would not be different if it were known from the solution of a dynamic equation (for example a solid with elastic restraint).

The complete system of equations governing u, v and p is the following:

$$\text{(incompressibility, Eq. 1)} \qquad \nabla.\mathbf{U} = 0 \quad \text{in } F \tag{9.1}$$

$$\text{(momentum, Eq. 2)} \qquad \frac{D\mathbf{U}}{Dt} = -\nabla p + \nu \Delta \mathbf{U} \quad \text{in } F \tag{9.2}$$

$$\text{(at wall)} \qquad \mathbf{U}(x, y) = \mathbf{U}_m(x, y) \quad \text{on } \partial S_m \tag{9.3}$$

$$\text{(far field)} \qquad \mathbf{U} \mapsto \mathbf{U}_\infty \quad \text{for } \|r\| \mapsto \infty \tag{9.4}$$

$$\text{(initially irrotational)} \quad \text{At } t = 0 \qquad \nabla \times \mathbf{U} = 0 \quad \text{in } F \tag{9.5}$$

$$\text{(no initial circulation)} \quad \text{At } t = 0 \qquad \oint_{C_m} \mathbf{U}.ds = 0 \tag{9.6}$$

where C_m is a contour that encloses S_m and ∂S_m. A more accurate definition of the contour within F is not necessary, because the velocity field is irrotational in F at time zero (Eq. 9.5), so that the line integral does not depend on the contour.

Let us turn our attention to the vorticity formulation. The vorticity ω is defined by Eq. 3. Since $\mathbf{U}$ is considered as being of class C_3, ω is considered to be of class C_2 in F for $t \geq 0$. In the exact solution the vorticity is known to decay exponentially at large distances from the body, provided that it did initially, at time zero [14]. All the flows considered here will be started

from rest, with zero vorticity in F; therefore exponential decay of ω can be assumed. As a consequence, all generalized integrals involving the vorticity over the infinite region are absolutely convergent and have the same behavior as if the vorticity had a finite support.

For the vorticity formulation it is convenient to formally extend the velocity field to cover the whole plane; inside F it is the fluid velocity and inside S_m it is the velocity $\mathbf{U}_m$ of the solid material. Naturally, the same dynamical equations do not apply in F and in S (in particular the pressure will not be extended to S), but this does not affect the kinematics of the extended velocity field. The reason for extending the various fields into S is that this will allow the use of Green's functions without any boundary terms or "images" for the solution of the Cauchy-Riemann equations.

Similarly, an extended vorticity field is defined by applying the definition, Eq. 3, both in F and in S. Inside S the velocity (given by Eq. 8) and the vorticity are both of Class C_∞.

We can now introduce the system of equations that will govern the vorticity:

$$\text{(vorticity conservation law, Eq. 4)} \qquad \frac{D\omega}{Dt} = \nu\Delta\omega \quad \text{in } F \tag{10.1}$$

$$\text{(vorticity inside solid)} \qquad \omega = 2\Omega_m \quad \text{in } S_m \tag{10.2}$$

(Biot-Savart)

$$\begin{pmatrix} u \\ v \end{pmatrix}(x,y) = \mathbf{U}_\infty + \frac{1}{2\pi} \int_{-\infty}^{+\infty} \int_{-\infty}^{+\infty} \begin{pmatrix} y'-y \\ x-x' \end{pmatrix} \frac{\omega(x',y')dx'dy'}{(x-x')^2+(y-y')^2} \tag{10.3}$$

$$\text{(at wall)} \qquad \mathbf{U}.\mathbf{n} = \mathbf{U}_m.\mathbf{n} \quad \text{on } \partial S_m \qquad (\mathbf{n} : \text{normal vector to } \partial S_m) \tag{10.4}$$

$$\text{(additional condition)} \qquad \oint_{\partial S_m} \nu \frac{\partial\omega}{\partial n} ds = -2A_m \frac{d\Omega_m}{dt} \qquad (A_m : \text{area of } S_m) \tag{10.5}$$

$$\text{(initially irrotational)} \qquad \text{at } t = 0 \quad \omega = 0 \quad \text{in } F \tag{10.6}$$

$$\text{(no initial circulation)} \quad \text{at } t = 0 \qquad \int\int_{D_m} \omega(x,y)\,dxdy = 0 \qquad (10.7)$$

where the domain D_m encloses S_m and ∂S_m like the contour C_m in Eq. (9.6).

The main result of this chapter is that the systems 9 and 10 are equivalent.

First let's prove that the system 9 implies the system 10:

- Equation 10.1 has already been derived as the curl of Eq. 9.2.
- Equation 10.2 is obtained by taking the curl of Eq. 8.
- Equation 10.3 is the Green's function integral giving the solution U of the Cauchy Riemann system formed by Eq. 9.1 and Eq. 3, subject to the boundary conditions, Eq. 9.4.
- Equation 10.4 is a consequence of Eq. 9.3.
- To derive Eq. 10.5 we use Eq. 9.2 and the identity:

$$\Delta \mathbf{U} = \nabla(\nabla.\mathbf{U}) - \nabla \times \omega$$

in addition $\nabla.\mathbf{U} = 0$ from Eq. 9.1. We then write Eq. 9.2 on ∂S_m and take its dot product with the tangent unit vector $\mathbf{t}$:

$$\frac{D\mathbf{U}}{Dt}.\mathbf{t} = -\frac{\partial p}{\partial s} + \nu\frac{\partial \omega}{\partial n} \qquad (12)$$

Since the particles, locally, adhere to the wall their acceleration is the same as the acceleration of the wall: $D\mathbf{U}/Dt = D\mathbf{U}_m/Dt$ on ∂S_m. Thus we have:

$$\frac{D\mathbf{U}_m}{Dt}.\mathbf{t} = -\frac{\partial p}{\partial s} + \nu\frac{\partial \omega}{\partial n} \qquad (13)$$

We then integrate Eq. 13 along the closed contour ∂S_m. The acceleration derived from Eq. 8 is integrated analytically, and the pressure term cancels. The final result is Eq. 10.5.

- Equation 10.6 is a consequence of Eq. 3 and Eq. 9.5.

• Finally, Eq. 10.7 is a consequence of Eq. 3, applied in F and S_m, and Eq. 9.6.

Let us now prove that the system 10, in return, implies the system 9:

• Equation 9.1 is automatically satisfied when the velocity field U is generated by the Biot-Savart law, Eq. 10.3.

• Equation 9.4 is also automatically satisfied due to Eq. 10.3 and the fact that ω decays exponentially away from the origin.

• To prove Eq. 9.3 it is convenient to introduce a stream function. The velocity U given by Eq. 10.3 is divergence-free and a stream function ψ can be associated with it and given by:

$$\frac{\partial \psi}{\partial x} = v \qquad \frac{\partial \psi}{\partial y} = -u \tag{14}$$

The solid body velocity field given by Eq. 8 is also divergence-free; a stream function ψ_m can be associated with it and defined over S_m by the same formula as Eq. 14. In both cases the stream function is defined except for an arbitrary additive constant. Then Eq. 10.4 can be rewritten:

$$\frac{\partial \psi}{\partial s} = \frac{\partial \psi_m}{\partial s} \quad \text{along} \quad \partial S_m \tag{15}$$

Thus $\psi - \psi_m$ is constant along ∂S_m. In addition, as a consequence of Eq. 3 and Eq. 14 the following Poisson's equation applies:

$$\Delta \psi = \omega \tag{16}$$

Now the (scalar) curl of U_m is $2\Omega_m$, and ω is also equal to $2\Omega_m$ in S_m, from Eq. 10.2. Therefore ψ and ψ_m satisfy the same Poisson's equation, and:

$$\Delta(\psi - \psi_m) = 0 \quad \text{in } S_m \tag{17}$$

The function $\psi - \psi_m$ satisfies Laplace's equation in S_m, which is bounded. It is also constant on ∂S_m (Eq. 15), which represents a Dirichlet boundary condition. This is a well posed problem and the unique solution for $\psi - \psi_m$ is a constant over S_m. Therefore its derivatives are zero, which can be written as:

$$\mathbf{U}(x,y) = \mathbf{U}_m(x,y) \qquad \text{in } S_m \tag{18}$$

The velocity field is equal to the solid body velocity inside the solid. Furthermore since ω is considered to be of class C_2 it is bounded (for $t > 0$) and the velocity field U generated by Eq. 10.3 is continuous; so if it is equal to $\mathbf{U}_m$ inside S_m it is also equal to $\mathbf{U}_m$ on ∂S_m, (the solid body is assumed to have a finite thickness) and Eq. 9.3 follows.

• To prove Eq. 9.2 we have to produce a pressure field. Let us consider the quantity:

$$\frac{D\mathbf{U}}{Dt} - \nu \Delta \mathbf{U} \tag{19}$$

with U given by Eq. 10.3. If we take the curl of Eq. 19 we get (since U is divergence-free):

$$\frac{D\omega}{Dt} - \nu \Delta \omega \tag{20}$$

which is zero from Eq. 10.1. Therefore the quantity defined by Eq. 19 is the gradient of a function p:

$$\frac{D\mathbf{U}}{Dt} - \nu \Delta \mathbf{U} = -\nabla p \tag{21}$$

We now write Eq. 21 on ∂S_m, rewrite the viscous term as in Eq. 13, use the same argument for DU/Dt and take the dot product with the tangent unit vector to obtain:

$$\oint_{\partial S_m} \frac{\partial p}{\partial s}\, ds = 2A_m \frac{d\Omega_m}{dt} + \nu \oint_{\partial S_m} \frac{\partial \omega}{\partial n}\, ds \tag{22}$$

The right-hand side is zero from Eq. 10.5. This means that p is single-valued around each solid S_m. Therefore p is the pressure (defined except for an additive constant) and Eq. 9.2 is satisfied.

- Equation 9.5 is a consequence of Eq. 10.6 and Eq. 3.
- Finally, Eq. 9.6 is a consequence of Eq. 10.7 and Eq. 3, applied in F and S_m.

This completes the proof.

b) Comments.

The first comment qualifies out assertion that "the system is well-posed". The far fieldcondition, Eq. 9.4, is imprecise in the sense that it does not specify how fast the difference $(\mathbf{U} - \mathbf{U}_\infty)$ tends to zero as $\|\mathbf{r}\|$ tends to ∞. How strong this decay should be to provide a well-posed system with the Navier-Stokes equations has not been rigorously established. The common practice one follows, when confronted with this question, is to assume a behavior in the far field that is as regular as possible. If we assume that the velocity can be expanded in negative powers of $\|\mathbf{r}\|$ and that the flow is effectively irrotational in the far field (the vorticity decays exponentially) then the terms of order $\|\mathbf{r}\|^{-1}$ are a source term and a vortex term. The source term must be zero for mass to be conserved. The vortex term gives the circulation around a large contour. This circulation must be a constant, from Kelvin's theorem (the viscous term $\nu\Delta\mathbf{U}$ has been written $-\nu\nabla\times\omega$ and therefore decays exponentially, if ω does). If a steady lifting flow is sought the circulation will not be zero. In our case the value of the circulation does not matter much since the flow is viscous and unsteady, and thus will wash away any excess circulation. We shall assume zero circulation; therefore the velocity disturbances decay like $\|\mathbf{r}\|^{-2}$. With this decay specified, the Cauchy-Riemann system has a unique solution, given by Eq. 10.3. Rigorously

this should not be considered as a pure boundary condition: it would be over-specified. It contains the boundary condition and an assumption about the far-field behavior of the solution.

The initial conditions were derived in the same spirit. They simulate an impulsive start of the flow. After such a start the vorticity will be confined to ∂S and be infinite in magnitude, with a finite jump of velocity across ∂S. This is simply a potential flow problem and it is well known that in such a case the circulation around each solid is arbitrary. It was set to zero.

The second comment concerns the boundary condition at the wall. If we examine the system 10 and especially Eq. 10.4, it seems that only the continuity condition (zero velocity normal to ∂S_m) is applied and that the no-slip condition (zero velocity parallel to ∂S_m) has been lost. However it was shown that Eq. 9.3, which includes no-slip, was satisfied. This paradox is clarified by noting, first, that the velocity fields produced by the formula 10.3 are not arbitrary (they are divergence-free and have the required vorticity $2\Omega_m$ in S_m), and second, that what we have shown is that the global normal velocity condition (Eq. 10.4 applied all along ∂S_m) implies the global no-slip condition. Naturally, the local normal velocity condition does not imply the no-slip condition.

Except for Chorin's first paper [29] and the recent paper by Lewis [34], all papers employing vortices imposed the boundary condition, Eq. 9.3, in two stages. First, they included image vortices in the Biot-Savart law, Eq. 10.3, to secure the normal velocity condition, and then, they introduced vortices to secure the no-slip condition. Here the complete boundary condition is obtained in one step by introducing vortices to satisfy Eq. 10.4, which becomes an integral equation for ω if U is replaced by Eq. 10.3. This is much more efficient since Eq. 10.4 and 10.3 can be written directly in the physical plane, whereas the image vortices could only be used after a conformal transformation had converted the body into a circle. This made

the Vortex Method awkward and limited the simulations to the few cases for which the mapping and its derivatives are known: ellipses, Joukovsky airfoils, etc.

The third comment is about the conservation of circulation. We mentioned previously Kelvin's theorem concerning the circulation around a large contour, Γ. Equation 10.5 has an interesting consequence which extends Kelvin's theorem. This result is due to Wu [14]. Γ is equal to

$$\Gamma = \int_{-\infty}^{+\infty} \int_{-\infty}^{+\infty} \omega(x,y)\, dxdy \tag{23}$$

(the integral includes the vorticity that is inside S). To evaluate $d\Gamma/dt$ it is convenient to use Lagrangian coordinates, because in Lagrangian coordinates F and S do not depend on t, so that points do not switch from F to S as the solids move. Let (a,b) be Lagrangian coordinates which coincide with (x,y) at the time considered. The Jacobian of the mapping $(a,b) \rightarrow (x,y)$ is 1 at any time since the flow is incompressible. Therefore Γ is also equal to:

$$\Gamma = \int_{-\infty}^{+\infty} \int_{-\infty}^{+\infty} \omega(a,b)\, dadb \tag{24}$$

we can integrate in either set of coordinates. Then $d\Gamma/dt$ is:

$$\frac{d\Gamma}{dt} = \int_{-\infty}^{+\infty} \int_{-\infty}^{+\infty} \frac{D\omega}{Dt}(a,b)\, dadb \tag{25}$$

This is Reynolds' transport theorem.

We can now revert to the (x,y) coordinates to evaluate Eq. 25. In S_m $D\omega/Dt$ is $2d\Omega_m/dt$ and integrates to $2A_m d\Omega_m/dt$. In F, $D\omega/Dt$ is $\nu\Delta\omega$ and

is easily integrated by parts, to yield:

$$\frac{d\Gamma}{dt} = \sum_{m=1}^{M} \left[2A_m \frac{d\Omega_m}{dt} + \nu \oint_{\partial S_m} \frac{\partial \omega}{\partial n} ds \right] \tag{26}$$

There is no contribution from the far-field, because of the exponential decay of ω. In addition, for each m the expression between brackets is zero, according to Eq. 10.5. The integral along ∂S_m that appears in Eqs. 10.5 and 26 can be interpreted as the total production of fluid vorticity along ∂S_m. Clearly each solid, while changing its internal circulation at the rate $2A_m d\Omega_m/dt$, releases an opposite amount of vorticity into F. If there is only one solid this is equivalent to Kelvin's theorem, which states that $d\Gamma/dt$ is zero. If there are several solid bodies Eq. 26 is a stronger result, since each solid separately contributes zero to the circulation.

Another point of interest is the way the pressure is computed. Computing the pressure is not necessary in order to solve the vorticity equation, but it is an excellent way to monitor the simulation. The common way to interpret boundary layer behavior is in terms of the pressure gradient along the wall. Formally, the pressure is given by Eq. 21; however this equation would be hard to use numerically with the Vortex Method. On the other hand Eq. 13 gives the wall pressure gradient as a function of $\nu \partial \omega / \partial n$, and we have seen that $\nu \partial \omega / \partial n$ is the rate of creation of vorticity at the wall; this quantity is well defined in the Vortex Method and will allow the wall pressure to be computed accurately, even inside the wake. Using Bernoulli's equation in the wake would be incorrect since the flow there is vortical.

A detail remains: Eq. 13 only yields the pressure gradient; thus the pressure is known except for an additive constant. If one wishes to determine this constant and the body is in contact with the irrotational region, it is possible to apply Bernoulli's theorem from infinity upstream to a point on the attached part of the boundary layer. In practice it is convenient to use the front

stagnation point.

Another useful boundary layer monitor is the wall shear stress. It is equal to:

$$\tau = \nu\omega \qquad \text{on } \partial S_m \tag{27}$$

2) Approximations for the outer and inner regions.

Matching procedure.

a) Motivation.

This section describes the approximations that are made and how certain considerations allow us to simplify the equations, by omitting terms that are known to be small or information that is not important.

Most of this section applies to all three versions of the program; when they differ, the description will apply only to $KPD3$. The theory implemented in $KPD1$ and $KPD2$ and their numerical aspects will be described in Appendix A.

The most important, and the most delicate, approximation is naturally the neglect of viscosity. The coefficient of viscosity is small, but it multiplies the highest derivative, and the perturbation problem is said to be singular [42] . The inviscid problem and the viscous problem have very different characters; in particular they do not require the same number of boundary conditions. Regions exist in the flow where the velocity gradients are so large that the viscous term is as large as the inertia term. This viscous term can change the local value of the vorticity by an amount of order 1, meaning that it does not tend to zero while the coefficient of viscosity does. Therefore the flow with small viscosity cannot be treated as slightly different from the inviscid flow in the usual sense, and a straightforward attempt to expand the solution as a power series in ν would fail.

The justification for omitting the viscosity is the following. The effect of viscosity will be to diffuse the vorticity over very short distances, without creating or destroying any. (The viscous term in Eq. 4 is the divergence of $\nu\nabla\omega$ and $\nu\nabla\omega$ is interpreted as a flux of vorticity. It is not a source term.) Let L be the length scale associated with the body, U_∞ the freestream velocity and ν the kinematic viscosity. The non-dimensional number LU_∞/ν is the Reynolds number, and is large in all cases under consideration (over 10^4). The length scale associated with the viscous diffusion is $\sqrt{\nu t}$ where t is the "age" of the vorticity. Let us consider some vorticity which is "born" at the solid boundary and in a time L/U_∞ is transported into the wake, to a distance L from the solid. The viscous scale becomes $\sqrt{\nu L/U_\infty}$ and the ratio of this scale to L is $\sqrt{\nu/LU_\infty}$, or $Re^{-1/2}$, and thus is small. Integrals like the one in equation 10.3 and in general the flow close to the solid boundary will not be sensitive to the displacement of the vorticity over such a small distance. Since predicting the stresses on the solid is the ultimate objective of the study, omitting detailed information about the vorticity diffusion in the wake is minor as long as the transport is correct.

However the vorticity is "produced" at the solid boundary [43] and its subsequent transport is very sensitive to its initial life, near the wall, during which the scales are small and the viscous term important. It is the convection with the fluid that carries the vorticity into the large structures of the wake, but the velocity is zero at the wall and only the viscosity can make the vorticity penetrate into the stream at all. Therefore the "justification" we just reviewed breaks down in the wall region.

This motivates the procedure, illustrated in Fig. 5, of coupling an inviscid outer flow and a viscous boundary layer flow. This procedure is common when the outer flow is not only treated as inviscid but also as irrotational. Here, the outer flow will be vortical. The effort will be worthwhile if an efficient solver is available for the simplified equations in each region.

The Vortex Method is efficient in the outer flow; it treats the transport term accurately and provides the necessary resolution in the wake. It does not cause any problem at large distances from the body. Its weakness in treating the detailed viscous features will not disturb the large scale structures which dominate in the wake. The implicit finite difference method is very good at treating thin viscous flows. For such a small and logically rectangular domain it is also very fast. Both methods are available and well tested. The new element that is needed is a procedure that makes the two regions interact through the boundary conditions at the interface.

In a previous investigation Shestakov also coupled the Vortex Method to an Eulerian method [44] ; however he used the Vortex Method in the wall region, and the Eulerian method away from it! Even though the conditions were slightly different (he treated an internal flow) our interpretation and Shestakov's appear to be totally opposite. His results appear reasonable, but it is not clear how much his flow depended on the wall region, or how much benefit he derived from using the Vortex Method near the wall.

The two approximate systems of equations will be described separately, followed by a discussion of the conditions at the interface.

b) Outer flow.

In the outer region, the viscous term in Eq. 4 is dropped, only the transport term is retained. The approximate equation is:

$$\frac{D\omega}{Dt} = 0 \tag{28}$$

The material derivative of the vorticity, or equivalently its time derivative in Lagrangian coordinates, is zero; this is what makes a Lagrangian method attractive.

The vorticity is zero at large distances (the system is always started with the fluid at rest) and no boundary condition is needed in the far field for Eq.

28. The far field behavior of the velocity is essentially the same as in the exact formulation, in which the vorticity decayed exponentially.

The proper boundary condition for the hyperbolic Eq. 28 at the interface with another domain depends on the sense of the velocity; ω itself is the characteristic variable and the velocity **U** gives the characteristic direction. If this velocity is into the other domain (outflow), no condition should be applied; if it is into this domain, the value of the vorticity, or equivalently the flux of vorticity, should be prescribed. Information travels in the same sense as the particles, and this is realized very simply with a Lagrangian method: an outflow boundary absorbs particles and information, an inflow boundary generates new particles which carry information.

c) Inner flow.

In the boundary layer the viscous terms are retained, but the thinness of the layer renders some terms negligible. Curvature effects will not be included. This is legitimate for shapes like a circular cylinder; for airfoils, it might be necessary to account for curvature near the trailing edg , or to round it off so as to increase its radius of curvature.

Let s and n be the coordinates along the wall and normal to it respectively, and u and v be the velocity components in the s and n directions respectively. The scale in the n direction being much smaller than that in the s direction allows Eqs. 1,3 and 4 to be approximated by:

$$\frac{\partial u}{\partial s} + \frac{\partial v}{\partial n} = 0 \tag{29}$$

$$\omega = -\frac{\partial u}{\partial n} \tag{30}$$

$$\frac{\partial \omega}{\partial t} + \mathbf{U}.\nabla\omega = \nu\frac{\partial^2 \omega}{\partial n^2} \tag{31}$$

Equation 1 has simply been reformulated in terms of (s, n, u, v), without approximation, to yield Eq. 29. The definition of the vorticity, Eq. 3, has

been simplified by dropping the $\partial v/\partial s$ term, giving Eq. 30, and the viscous term in the s direction has been dropped from Eq. 4 to give Eq. 31.

These differential equations are the same as the conventional time-dependent boundary layer equations, but the boundary conditions employed will be different. The inner region extends around the whole body, and the boundary conditions in the s direction are periodic. The equation is advanced in time, not by "marching" along the boundary layer in the direction of the local velocity. Thus the type and stability of the equation are not affected when this velocity changes sign, for instance at separation. The other major difference is that, whereas conventional boundary layers are imbedded in an irrotational outer flow, this one is not. In particular, there is no Bernoulli relation linking the outer velocity to the pressure gradient. Also, the vorticity does not necessarily tend to zero at the outer edge of the inner region, and the boundary condition at this edge must allow a transfer of vorticity to or from the outer flow.

The edge of the inner region is at $n = \delta$, where δ is a parameter. δ should be small enough for the boundary layer assumptions to be valid; on the other hand δ should be large enough for the physical viscous region to be contained in the computational region. Naturally, the "viscous region" cannot be precisely defined; however, if the inner solution reveals strong gradients confined to the vicinity of the wall and a quieter region elsewhere, δ is probably large enough. Another test is to compute the various physical thicknesses of the boundary layer (displacement, momentum, etc) and to compare them to δ. Along the attached region, the boundary layer is well within δ; after separation almost all the vorticity is in the outer region and there is no boundary layer in the usual sense. Examples will be given to illustrate how δ is chosen.

In the boundary layer the velocity is obtained by integrating Eqs. 29 and 30 in the n direction. Both components of the velocity are zero at the wall.

This provides a well posed system with Eqs. 29 and 30 since these are first order.

Equation 31 is of second order in the n direction and thus requires two boundary conditions.

Instead of a boundary condition at the wall, the integral equations, Eqs. 10.3, 10.4 and Eq. 10.5, are used. This is natural since we have shown that in the exact formulation Eqs. 10.3, 10.4 and 10.5 regulate the flux of vorticity from the wall.

The other condition regulates the flux of vorticity through the interface.

d) Interface conditions.

Both the velocity and the vorticity field should be matched at the interface. The matching of the velocities is done in the same spirit as in classical boundary layer theory. The component of velocity parallel to the wall, u, will always be matched since it is of order 1. The normal component v is small, of order δ, at $n = \delta$ and at the lowest level of approximation it is neglected; we shall adopt the next level of approximation and match the v components as well(still assuming that the inner region is thin).

As for the vorticity, since Eq. 28 is first order and Eq. 31 is second order, they cannot be matched without making an additional approximation.

The two domains exchange vorticity through the interface. Since Eq. 28 is applied down to the interface, it is consistent to derive the approximate interface condition in the same spirit. Thus it is assumed that the interface is far enough from the wall for the viscous term to be dominated by the convection term, and the transfer of vorticity is taken as $v\omega$ and imposed by the upstream region. The boundary condition has thus dropped to the level of the inviscid approximation. For Eq. 31, this means that the viscous term $\nu \frac{\partial^2 \omega}{\partial n^2}$ is neglected at the outer edge of the boundary layer.

III) NUMERICAL IMPLEMENTATION.

Discrete approximations to the continuous equations are derived as a basis for the following discussion of the numerical method. The algorithm used for each region are described first, and then the coupling procedure is introduced. Each method converges in its domain as the scale of the discretization is reduced in space and time. However, the complete algorithm should not be expected to converge to the Navier-Stokes solution since the errors introduced by the inviscid and the boundary layer approximations remain finite. Convergence at a given Reynolds number could only occur if the order of the boundary layer approximation (among other things) was increased in parallel with the numerical refinement.

This chapter applies to the $KPD3$ program; $KPD1$ and especially $KPD2$ use a different logic which will be described in Appendix A.

1) Outer flow.

a) Extent of the outer region and discretization in space.

The outer region covers the whole (x, y) plane except the solid and a narrow band of thickness δ around it. It extends to infinity and no grid is involved.

The vorticity field is described as the sum of a large number N_v of mobile functions of small support, referred to as "vortices". Each vortex is defined by the position $\mathbf{r}_i = (x_i, y_i)$ of its center, its circulation Γ_i which is the integral of the vorticity it carries, and the shape γ of the distribution of the vorticity around the center (see Eq. 5). This distribution is in general bell-shaped; this is the "vortex blob" method.

An individual vortex does not live for the full duration of the computation New vortices are created at the interface, where they enter the outer flow. Vortices can also be absorbed by the wall region and thus removed from the computation. Finally, vortices are allowed to merge when certain conditions are fulfilled. The vortices are independent entities; they form a "jungle" except maybe just after separation, where the free shear layer has not yet undergone instability and broken down into circular eddies.

In this study, the shape of the blob, γ is taken to be axisymmetric, and is the same for all vortices at all times. The whole blob moves at the velocity of its center. Clearly, no diffusion of the blob takes place, and the straining of the blob by the velocity gradients is also neglected. This straining is the source of the spatial error, as analyzed in [9] and [19].

Simple cores, defined by algebraic functions, were used. Being everywhere positive, these cores are expected to yield second order convergence in an inviscid problem [19]. The superiority of the more elaborate cores (which should yield higher order convergence) has not been clearly demonstrated [45] ; therefore the simplest possible approach was chosen. The cores chosen also require less computing time. The computation of the interactions is the most time-consuming part of the program and it might be advantageous to have many "inexpensive" vortices rather than a smaller number of "sophisticated" ones. Finally, it is very likely that the main source of error is not in the treatment of the inviscid transport of vorticity, but in the neglect of the small scale turbulence, and even more in the interaction with the walls. In the wall region the solution is not smooth at the scale of the vortex core radius, and the rate of convergence of the method becomes less relevant.

Two cores were used and are defined by

$$\text{Core 1} \qquad \gamma(r) = \begin{cases} \frac{(1-\frac{r^2}{\sigma^2})^2}{\pi\sigma^2}, & \text{if } r < \sigma; \\ 0, & \text{if } r > \sigma. \end{cases} \tag{32.1}$$

$$\text{Core 2} \qquad \gamma(r) = \frac{\sigma^2}{2\pi(r^2+\sigma^2)^2} \tag{32.2}$$

σ is the "core radius". These functions are plotted in Fig. 6, as well as the corresponding velocity and stream function distributions, with the point vortex as a reference. In Core 1 the vorticity is continuous and the velocity continuously differentiable, while Core 2 is infinitely differentiable. Core 1 has a finite support and a vortex is not allowed within a distance σ of the wall, so that the vorticity is entirely outside the solid. Core 2 does not have this property: its support is infinite (the vorticity decays like r^{-4}) and penetrates the solid. Although this does not appear to be very natural, the differences in the results were negligible.

Core 1 was used in some versions of $KPD1$ and $KPD2$, in particular for the case of dynamic stall (on a CDC 7600). It was then decided to switch to Core 2 for the CRAY version of the program, because Core 1 involves an "IF" test which inhibits the vectorization of the loop.

b) Computation of the velocity.

The velocity field must be computed in order to solve Eq. 28 for ω. If we introduce the value of ω from Eq. 5 into the Biot-Savart law, Eq. 10.3, the velocity induced at a point r by the vortices is given by:

$$\begin{pmatrix} u \\ v \end{pmatrix}(\mathbf{r}) = \sum_{i=1}^{N_s} \frac{\Gamma_i}{2\pi} \eta(|\mathbf{r} - \mathbf{r}_i|) \begin{pmatrix} y_i - y \\ x - x_i \end{pmatrix} \tag{33}$$

with η defined by:

$$\frac{d(r^2\eta)}{dr} = r\gamma(r) \text{and } \eta \approx r^{-2} \text{for } r \text{large.} \tag{34}$$

The formula is greatly simplified by the fact that the blobs are axisymmetric. If point vortices were used η would be equal to r^{-2}. With vortex blobs η is regular near zero, and the velocity field is smooth.

The uniform freestream velocity also contributes to the velocity field, as well as the velocity induced by the inner flow vorticity, which is not included in the blobs. Since the inner region is a thin shear layer, even compared to the

core diameters of the vortices, it can be represented to a good approximation by a vortex sheet of zero thickness. The strength of the vortex sheet will be designated by U_e; it is the circulation per unit length of the sheet, and also the jump of tangential velocity across the sheet. The sheet is made up of segments, each segment covering the interval between two wall points (see Fig. 7). The strength of the vortex sheet is assumed piecewise linear. The velocity field of such a segment of vortex sheet can be expressed analytically. In complex variables it is

$$\mathrm{U}(z) = \frac{i}{2\pi}\frac{(z_2 - z_1)}{|z_2 - z_1|}\overline{\left[U_{e1} - U_{e2} + \frac{U_{e1}(z - z_2) - U_{e2}(z - z_1)}{(z_2 - z_1)} \log\left(\frac{z - z_2}{z - z_1}\right)\right]} \tag{35}$$

where z_1 and z_2 are the two ends and U_{e1} and U_{e2} are the strength at each end and the overbar denotes the complex conjugate. This field jumps across the sheet but is smooth on each side: this is why segments are used instead of circular vortices to represent the inner flow vorticity. The velocity field however has a logarithmic singularity at the junction of two adjoining segments unless they have the same slope. Therefore it is desirable to keep this slope as smooth as possible.

Thus the velocity of each vortex is the sum of the freestream velocity U_∞, N_w terms of the type given by Eq. 35 for the N_w wall intervals, and N_v terms of the type given by Eq. 33 for the N_v vortex blobs. This is the discrete analog of Eq. 10.3.

The computation of the interactions has to be performed at each time step and this is the most time-consuming part of the program. $N_v(N_v + N_w)$ interactions have to be computed, and each of the $N_v N_w$ interactions with the wall segments involves a complex logarithm. Fortunately, the simplicity of the data base makes vectorization easy, provided that the function η does not involve "IF" tests or any non-simple function. Even then, it is worthwhile to apply analytical tools to reduce this cost.

The high cost of implementing the Biot-Savart law, Eq. 33, comes from the fact that each vortex interacts with vortices in the whole domain, with

distant vortices as well as with its neighbours. On the other hand, the velocity field induced by a distant cluster of vortices does not depend much on its detailed shape, and this should be taken into account by the program. The velocity induced at a large distance R by a cluster of diameter l has a Taylor expansion in terms of l/R. The first terms of this expansion are a vortex term, a dipole term, and so on.

To implement this in a controlled way, with a known and bounded error, the clusters are first given a precise definition. The plane is divided into a number n of identical square cells of side l, surrounded by an external cell which is treated separately (Fig. 8). For the scheme to achieve its purpose, each cell should contain more than a few vortices; so n should be much smaller than N_v. Each time the interactions are to be computed, the vortices that are in the same cell are linked, logically. Their distance to the center of the cell is smaller than $l/\sqrt{2}$.

It is convenient to use complex notation here. The function that is expanded is $(z_i - z_j)^{-1}$, where z_i is complex for (x_i, y_i). Let z_i be in the K^{th} cell, with center Z_K, and z_j in the L^{th} cell (see Fig. 9). Thus $(z_i - z_j)^{-1}$ is expanded in the vicinity of $(Z_K - Z_L)^{-1}$. The function z^{-1} has a rapidly converging Taylor expansion, and the error can be bounded as a function of $l/|Z_K - Z_L|$ and of the number of terms that are retained. This number of terms is chosen to make the error as uniform as possible. If the two cells are far from each other, compared to l, only the first term of the expansion will be kept. If they are not very far, up to four terms will be included. If they are neighbours, the Taylor expansion does not apply; in that case, the interactions are computed vortex by vortex. If either vortex is in the external cell, the Taylor expansion is not used either, since the external cell is infinite in extent and has no "center".

In the final version of the program, enough terms were taken to ensure a maximum relative error of 1% in each interaction. The actual error was computed in a test case by also computing the velocities without using Taylor

expansions. The maximum difference that was observed was about 0.5% of U_∞, and the "L_2" average was less than 0.1%. This level of error is very moderate, in comparison to the other possible sources of error.

With a proper choice of l and n, computing the interactions this way instead of applying Eqs. 33 and 35 directly can save 65% of the time on a serial computer like the CDC 7600. Typical values are $N_v = 1000$, $n = 100$, $l = .5$ with a body of size 2. Vectorizing the Taylor expansion for the CRAY was possible, but resulted in a program that was more complex and less "smooth" logically, with shorter loops. As a result, $KPD1$ and $KPD2$ run faster without the Taylor expansions; $KPD3$ still runs faster with them, because using them saves the time of evaluation of most of the complex logarithms in Eq. 35.

c) Time integration.

The system of ordinary differential equations, Eqs. 7 and 24, is integrated by the Adams-Bashforth second order method. The velocity of each vortex is computed at uniform time intervals and the positions updated according to the formula:

$$\mathbf{r}_i(t + \Delta t) = \mathbf{r}_i(t) + \Delta t(\frac{3}{2}\mathbf{U}_i(t) - \frac{1}{2}\mathbf{U}_i(t - \Delta t)) \tag{36}$$

Δt is the time step and the accuracy in terms of Δt is of second order [46] .

As with any multistep method, the first step of integration must be treated differently because $\mathbf{U}_i(t - \Delta t)$ is not available. Thus the first step in the life of each vortex is handled by the explicit Euler scheme:

$$\mathbf{r}_i(t + \Delta t) = \mathbf{r}_i(t) + \Delta t\, \mathbf{U}_i(t) \tag{37}$$

The Adams-Bashforth scheme was chosen because it is second order accurate, while requiring only one evaluation of the derivative per step. It is weakly unstable when applied to linear equations, but the non-linearity of equations 7 and 24 actually stabilizes the integration and no stability problem has been

encountered (see subsection e)). The need to store two levels of the velocity values is not a problem since the Vortex Method involves only a very moderate number of variables.

It should be noted, however, that since the inner region solution is only first order accurate in time, the overall accuracy is of first order at best. The Adams-Bashforth scheme is used mainly to gain quantitative accuracy (over the first order Euler scheme) and especially reduce the scattering of the vortices (see subsection e)).

d) Vortex merging device.

The boundary layer releases a significant number of vortices near the wall at each time step: typically 100 new vortices, compared to a total number of 1000. (Naturally, these 100 vortices do not carry 10% of the vorticity; they are numerous but weak. Typically, in one time step the new vortices of one sign might add up to a circulation of 0.03, while each one of main "Karman Street" eddies carries a circulation of the order of 10). This continuous addition of new variables should be balanced by the suppression of some of the old variables at approximately the same rate; this is done by merging pairs of vortices into one when appropriate conditions are fulfilled. As a result, the vortices are dense near the body, where fine resolution is desirable, and become progressively sparser away from it.

Deffenbaugh and Marshall introduced a merging method but did not make all the details available [28]. R. Rogallo (personal communication) used a device which was very similar in spirit to the one used here; however the error estimate was different.

If nothing was done to keep the number of vortices under control the program would only be able to compute flows of relatively short duration before the number of vortices and the associated computing cost would become excessive. This would be acceptable for some applications (slender body "2D-3D" analogy, for instance) but not for the ones considered in this study.

Furthermore, if all the vortices are kept, there is a strong incentive to create fewer at each step; as a result the wall boundary condition is more loosely satisfied: typically only 20 discrete equations are retained [29]. It is preferable to have a much greater resolution near the body, typically 200 discrete equations, and then let these many small vortices progressively merge into larger ones. Furthermore the description of the flow is more homogeneous in time and can actually reach an asymptotic state.

The procedure is the following. Only the merging of two vortices into one is attempted, at each time step. If we consider two vortices of circulation Γ_1 and Γ_2 and position z_1 and z_2, the velocity field they create before merging is, in complex notation:

$$\mathbf{U}(z) = \frac{i}{2\pi}\left(\frac{\Gamma_1}{(z - z_1)} + \frac{\Gamma_2}{(z - z_2)}\right) \tag{38}$$

The field they create after merging is:

$$\mathbf{U}'(z) = \frac{i}{2\pi}\frac{\Gamma}{(z - Z)} \tag{39}$$

where Γ and Z are the circulation and position,recpectively, of the new vortex. The first few terms of the expansion of the difference $\mathbf{U}(z) - \mathbf{U}'(z)$ at large distance z are (the complex conjugate of):

$$\frac{i}{2\pi}\left(\frac{(\Gamma - \Gamma_1 - \Gamma_2)}{z} + \frac{(\Gamma_1 z_1 + \Gamma_2 z_2 - \Gamma Z)}{z^2} + \frac{(\Gamma Z^2 - \Gamma_1 z_1^2 - \Gamma_2 z_2^2)}{z^3}\right)$$

$$+ O(|z|^{-4}) \tag{40}$$

The two leading terms can be removed by taking:

$$\Gamma = \Gamma_1 + \Gamma_2 \tag{41.1}$$

$$Z = \frac{\Gamma_1 z_1 + \Gamma_2 z_2}{\Gamma} \tag{41.2}$$

This means that the new vortex is given the sum of the circulations of the old ones and placed at their centroid (Fig. 10). It is worth noting that two vortices, if they are isolated, orbit precisely around this centroid, which is itself stationary. Thus by merging we replace two vortices, which would move on two concentric circles, by one stationary vortex at the center of these circles. This way of merging also preserves the total circulation, and the first moment of vorticity, which is equal to the impulse of the flow (this results from an integration by parts [14]). It should also be noted that if the two vortices have opposite signs the centroid is aligned with them but not between them (Fig. 10.b).

The third term cannot be removed within this framework, and is therefore taken as an estimate of the error introduced by the merging. At each step the vortices are examined pair by pair and the merging done only if the estimate is within a tolerance V_0. The exact estimate used is:

$$\frac{|\Gamma_1\Gamma_2|}{|\Gamma_1+\Gamma_2|}\frac{|z_1-z_2|^2}{(D_0+d_1)^{1.5}(D_0+d_2)^{1.5}} < V_0 \tag{42}$$

where d_1 and d_2 are the distances from z_1 and z_2 to the nearest wall and D_0 is a parameter. The expression in Eq. 42 has the dimension of a velocity and is our estimate of the disturbance that a merging would impose on the boundary layer. Typically, V_0 is of the order $10^{-4}U_\infty$ or less.

The disturbance estimate is the product of two factors. The first factor depends only on the circulations:

$$\frac{|\Gamma_1\Gamma_2|}{|\Gamma_1+\Gamma_2|} \tag{43}$$

Clearly, merging of vortices with large circulations is discouraged, as is the merging of two vortices that have nearly opposite circulations. (In that case the new vortex would be very far from the original ones. See Fig. 10b)

The second factor depends only on the positions:

$$\frac{|z_1-z_2|^2}{(D_0+d_1)^{1.5}(D_0+d_2)^{1.5}} \tag{44}$$

Clearly vortices are more likely to merge if they are close to each other and far from the body. The parameter D_0 controls the relative variation of the estimate as a function of d_1 and d_2. If D_0 is large $(D_0 + d)$ has a slow relative variation near the wall and the density of vortices will be quite uniform. If D_0 is small $(D_0 + d)$ gets very small near the wall, which discourages merging and will result in more small vortices subsisting near the wall. Thus, the parameter D_0 allows the user to shift the resolution from the wall region to the wake or vice versa, as illustrated in Fig. 11.

The value of the tolerance V_0 is not held constant for every time step. Instead, the programs slowly adjusts it to keep the number of vortices near the chosen number, raising V_0 to make mergings easier if it sees too many vortices and lowering V_0 if it sees too few. The number of vortices thus remains close to the input value, which is very desirable from a practical point of view.

In contrast with some earlier approaches [22], this method of merging vortices is totally automatic and has a mathematical rather than a physical basis. For instance no effort is made to "manually" obtain a well defined Karman street; the vortices will probably take on this pattern at some distance from the body, but it will be destroyed as they move farther downstream.

e) Numerical diffusion.

The Vortex Method, at least in an unbounded fluid, has been shown to converge to the solution of the Euler (inviscid) equations. In reference [45] , (written with Dr. Y. Nakamura and Dr. A. Leonard) we applied the Vortex Method to several simple problems and by comparison with the known exact solutions confirmed the mathematical estimates: second order convergence, in terms of the core radius, was observed. These flows were all inviscid and unbounded, and the initial data had to be sufficiently smooth. Gaussian cores were used, but any core for which γ is smooth and everywhere positive should also give second order convergence [19].

Although the Vortex Method solves the inviscid equations, there is evidence

of a significant "numerical", or "parasitic", diffusion in the solutions it produces. Essentially, strong velocity gradients induce strong accelerations which deteriorate the accuracy of integration of the motion of the vortices. This effect is different from the numerical diffusion present in many finite-difference methods, in that it is caused by velocity gradients instead of the velocity itself. Naturally this diffusion tends to zero as more vortices are used and shorter time steps taken, but it cannot be ignored when doing computations with a practical level of resolution. To describe this numerical diffusion better we shall consider some of the invariants of the system. In this section only unbounded flows will be considered; the presence of a solid and the creation of vorticity at its surface would only complicate the discussion.

It is well known that a system of point vortices is a Hamiltonian system [47] . The Hamiltonian of the system is the Kirchhoff function, defined by

$$W = \sum_{i \neq j} \frac{\Gamma_i \Gamma_j}{2\pi} \log(|\mathbf{r}_i - \mathbf{r}_j|) \tag{45}$$

and the equations of motion become

$$\Gamma_i \frac{dx_i}{dt} = -\frac{\partial W}{\partial y_i} \tag{46.1}$$

$$\Gamma_i \frac{dy_i}{dt} = +\frac{\partial W}{\partial x_i} \tag{46.2}$$

Naturally W itself is an invariant. Other invariants are the total circulation, the first moment of the vorticity (equivalent to the momentum of the fluid) and the second moment (equivalent to the angular momentum) [14], [48]. W is also the energy of interaction of the vortices (their internal energy is infinite and has been separated from the interaction energy). These quantities are also invariants of the exact inviscid solution; these built-in invariants provide a basic advantage in using the Vortex Method.

For a system of vortex blobs a Kirchhoff function can still be defined, by replacing the logarithm in Eq. 45 by an appropriate regular function. For

example Core 2 results in the Kirchhoff function

$$W = \sum_{i \# j} \frac{\Gamma_i \Gamma_j}{2\pi} \log(\sqrt{|\mathbf{r}_i - \mathbf{r}_j|^2 + \sigma^2}) \tag{47}$$

and Eq. 46 is satisfied.

If we give all the vortices the same core shape, the vortex blob system has the same 4 invariants as the point vortex system (this is the "semi-discrete" system: discretized in space but continuous in time).

On the other hand it is clear that errors in the integration of the ordinary differential equations, Eq. 7, tend to scatter the vortices and therefore act in the same sense as a diffusion term. One way to describe this diffusion more precisely is to determine which of the invariants we mentioned are actually conserved and which ones are not in the solution of the fully discrete system (discretized both in space and time). Any deviation will be a result of the time integration errors.

The total circulation is obviously conserved because each value Γ_i is kept constant. The first moment of vorticity, $\int\int \omega r$, is conserved too if the time integration scheme is linear (which is the case for all the classical schemes) because it is a linear combination of the r_i's.

The second moment of vorticity, $\int\int \omega r^2$, is not conserved in general. It reflects the scattering of the vortices. In Ref. [45] we defined an effective viscosity ν_e by:

$$\frac{d}{dt}\left[\int_{-\infty}^{+\infty}\int_{-\infty}^{+\infty} \omega(x,y)(x^2+y^2)dxdy\right] = 4\nu_e \left[\int_{-\infty}^{+\infty}\int_{-\infty}^{+\infty} \omega(x,y)dxdy\right] \tag{48}$$

It is shown in Reference [48] that an exact viscous solution satisfies Eq. 48 with ν_e replaced by ν; this motivates the definition of ν_e. The viscous diffusion steadily increases the second moment of vorticity, which is a measure of the spreading of the vorticity. The effective viscosity was calculated in

several cases and shown to tend to zero with the size of time step, for a given space discretization. This why we called the Vortex Method "semi-inviscid", meaning that the space discretization itself was not responsible for the diffusion, but that it allowed the time integration scheme to introduce a diffusive error (the same terminology is used when a method is said to "semi-conserve" energy, i.e. it would conserve energy if the time integration were exact).

The concept of effective viscosity according to Eq. 48 however has several weaknesses. It breaks down if the total circulation is zero, which is often the case, and if there are solid walls boundary terms appear which cannot be defined very reliably in a vortex simulation. More importantly, it is a global quantity. A concept that would yield a local effective viscosity would be much more useful, but has not been found yet. Thus it is not possible to produce the "modified equation" the way it is commonly done with finite difference methods, or to produce an "effective Reynolds number" of the computation. If that were possible, one could think of using the integration errors to introduce the desired diffusion.

The reason why the second moment is not conserved is that it is not a linear combination of the r_i's; similarly, W is non-linear and will not be conserved. Delcourt and Brown used W (interpreted as the energy) for their definition of an effective viscosity [31]. The effective viscosity turned out to be positive, since the energy decayed steadily. For the time integration they used the Euler explicit and the Huen scheme (also called Runge-Kutta, first and second order).

We showed in Ref. [40] that the non-linearity of Eqs. 7 and 35 has a strong influence, even in a very simple case: two vortices isolated in space. If their circulations are Γ_1 and Γ_2, their (complex) positions are given Z_1 and Z_2, and they are treated as point vortices, then their spatial separation $Z = (Z_1 - Z_2)$ satisfies the first order ordinary differential equation:

$$\frac{dZ}{dt} = \frac{i(\Gamma_1 + \Gamma_2)}{2\pi\overline{Z}} \tag{49}$$

If Z_0 is the initial separation, at $t = 0$, the solution is:

$$Z(t) = Z_0\, e^{i\Omega_0 t} \tag{50}$$

where Ω_0 is defined by $\Omega_0 = (\Gamma_1 + \Gamma_2)/(2\pi|Z_0|^2)$. The vortices orbit together, and the second moment of vorticity is constant; in that sense the discretization by vortices did not introduce any diffusion. The linear ordinary differential equation:

$$\frac{dZ}{dt} = i\Omega_0 Z \tag{51}$$

has the same solution and is more familiar. In finite difference methods, convection terms generally produce pure imaginary eigenvalues, which makes Eq. 51 a good model problem.

Although the two equations have the same exact solution their numerical integration, by the same scheme, can give widely different results in terms of stability. We shall concentrate on the modulus of Z since we are mostly interested in scattering. Fig. 12 shows $|Z|$ as a function of time as found in a numerical solutions to Eqs. 49 and 51 for a typical case: Adams-Bashforth 2 and Lomax schemes, and several values of the time step. The Lomax scheme is especially adapted to the integration of Eq. 51 [46] . With Adams-Bashforth-2 the nonlinearity of Eq. 49 reduces the error, compared to the linear equation, because as $|Z|$ increases the angular velocity decreases, and the integration becomes more accurate. The solution to Eq. 51 grows exponentially, which is a strong instability, while the solution to Eq. 49 only grows like $t^{1/8}$. The integration of the linear equation by the Lomax scheme shows exponential decay, while the integration of the non-linear equation keeps $|Z|$ finite. In this case the second moment increases and decreases periodically; the effective viscosity is not constant, and even takes on negative values. It appears that the angular velocity cannot remain below a given value (about $0.24/\Delta t$ with the Lomax scheme).

Similarly, in practical cases with many vortices the time integration scheme does not allow values of angular velocities above a certain level, and scatters

the vortices when the local velocity gradients are too strong (in that sense the Vortex Method is stabilized by its own integration errors).

In the computations done in this study, a typical value of the angular velocity in the near wake is 10, and the time step is 0.03 (in compatible units). The product is non-dimensional and of the order of 0.3: obviously integration errors will be significant at the scale of the individual vortices. Considering the fact that at high Reynolds numbers the angular velocities in the exact solution would be as high as several hundred units, at least an order of magnitude greater, it is also clear that resolving all scales is not possible. The Vortex Method performs well in spite of such errors partly because the conservation of circulation and momentum are built-in.

The effect of merging can be examined in the same spirit. When two vortices of the same sign (the more likely case) merge the second moment of the vorticity distribution decreases. The merging concentrates vorticity and this is especially apparent in the far wake. If the mergings occur far enough from the solid body the effect of this "reverse diffusion" is small.

2) Inner flow.

The boundary layer equations, Eqs. 29, 30 and 31, are solved using a finite difference discretization in space and an implicit method in time. The accuracy is of second order in one space direction, fourth order in the other, and first order in time. The Baldwin-Lomax algebraic turbulence model is used.

a) Extent of region and discretization in space.

The region is a band of width δ placed around the body. δ is small, compared to the radius of curvature, and the curvature of the band is neglected.

The functions ω, u and v are assigned values at the nodes of a grid. The grid is stretched in the s direction, according to the distribution of the points along the wall. In the n direction an exponential stretching is used to give

a finer resolution near the wall. This is especially useful for turbulent cases, in which the viscous sublayer is very thin. With the grids used the cell size near the wall was of the order of 5, in "wall units", so that the first point was well within the viscous sublayer [50]. The equations are transformed to a computational plane where the grid is uniform. Centered differences are used for all derivatives in all directions. Second order accurate differences are used in the n direction, in which the grid can be made very fine without penalty. In the s direction, the grid repoduces the intervals involved in the outer flow, and these cannot be made very short. For this reason, and to make the convection of vorticity as accurate as possible, fourth order accurate Pade differences are used in the s direction. Naturally, to actually obtain fourth order accuracy the grid should be smooth enough, which is not always easy when generating complex shapes.

b) Computation of the velocity field.

The u velocity in the grid is obtained by integrating Eq. 30 upwards from the wall, where $u = 0$. The v velocity is then obtained by integrating Eq. 29 with $v = 0$ at the wall. In both cases, the second order accurate "trapezoidal rule" is used in the n direction, and $\partial u/\partial s$ is obtained by Pade differences.

c) Time integration scheme.

The integration in time is done using a first order accurate implicit scheme: it is the Euler implicit scheme, except that the velocity components are "frozen" at the old time level. Completely linearizing the non-linear convection term, $\mathbf{U}.\nabla\omega$, would make the matrix inversion much more costly without formally improving the accuracy. Furthermore the Euler implicit scheme is very stable according to a "frozen velocity" analysis, and there is no evidence that the incomplete linearization hurts its stability.

This first order scheme is used because the time variations in the boundary layer are very slow (typically 300 steps per period) and because implementing

a higher order scheme would be much more complex, again because of the difficulty in linearizing the velocity components.

The boundary condition in the s direction is periodic and does not require special attention. The boundary conditions in the n direction are implicit, which is desirable in the presence of a viscous term and with a fine grid.

d) Approximate factorization.

The time evolution equation is written in "delta" form and the implicit operator is approximately factored into two tridiagonal operators, one in each direction. This simplifies the solution without degrading either the first order accuracy in time, or the accuracy of the steady state.

The operator in the s direction is periodic and tridiagonal. It is solved by the Thomas Algorithm, adapted to periodic matrices. The operator in the n direction has the three diagonals plus a full first line representing the integral across the layer. This integral condition replaces the boundary condition at the wall; more details will be given in the chapter on the coupling. The boundary condition at δ will also be described later; it is included by modifying the last line of the matrix. This matrix is solved by the Thomas Algorithm, this time adapted to start the elimination from the bottom and eliminate the first line too.

e) Artificial dissipation.

Finally, an artificial dissipation is added in the s direction. The centered differences used to approximate the first derivatives in the s direction do not couple the even and odd lines, and a small positive term representing a derivative of even order is added to the time derivative to absorb energy and avoid the appearance of oscillations. A fourth order derivative is generally used, to disturb the slow varying components as little as possible. Depending on the amount added, it might be necessary to treat the artificial dissipation implicitely to preserve stability.

Probably because of the constraints imposed by the outer flow, and of the non-linearity, a catastrophic instability does not result if the dissipation is omitted in this program: the solution remains bounded. However it exhibits short wave undulations in the s direction, which have half-periods close to the grid size, and are very probably caused by the inaccuracies of the finite difference method when treating the convection term with non-constant velocity. Naturally the coefficient of artificial dissipation, ϵ, is given a value as low as possible. This will be illustrated in the "Results" chapter.

As a whole the numerical method used for the inner flow closely follows the theories developed by Beam, Warming, Steger and Pulliam at NASA Ames [49] .

f) Turbulence model.

The Baldwin-Lomax turbulence model was chosen because it is simple to use and was designed for separating flows [50] . It is based on the Cebeci-Smith model, but modified to ensure a normal behavior even when the boundary layer thicknesses become very large. It is an algebraic, or "zero-equation", model; it does not require the solution of any additional differential equations, or any special conditions at the outer edge of the inner region.

The turbulent stresses predicted by the Baldwin-Lomax model are multiplied by an intermittency factor β which is a function of s only, and switches from 0 to 1 as the boundary layer undergoes transition. The transition model proposed by Baldwin and Lomax is not used; it does not seem to take sufficiently into account the pressure gradients which are very strong in flows around cylinders for instance. The criterion described by Schlichting, which is based on his own stability theory and an empirical correlation by Granville, incorporates the dependence on the pressure gradient and is used instead [51] . This transition model produces a position s_i of instability of the laminar boundary layer, and a position s_t of full transition. This delay is used in the program to make the transition smoother: the intermittency

factor $\beta(s)$ is defined by:

$$\beta(s) = 0 \qquad \text{if } s < s_i \tag{52.1}$$

$$\beta(s) = 3\left(\frac{s - s_i}{s_t - s_i}\right)^2 - 2\left(\frac{s - s_i}{s_t - s_i}\right)^3 \qquad \text{if } s_i < s < s_t \tag{52.2}$$

$$\beta(s) = 1 \qquad \text{if } s > s_t \tag{52.3}$$

The choice of a cubic function for Eq. 52.2 was arbitrary; it was chosen merely to make β a smooth function of s.

The turbulence model is present in the algorithm regardless of the Reynolds number. However, for Reynolds numbers of 10^5 or less, transition is not predicted (although instability often is) and the turbulent stresses are never activated. Thus the computation is fully laminar in such cases.

3) Coupling.

The interaction of the two regions involves the matching of the velocity fields and the transfer of vorticity across the interface.

The velocities are matched by properly setting up the vortex sheet that represents the inner flow vorticity in the Biot-Savart integral. The outer velocity field is a function of the $\mathbf{r}_i$'s and Γ_i's, the values of U_e and the position of the vortex sheet. If it satisfies Eq. 10.4 then the velocity at the wall (under the sheet) will be zero, and the tangential velocity over the vortex sheet will be U_e. Thus U_e is the value of the tangential outer velocity at $n = \delta$.

On the other hand the tangential component of the inner velocity at $n = \delta$ is:

$$u(s, \delta) = -\int_{n=0}^{\delta} \omega(s, n) dn \tag{53}$$

in view of Eq. 30. For the tangential velocities to match, this integral must be equal to U_e.

Matching the normal velocities is not as crucial, because the normal velocity is still small at δ. The program runs quite well without any effort to match the normal velocities. However some finer effects can be added by doing so. Since the vortex sheets is a simplified representation of a layer of vorticity of finite thickness δ, the vertical position of the vortex sheet is arbitrary within the thickness δ; it is natural to place it at the centroid of the inner flow vorticity, defined by:

$$\delta^*(s) = \frac{\int_{n=0}^{\delta} n\omega(s,n)\,dn}{\int_{n=0}^{\delta} \omega(s,n)\,dn} \tag{54}$$

Fig. 13 shows that if the vortex sheet is placed at δ^* the normal velocity at a distance δ from the wall must be

$$-\frac{d}{ds}(U_e(\delta - \delta^*)) \tag{55}$$

for mass to be conserved.

Now from Eq. 29, the normal component of the inner velocity, at $n = \delta$, is:

$$v(s,\delta) = -\int_{n=0}^{\delta} \frac{\partial u}{\partial s} dn \tag{56}$$

Using integration by parts we obtain:

$$v(s,\delta) = -\left[n\frac{\partial u}{\partial s}\right]_0^{\delta} - \frac{\partial}{\partial s}\int_{n=0}^{\delta} n\omega(s,n)dn \tag{57}$$

This equation, combined with Eqs. 53, 54, and 55, and the fact that $\partial\delta/\partial s = 0$ shows that the normal velocities at δ indeed match.

The vortex sheet is placed at δ^* because δ^* is the centroid of the vorticity. However integration by parts shows that, if the boundary layer is entirely contained in the band of thickness δ, δ^* is the classical displacement thickness defined in boundary layer theory [51] . The line defined by δ^* acts as an

effective boundary for the outer flow; its slope introduces the small amount of normal velocity due to the thickening of the boundary layer. This yields a boundary layer procedure of higher order and the incorporation of the displacement effect is necessary to avoid the singularity that otherwise appears in the boundary layer solutions near separation or reattachment [52] , [53] , [54] The boundary layer acts on the pressure both by the emission of vorticity into the outer region and by the displacement effect inherent in δ^*; the outer region vorticity controls the broad features of the pressure distribution while the δ^* effect corrects the pressure locally, especially near separation.

Although many questions are still open the consensus seems to be that a truly unsteady boundary layer, even in a direct solution (U_e imposed), does not have a singularity at separation [52] , [53] , [54] , [55] , [56] . However, if the solution as time progresses tends to a steady state, the shear stress distribution will steepen and tend to a singular distribution unless the boundary layer is allowed to relieve the pressure gradient by the displacement effect. This is what is sought in this algorithm; fairly smooth solutions are obtained but some oscillations near separation suggest that the problem might not be entirely solved. Naturally, the production of fair numerical solutions is not a proof of the regularity of the differential system unless a thorough convergence study is made like in reference [54] . This was not possible here, mostly because of the high cost of the vortex part of the computation.

In some plots of the computated results (especially in Figure 36), the vortex sheet is shown as a solid line over the wall and it is apparent how it lies very close to the wall in the part of the boundary layer having a favorable pressure gradient, then leaves the vicinity of the wall, until the boundary layer separates and injects itself into the outer region, becoming a free shear layer made of vortices.

One problem persists regarding the positioning of the vortex sheet at δ^*. It is that δ^* can take on negative values, or values larger than δ, and in general is not very smooth in the regions where U_e is small. Values of δ^* larger than

δ are not acceptable, because then some vortices would be under the vortex sheet and their tangential velocity would not be correct. In addition, we have seen that the vortex sheet should be kept very smooth. For these reasons, the function δ^* is filtered and truncated between 0 and δ, giving $\hat{\delta}$, and the sheet is placed at a distance $\hat{\delta}$ over the wall, instead of δ^*.

The thickness δ^* is obtained from the inner flow solution. The determination of the quantity U_e is more complex and coupled to the transfer of vorticity. The whole procedure will now be described; it reflects the flux of information from one module to the other and was devised on an intuitive basis. The flow chart in Fig. 14 illustrates it.

A buffer is used that communicates alternatively with the outer flow and with the inner flow. It is a vortex sheet of intensity B_f. Starting from the outer flow, at each time step the vortices that crossed the interface are put into the buffer and considered as candidates for absorbtion by the inner flow. The buffer then communicates with the inner flow.

The circulation per unit length, under the old vortices, will be $(U_e + B_f)$. Equations 10.3, 10.4 and 10.5 are then solved. In one time step the vorticity that is generated at the wall will not reach the outer flow in significant amounts (the vorticity diffuses to distances of order $\sqrt{\nu \Delta t}$ and $\sqrt{\nu \Delta t}$ will be .002 or less while δ will be .015 or more). Therefore Eq. 10.3/10.4/10.5 can be solved to a very good approximation by considering the outer flow vorticity as known and the strength $(U_e + B_f)$ of the inner shear layer as unknown. This amounts to assuming that for one time step the flux of vorticity through the wall, which is also the pressure gradient, does not depend on the shift of inner region vorticity in the n direction.

In that sense the boundary layer solution is "direct" at each step and the coupling is not "strong" in the sense of [53] ; the pressure distribution is imposed on the boundary layer for this step, and will respond to the boundary layer only for the next time step. This should be sufficient since the variations in the boundary layer are very slow.

$(U_e + B_f)$ is computed by solving a linear system. If N_w is the number of wall intervals, the N_w unknowns are the values of $(U_e + B_f)$ over each wall interval. The first $N_w - 1$ equations govern the differences between the values of the stream function at the N_w wall points (this is the integral form of Eq. 10.4, which is considered less sensitive and therefore more efficient than the colocation form), and the last equation governs the total circulation emitted by the solid (Eq. 10.5). The stream function is the sum of the stream function generated by the freestream and the existing vortices (which is known and forms the right hand side), and of the stream function generated by the vortex sheets (which is the unknown). The matrix is computed at the beginning of the run and "Gauss eliminated" once and for all, since it does not change. Note that a rotation of the solid does not affect the matrix; but if several solids were to move independently, this would affect the distance between wall points, and a different matrix would have to be inverted at each time step. The cost would then be higher.

The linear equations are set up to strongly couple each unknown with the equation of the same index, so that the matrix has its larger elements near the diagonal. As a result, the matrix is well conditioned enough for Gaussian elimination with partial pivoting or even without pivoting (both on the CDC 7600 and the CRAY).

Then the inner flow is advanced. In particular, the transfer of vorticity through the interface is computed. This vorticity is transferred between U_e and B_f, but $(U_e + B_f)$ takes the value that was just computed. Two cases are possible: $v_e < 0$, and $v_e > 0$. v_e is the normal velocity at δ and is obtained from the inner solution (Eq. 56). As was done for the inner flow solution, the velocity v_e lags by one time step.

If $v_e < 0$ the transfer is imposed by the outer region, in keeping with Eq. 30 The buffer vorticity is injected into the boundary layer; after the transfer the buffer is empty and all the vorticity is in U_e. This injection of the buffer constitutes the boundary condition at $n = \delta$ for the inner flow.

If $v_e > 0$ the transfer is imposed by the inner flow. The inner flow rejects the buffer and injects additional vorticity into it. The flux is $v_e\omega_e$, where ω_e is the value of the vorticity at $n = \delta$. This in itself constitutes the boundary condition at δ, since it amounts to setting the viscous flux to zero (it can also be interpreted as a linear extrapolation).

In both cases, the sum of B_f and of the integral in Eq. 53 is equal to the value that was computed for $(U_e + B_f)$. This yields the integral condition for the inner flow vorticity.

The new values of U_e and B_f have now been determined and the program returns to the outer region. The U_e vorticity stays in the boundary layer and U_e gives the strength of the vortex sheet. The buffer vorticity is injected into the outer flow under the form of new vortices if $v_e > 0$. (If $v_e < 0$ the buffer is empty.) The values of δ^* have also been computed and the vortex sheet is repositioned.

The outer flow is then advanced, which involves the computation of the velocities, the motion of the vortices, and the mergings. The program is now ready to start a new loop by determining the vortices to be put into the buffer (Fig. 14).

IV) RESULTS.

1) Parameters.

The main parameters are the number of vortices, N_v, the time step, Δt, the core radius, σ, the distance, R_0, from the wall where newly created vortices are placed, the grid thickness, δ, and the artificial dissipation coefficient, ϵ, if $KPD3$ is used, and the parameter, D_0, of the merging device.

a) Number of vortices, N_v.

The cost of a computation depends strongly on N_v since the computer time per time step is roughly proportional to N_v^2; naturally, the larger N_v is the greater the details that are reproduced and the more accurate the simulation. It is impossible to rationally select a minimum value of N_v for a particular situation. One should observe the solution and ascertain whether the smallest features considered significant contain at least several vortices and therefore have some degree of structure and some ability to be strained. (A good graphics system is essential for the monitoring of vortex computations). If an eddy contains only one computational vortex it is effectively circular, and of size σ.

A more quantitative estimate of accuracy, in selecting the value of N_v to be used, is the tolerance V_0 for merging. The larger N_v is the later the mergings will occur and the smaller V_0 will be. As an example the same code ($KPD1$) was run for the same case (a square) with $N_v = 800$, then with $N_v = 1200$ (Fig. 15). At the end of the simulations V_0 was 7.6×10^{-4} in the first case and 1.7×10^{-4} in the other case. The difference is significant: with 800 vortices, mergings occured that caused a disturbance four times as strong as would be allowed with 1200 vortices. However both values are small compared to U_∞.

For a single smooth body a value of 1000 is generally sufficient: the significant eddies in the flow are not very small and the other sources of error (boundary layer assumptions, turbulence model, etc.) probably dominate. If the body has sharp corners or a trailing edge then larger values of N_v might be desirable. The need for resolution is also stronger if the separating boundary layer is very thin; for example, the circular cylinder in the critical range of Reynolds numbers. In that case 1600 vortices were used. Finally, with several bodies the wake of the first body interacts with the other bodies; then it is justified to use much more vortices. The Vortex Flowmeter simulations described in Reference [41] used $N_v = 3600$.

b) Time step, Δt.

As was the case for N_v, the choice of Δt is a compromise between cost and accuracy.

The Lagrangian method can be quite accurate in the wake without a very short Δt because accelerations are moderate there, which makes Eq. 7 easy to integrate accurately. Similarly the Eulerian method in the boundary layer can be accurate without a very short step: the boundary layer often evolves slowly and in that case C. F. L. numbers much larger than 1 are acceptable (the C. F. L. number is $|U|\Delta t/\Delta s$, with U the local velocity and Δs the grid size in the s direction). The region that demands a short step is in general the intermediate region, and this is for two reasons. First, the vortices that are just outside the inner region often pass several grid points in one step while the inner region points interact only with their immediate neighbours. This can create an imbalance because the signals do not travel at the same celerity in the two layers. Second, if the time step is long the newly-created vortices are stronger (their circulation is proportional to Δt) and such strong vortices disturb the inner region.

To estimate an acceptable value for Δt the user should observe the simulation where the body has tight curves; if Δt is too long the vortices will not follow the wall. The C. F. L. number should not be much larger than 1. In general the results depend on Δt more directly than on N_v; one of the

weaknesses of the method is that it is only first order accurate in terms of Δt.

c) Core Radius, σ.

Unlike N_v and Δt the core radius does not influence computing cost and an optimum value exists, instead of a compromise between cost and accuracy (in Ref. [45] we systematically determined this optimum value in a few simple cases). If σ is large, the velocity is very smooth locally and the noise is low: as a result the vortices will not scatter much. On the other hand a large core radius can suppress velocity gradients that are physically significant and "freeze" a coherent structure that would be better represented if the cores were small enough and allowed it to evolve.

Fig. 16 shows the same flow computed with $\sigma = .005$ and then $\sigma = .05$. It is clear that the simulation is not very sensitive to the value of σ: changing it by a factor of 10 did not cause a striking difference. As a rule, σ should be of the order of $\Delta s/2$, where Δs is the spacing of the points along the wall. The value of σ influences the coupling between wall points and creation points, in the same way as the value of R_0 does (see subsection d)).

d) Distance R_0.

The points where new vortex blobs are introduced are located at a distance R_0 over the wall. In addition, vortices that are found within a distance R_0 of the wall are treated as being absorbed by the wall layer. Thus R_0 is a rather important parameter.

If $KPD3$ is used, R_0 is equal to δ, so that the vortices are created at the edge of the viscous region. If Core 1 is used, R_0 is equal to the core radius σ, so that the edge of the core is tangent to the wall.

If Core 2 is used in $KPD1$ or $KPD2$, R_0 is an independent and non-physical parameter. A good value for R_0 is about $\Delta s/2$, where Δs is the spacing of the points along the wall. Much smaller values would let the vortices go too close to the wall points (where the stream function is sampled) and create noise in the pressure. Much larger values would weaken the

coupling between each creation point and the wall point below it; again, the result might be oscillations in the pressure distribution. Such oscillations are a sign that the system is not functioning properly, and will also strongly disturb the integral boundary layer solver.

For simplicity R_0 is held the fixed for all the points along the wall. On the other hand Δs might vary, for instance if wall points are clustered in a region that is thought to require more resolution. (The selection of the wall points and their clustering is left to the user). To keep the ratio $R_0/\Delta s$ at a value of the order of 1/2, the clustering of points should be moderate. In the applications presented here points were clustered near sharp edges or trailing edges, or sometimes in the separation regions, but the ratio of the largest value of Δs to its smallest value did not exceed about 2.

e) Selection of δ, for $KPD3$.

The thickness δ of the computed viscous region results from a compromise and can be chosen by observing the solution.

On the one hand, the larger the value of δ, the greater the domain treated by the viscous solver, which is good. (In addition, extending the computational viscous region is not very costly). The attached part of the boundary layer clearly must be contained in the grid; the vorticity contour plots are helpful in ascertaining this. Another way to assure it is to compute the displacement thickness, δ^*: it should be of the order of $\delta/2$ or less along the entire attached boundary layer. Near separation it is normal for δ^* to become comparable to δ or even exceed it (vorticity of the two signs is present, and as a result the centroid can have large excursions). Fig. 17a shows a computation in which δ was too small: the boundary layer reaches the edge of the grid, even in a region with favorable pressure gradient. This defeats the purpose of having an inner viscous region.

On the other hand, the larger δ is the less the boundary layer assumptions are justified. The errors associated to these assumptions grow. These errors are hard to estimate quantitatively, but the results often give indications when δ is too large: the stability decreases and oscillations appear near

separation. Probably, the variations of the displacement thickness become too steep and disturb the algorithm. Fig. 17b shows such a case.

f) Selection of ϵ.

A small amount of artificial dissipation proves to be necessary to keep the solution smooth in the inner region, so that the finite difference approximations are accurate. Since fourth-order dissipation is used, it is difficult to compare the effect of the artificial dissipation with other sources of dissipation, for example the viscous stresses which are a second-order term. Fig. 18a shows a simulation with $\epsilon = 0$. Ripples appear in the vorticity contours and the other quantities involved with the inner region. The ripples are in the s direction, which was to be expected since that is the direction in which the grid is coarse and viscous stresses comparable in magnitude to the convection terms are not present.

This is why artificial dissipation is added only in the s direction. In Fig. 18b the flow is simulated with the grid and other parameters the same, but $\epsilon = 0.8 \times 10^{-5}$. The solution is now smooth. ϵ can be increased further, even by a factor 10, without any apparent effect. This is important since it shows that the dependence of the solution on ϵ is weak, provided that ϵ is large enough to eliminate the ripples.

g) Merging parameter, D_0.

The effect of D_0 was described in Chapter III. In this case also, the only way to determine a good value for the parameter is to observe the simulation. However, a good rule is to make D_0 about 5% of the body size if only one body is present. If there are several bodies, more vortices are devoted to computing the wake of the first body, so that it is not too coarsely represented when it strikes the second one. To achieve this, D_0 is made larger: about 50% of the distance between bodies.

2) Memory requirements and computing times.

a) Codes $KPD1$ and $KPD2$

The codes $KPD1$ and $KPD2$ have very similar requirements; the integral boundary layer solver requires very little memory and computing time. The total memory is about 10^5 words, and little effort was spent trying to reduce it. It could certainly be reduced to about 0.7×10^5. With 200 wall points the matrix alone requires 0.4×10^5 words. The computing time with $N_v = 1100$ and $N_w = 200$ is about 0.4 seconds per step on the CRAY-1. This figure is probably close to the minimum; the program was carefully written to reduce the CPU time and all the major operations were vectorized. Theses operations are the computations of the interactions ($O(N_v^2)$), the merging tests ($O(N_v^2)$), and the computation of the stream function at the wall points ($O(N_v N_w)$). The non-dimensional time step $U_\infty \Delta t/c$ was 0.015. Thus a complete period of oscillation for the square body requires about 250 seconds on the CRAY-1.

b) $KPD3$ code.

The $KPD3$ code requires a fair amount of additional memory for the differential boundary layer solver; the total is now about 2.8×10^5 words in the high resolution runs (again, no special effort was devoted to lowering the memory requirements). The additional CPU time required for the boundary layer is modest: about 15%. The other operation that is more time-consuming is the computation of the velocity field induced by the vortex sheet at the wall. It is $O(N_v N_w)$ and now involves a complex logarithm, whereas in $KPD1$ and $KPD2$ only arithmetic operations were involved.

Simulations of the circular cylinder with $KPD3$ were run with two levels of resolution. At the lower level $N_v = 1100$, $N_w = 200$ and $\Delta t = 0.025$, and the CPU time was about 1.1 seconds per step, or 450 seconds per shedding cycle. The high resolution runs used $N_v = 1600$, $N_w = 300$ and $\Delta t = 0.02$, resulting in a CPU time of 2.1 seconds per step, or 1050 seconds per cycle.

3) Results from the program $KPD1$.

a) Flow around a square.

The flow around a square is a good test because the viscous effects seem to be reduced to a minimum. The experiments exhibit a flat drag curve from $Re = 10^4$ to $Re = 10^7$ [57], probably because the primary separation occurs at the front corners irrespective of boundary layer thickness or of its laminar or turbulent character.

The computed mean drag coefficient is 1.8; the experimental value is 2. The computed Strouhal number is .11, which agrees with experiments. These results were obtained with Core 1, $N_v = 1000$, $N_w = 320$, $\sigma = R_0 = .02$ and $\Delta t = .03$ ($U_\infty = 1$ and $c = 2$). The tendency to underpredict the drag of the square is real: with other sets of parameters the drag was often even lower than 1.8, of the order of 1.4. This is a little disturbing since the case of a square was chosen precisely because complex viscous effects are not thought to be present. One possible cause for the inaccuracy is the difficulty for the algorithm to model the flow near a sharp corner, where the radius of curvature is small even compared to the size of the vortex cores and the spacing of the vortices.

b) Starting vortex at a sharp corner.

This example illustrates "viscous" behavior in the simulations done using the Vortex Method. In this case the viscous character is properly, although fortuitously, reproduced.

The body is a diamond and is a fair representation of the experimental situation in Ref. [1] , for short times after the start. The case chosen here is an angle of 60° and a constant velocity after the impulsive start ($\beta = 1/3$ and $m = 0$ with the notation in [58]). We shall focus on the flow pattern near one of the corners a short time after an impulsive start (the Kaden Vortex), and compare it with the experimental pattern. At time zero the flow is irrotational and as a result the velocity tends to infinity at the corner. This is the solution to the inviscid equations and it would stay unchanged

at all times. However, in the numerical solution, vortices are seen to leave the wall and form a starting vortex that resembles a spiral (Fig. 19a). The streamlines also show that the flow leaves the surface at the corner along the tangent to the upstream face; this pattern is generally accepted as correct and consistent with the Kutta condition. The streamlines are also shown in Fig. 19a and reveal the topological structure of the velocity field, with a half-saddle point at the corner and one on the back face.

Visual agreement with experiments is good. In addition, the growth of the length scale with time was compared with similarity theory. This theory, for an angle of 60°, predicts that the length scale will be proportional to $t^{5/7}$ (B. Cantwell, personal communication). In Fig. 19b, the distance from the tip to the point of zero velocity (near the center of the spiral) is plotted as a function of time, in Log-Log coordinates. The curve is close to being a straight line and its slope close to 5/7. The Vortex Method has succeded in simulating the formation of a starting vortex and associated establishment of the Kutta condition.

In this case it is clear that the motion of the vortices being advanced finite step by finite step, cannot accurately follow the sharp kink in the wall, especially if the magnitude of the velocity is large. After the first vortices have separated from the corner the flow pattern changes, the streamlines become smooth and the velocities smaller, and the simulation can be quite accurate. However the process, originally, is caused by inaccuracies in the numerical solution of Eq. 7.

c) Airfoil at low incidence.

This case is shown only to illustrate how $KPD1$, a pure Vortex algorithm, can become inaccurate when long stretches of attached flow are present. This is a major issue about the Vortex Method in general.

The flow around an airfoil at a low incidence, 10°, is shown on Fig. 20, treated by $KPD1$. The correct solution is a flow that remains attached almost to the trailing edge, with a very narrow wake and very low drag. The lift is accurately specified by potential flow theory and the Kutta condition

is satisfied.

In the numerical simulation, on the other hand, separation (defined as a departure of the flow from the solid surface) is seen to occur just downstream of the leading edge on the upper surface. As a result the wake is much too wide, the drag is significant and the lift too low, probably because the trailing edge is immersed in the wake and the Kutta condition is not satisfied.

The strong thickening of the boundary layer is a clear manifestation of the numerical diffusion that was described earlier (Chapter III). Basically, the boundary layer as represented by vortices can remain attached only in a significantly large and favorable pressure gradient (it actually does along the lower surface). Thus *KPD*1, and pure Vortex methods in general, are not well adapted to the simulation of flows past streamlined bodies. For these bodies, especially for airfoils, the accuracy will improve dramatically when the boundary layer is treated properly. In Fig. 20b the same flow is shown, treated by *KPD*2. The pattern is now correct and the quantitative features like lift, drag and moment much more accurate (see section 4).

4) Results from the program *KPD*2.

*KPD*2 is used mostly to compute airfoil flows. *KPD*1 would not be accurate because airfoil flows have long boundary layers, and *KPD*3 is still restricted smooth shapes.

a) Attached flow on an airfoil.

This example is a direct test of the accuracy of the method, in an admittedly simple case, by comparing it to an exact solution. A Joukovsky airfoil is treated at an incidence of 5°. The solution for potential flow with the Kutta condition satisfied is known analytically; the pressure coefficient predicted by the numerical method together with the exact one are compared in Fig. 21. The agreement is very good, which proves two facts. First, the flow as a whole is very well predicted and the circulation has been properly chosen by the algorithm to satisfy the Kutta condition. Second, the method of com-

putation of the pressure, using Eq. 13, is accurate; this is important because Eq. 13 does not involve Bernoulli's theorem, which happens to be valid here but is not valid when vortical flows are simulated.

b) Starting vortex on an airfoil.

Formation of the starting vortex and establishment of the Kutta condition are key features of the flow around airfoils; they are responsible for the existence of lift. Traditionally, the Kutta condition has been added to inviscid models in order to mimic a viscous phenomenon, namely the separation of the boundary layer that takes place at the trailing edge if the fluid attempts to flow around it. However the Vortex method, although it is in principle inviscid, reproduces this viscous feature without any intervention. This is another case in which the algorithm conveniently disobeys the inviscid equations: vortices are "thrown away" from the trailing edge if large velocities are present, until the circulation is correct and the trailing flow is smooth.

A convincing and probably accurate simulation of the starting vortex has been obtained and compared with the results of Wagner's theory [2] . An airfoil is started impulsively in an irrotational fluid. The airfoil is at incidence but there is no circulation around it; thus the Kutta condition (in classical terms) is not satisfied at time zero. The boundary layer is seen to separate from the lower surface at the trailing edge in Fig. 22. The vortex sheet it carries curls up into a vortex that is swept downstream. Since the total circulation remains zero, a circulation of the opposite value is established around the airfoil. This circulation grows with time, as does the lift on the airfoil. This lift starts at about half the steady value; Wagner's theory predicts an initial lift of exactly half the steady value. In general, agreement between the two curves, shown on Fig. 23, is very good. Wagner neglected the curling up of the vortex sheet and this might account for some of the disagreement. Also, Wagner used thin airfoil theory and the steady lift curve slope was 2π; here the airfoil was 12% thick, which results in more lift. The convergence of the lift to the steady value is made slower by the downwash of the starting vortex; this downwash decays only like t^{-1}.

Also of interest are the motion of the center of pressure, and the presence of drag, due to the downwash created by the vortex. At later times the center of pressure is at the quarter-chord point and the drag is zero (Fig. 22).

c) Dynamic stall.

The next case is the dynamic stall of the same NACA 0012 airfoil. Dynamic stall is a challenging problem, and a case was chosen for which experimental results are available [60]. The airfoil performs prescribed oscillations in pitch with the pivot at the quarter chord. The incidence is a sinusoidal function of time given by

$$\alpha(t) = \alpha_0 + \alpha_1 sin(kU_\infty t/c) \tag{99}$$

The Reynolds number is $2.5\,10^6$. In the simulation, the lower boundary layer was in a favorable pressure gradient and generally it did not undergo transition and did not separate until the trailing edge. The upper boundary layer tended to undergo transition and remain attached at low angles of attack; at high angles of attack, it separated while still laminar. It switched instantaneously from one state to the other; this is not very satisfactory, but is inherent in the transition model that was used. Also, separation bubbles in which the separated shear layer makes a transition and reattaches on the upper surface cannot be reproduced by the algorithm. This is unfortunate since such a bubble is probably present, at least during part of the cycle ($KPD3$ was written to eliminate these shortcomings as far as possible).

The history of the flow during one cycle can be followed on Fig. 24. The airfoil together with the vortices are shown; the force is displayed in terms of its magnitude, direction and axis of application (the center of pressure). Finally, the dashed line shows the suction distribution, measured normal to the surface and referenced to the stagnation pressure. The cycle begins with attached flow at 5° incidence; the Kutta condition is satisfied as evidenced by the smooth wake emanating from the trailing edge. The center of pressure is very close to the quarter-chord, which is expected for a symmetrical airfoil. As the incidence rises, counterclockwise circulation is shed; lift on the airfoil rises and the suction peak at the nose gets larger. At about 20°, the pressure

gradient that follows this suction peak becomes too severe and the upper boundary layers fails to undergo transition; it separates instead from the nose of the airfoil. A vortical region of moderate thickness forms on the upper surface. The flow then reattaches for a short time before entering the fully stalled condition (it is not certain whether this reattachment is physically correct).

After the incidence passes its maximum of 25°, the flow on the upper surface remains separated and large eddies form on the upper surface. These eddies are accompanied by low pressure regions. The surface pressure distribution is strongly disturbed; the center of pressure moves away from the quarter-chord, mostly towards the trailing edge. The lift stays roughly constant until the incidence is back to about 15°, then falls. During the rest of the cycle, the large vortices are progressively washed away and the flow reattaches on the upper surface. The center of pressure still has large excursions: this would be felt as buffeting in an airplane.

Figure 25 presents the numerical results for the normal force coefficient and the moment coefficient, compared with experimental results reported in [60]. The experimental results are phase averaged over a large number of cycles. Three successive cycles of computation are shown; the first cycle is not as representative since it started from fully irrotational flow. Three cycles are too small a sample for phase-averaging and this is why individual cycles are shown.

The agreement is quite good. However, the peak value of the normal force is lower in the computations. The peak value of the moment is also significantly lower; the experiments exhibit a large peak during the phase called "moment stall". Another area of disagreement is during the low incidence period. Reattachment often seems to take an unexpectedly long time in the computations and this might account for the difference. It is hoped that these disagreements will be better understood when the tunnel walls are included in the computation.

Figure 26 shows the pressure distribution on the airfoil during dynamic stall, after it has been Fourier-transformed in time. The mean pressure is

shown, as well as the in-phase component (the phase being given for the incidence by Eq. 99) and the out-of-phase component. Each component has been non-dimensionalized, the mean is divided by the mean incidence α_0 and the first harmonics are divided by the amplitude α_1. The agreement between data extracted from different cycles is fair. The difference between the mean and the in-phase components, and the existence of an out-of-phase component, are manifestations of the non-linear behavior of the flow.

d) Tilt-Rotor wing in hover.

The "Tilt-Rotor" concept combines many of the advantages of wingborne aircraft and of helicopters and has been studied for many years. NASA and Bell have recently conducted a very successful experimental program which included the construction and testing of the XV15 aircraft. A production version called JVX is now being developed and more emphasis is being placed on performance. One factor in the hover performance is the download experienced by the wing in the downwash of the rotors; both an experimental program and a numerical study are under way at NASA Ames to improve this aspect of the system.

A Tilt-Rotor aircraft has two rotors that can point vertically for vertical, helicopter-like take-off and landing, and also point forward for airplane-like forward flight. The Tilt-Rotor is much more efficient than a helicopter in forward flight because it avoids the asymmetric conditions than deteriorate the operation of the helicopter rotor, with the advancing blade experiencing drag rise from high subsonic Mach numbers and the retreating blade experiencing low dynamic pressures and stall. As a result the Tilt-Rotor is much faster and has a lower fuel consumption than the helicopter; its development was delayed mostly by aeroelasticity and control problems.

The Tilt-Wing concept, in which the wing tilts with the rotors, was not as successful probably because it required a heavy articulation at the wing root, and had more severe control problems. However, for a Tilt-Rotor when the rotors are pointing up the wing is still horizontal and placed in the downwash of the rotors; this creates a downward force on the wing which is

very significant especially since hover is the most critical condition in terms of payload. The objective is to decrease this force by improving the shape of the clean wing and by adding devices, like flaps, that could also serve as high lift devices for slow forward flight.

Almost all of the wing is in the downwash, which is far from being uniform. An accurate computation of the three dimensional flow is presently out of the question; the computations will be done in two dimensions and are expected to show trends and provide guidelines for the choice of the airfoil and landing devices on the wing.

The Tilt-Rotor wing can be quite thick since the Mach numbers it reaches are not very high; the main advantage is a lighter structure and more space for fuel and other components, but the larger thickness coincidentally improves the situation with regard to download. The NACA 4421 airfoil was chosen for the first stage of the numerical study and three landing devices were considered: two kinds of trailing edge flap and a leading edge device. Both flaps span 25% of the chord; the first one pivots about a hinge that is within the thickness of the airfoil and the second one has the hinge at the lower surface. The deflection of the flap introduces an arc of a circle as part of the top surface; the first flap has a circle of smaller radius than the second. This curvature was expected to strongly influence the separation of the boundary layer and therefore the global force. The leading edge modification involved removal of about 10% of the chord, thus reducing the effective chord and increasing the leading edge radius, with again a favorable effect on separation (the part of the airfoil that is removed would be placed under the leading edge and thus shielded from the mainstream).

The *KPD2* program was chosen. All cases were run with the same parameters to allow a comparison. The Reynolds number was 10^7, and the boundary layer underwent transition; all the shapes were defined by about 200 points, with $\Delta t = 0.03$, $R_0 = c = 0.02$, $D_0 = 0.2$ and $N_v = 1000$. Several thousand time steps were necessary for an average value to emerge; this represents 20 to 30 minutes on the CRAY-1.

The flat plate was treated under the same conditions to provide a reference; the result for the drag was about 3.5, compared to the experimental value of

about 2 [5]. Thus all the results are probably higher than the correct values; however, this does not prevent a comparison between different configurations, which was the main objective of the study.

Figure 27 shows the drag computed for the flat plate reference, both flaps with deflections ranging from 0 to 90°, and the modified leading edge with the large radius flap. The clean airfoil had a drag coefficient of 2.8, which is also thought to be higher than the correct value.

It appears that the two flaps give results that are much closer than one would have expected, and that the small radius flap can even have less drag. In retrospect, the reason is probably that even when the flow separates from the top surface at the hinge it can reattach on the flap; see Fig. 28 (in Fig. 28 the airfoil, vortices and force are shown, as well as the instantaneous streamlines). The size of the separation bubble will not influence the drag. Furthermore, at low deflections the large radius flap actually increases the chord of the airfoil, compared to the small radius flap; this could explain why the small radius flap is better below 45°. At higher deflections the advantage of the large radius flap in terms of delaying the separation seems to come into play; however the difference is probably not large enough to override the structural considerations and dictate the choice of the flap.

Another lesson learned is that low flap deflections barely reduce the drag; here, a linear decrease could have been expected. The drag then reaches a minimum around 75°, and then rises again; this is probably because the flow does not reattach on the flap any more (Fig. 28). This character of the drag curve, with a plateau at low deflections and a minimum at less than 90°, was observed in measurements performed on the aircraft itself; a more quantitative comparison will not be attempted since the flow is strongly three-dimensional.

A third lesson learned is that the leading edge modification reduces the drag appreciably without flap deflection, but loses almost all of its effect when the flap is deflected to 75° (Fig. 29). This was disappointing and no convincing explanation has been found. Other types of leading edge devices are now considered.

The flows exhibited a shedding of large vortices; the Strouhal numbers were

of the order of 0.15, which represents rather slow variations of the loads. Some configurations also gave rise to a significant force normal to the airflow. The clean airfoil had low pressure near the leading edge and a small forward force. With the flap deflected, rearward forces of the order of 0.5 were observed. These might have to be taken into account since the available control power is not very high in a hover condition.

As a whole this study demonstrated the flexibility of the method in treating many different shapes, and produced consistent and useful results even in a "first pass" with a set of parameters that was not optimal. It also gave clear indications about the structure of the flow, for instance the presence of a bubble at the hinge. In the near future a more extensive study will involve the actual XV15 airfoil, flaps and other possible devices, wall effects, and will be directly compared to wind tunnel tests.

5) Results from the program KPD3.

The program *KPD3* has been applied only to the circular cylinder. Attempts to treat airfoils with *KPD3* were unsuccessful; the algorithm seems to be unable to treat the trailing edge region properly. The most likely explanation is that the boundary layer assumptions are simply not applicable in a region where the wall has so much curvature.

The flow around a circular cylinder is the most classical bluff body problem and the best documented. It is also a good test of the ability of the program to predict the stucture of the boundary layer. Its dependence on the Reynolds number is known to be strong. The range of Reynolds numbers that were considered is from 10^4 to 3.16×10^7.

The value 10^4 is considered to be roughly the lower limit because at $Re = 10^4$ the thickness of the viscous region is about 0.035, which is not very small any more compared to the radius of cutvature, which is 1. As the Reynolds number decreases, use of the boundary layer assumptions become less justifiable.

The value of 3.16×10^7 was chosen as the upper limit; experiments have

been conducted up to about 0.8×10^7. Agreement between numerical and experimental results was found to be quite good in the upper range. Therefore it seems reasonable to consider extending the range of the numerical simulations by this factor of 4 in Reynolds number. Furthermore, the turbulence model has been validated at Reynolds numbers slightly higher than 10^7 [50].

Fig. 30 shows the global numerical and experimental results for the drag of a circular cylinder. Fig. 31 shows the Strouhal number and Fig. 32 the mean separation angle. Fig. 33 shows the pressure distribution at eight different Reynolds numbers. These cases include $Re = 10^4$, 10^5, 10^6 and 10^7, some extra cases in the critical region: $10^{5.5}$ (3.16×10^5), $10^{5.75}$ (5.62×10^5) and $10^{6.5}$ (3.16×10^6), and finally $10^{7.5}$ (3.16×10^7). Experimental results are also shown when available, [61],[62],[63],[64]. Fig. 34 shows the wall shear stress coefficient at the same Reynolds numbers. In order to make comparisons easier the scales are the same for all the pressure plots and for all the shear stress plots, except 10^4.

The Strouhal number was determined by counting the apparent number of periods in the lift signal during the simulation, using plots like the ones in Fig. 40. If the length of the sample is of the order of 5 periods, this way of determining the Strouhal number is accurate although somewhat arbitrary. Another way is to Fourier-analyze the signal; however one still has to "clip" the sample to simulate a periodic signal, which is also arbitrary. The Fourier analysis method is reliable only if long samples are available; experimental results often provide hundreds of cycles, but computations do not, for obvious cost reasons. As a result, the spectra contain subharmonics which would probably disappear if longer samples were available. In that sense, these harmonics are not meaningful, physically (see Fig. 41).

The mean separation angle was defined as the time-average of the angle at which the instantaneous shear stress is zero. This does not coincide with the angle at which the time-average of the shear stress is zero, because the shear stress is a strongly non-linear function in that region. Actually, in some cases the numerical results for the shear stress do not cross zero. This point will be developed later.

a) Subcritical regime.

This regime exists for Reynolds numbers under approximatively 10^5. The drag and Strouhal number are almost constant, and the evolution of the flow as the Reynolds number increases is weak (although the base pressure does change, and the lack of change in the drag is fortuitous [65]). Both boundary layers separate while still laminar and the separation point does not move significantly. The shear layers transition in the wake and transition occurs closer to the cylinder as the Reynolds number increases [65]. Apparently the "drag crisis" starts around $Re = 2 \times 10^5$ when the process is complete and transition occurs in the boundary layer just before or after separation, rather than in the wake. As a result, the boundary layers reattach and separate again, only farther downstream.

In the numerical results the boundary layers never transitioned for Reynolds numbers of less than 3.16×10^5. Thus the only evolution with Reynolds number is the thickness δ of the viscous region, which scales with $Re^{-1/2}$, from 0.035 at 10^4 to 0.015 around 10^5. The average separation angle is almost constant around 84°. The Strouhal number is between 0.205 and 0.195, which is considered a good prediction. The drag coefficient on the other hand slowly decreases from 1.42 at 10^4 to 1.03 at 10^5 and 0.88 at 3.16×10^5. This is not very good since, experimentally, the drag does not decrease in that range.

The pressure and shear stress distributions are correct qualitatively, but the quantitative differences which cause the inaccuracy in the predicted drag are obvious. At 10^5 the base pressure is -0.85, compared to -1.25 in the experiments. There is a significant pressure rise downstream of the separation point, which is not correct physically.

The average shear stress remains positive until the 110° point is reached, while the mean separation angle is 85°. The reason for this paradox is clear on Fig. 35b, which shows a still of the simulation at $Re = 10^5$. The instantaneous shear stress crosses zero, but has significant oscillations downstream of that point. As the flow oscillates the separation point moves back and forth and, in the average, the shear stress remains very close to zero instead of being frankly negative as in the experiments. This value

of the shear stress is small and results from the averaging of much larger numbers; therefore, although the situation seems inconsistent physically, the inaccuracy is quantitatively small.

Figure 35a shows the state of the inner flow at the same instant. It includes vorticity contours and the values of U_e, V_e and C_p (the inner region has been unwrapped from the cylinder and the scale expanded in the n direction).

Starting from the center of the figure (front of the cylinder) the two boundary layers of opposite sign divide and progress along the walls. The magnitude of U_e increases, the pressure decreases (favorable gradient) and V_e is negative (flow into the inner region). The wall shear stress (plotted in Fig. 35b) reaches a maximum. In the region near 90° the situation changes. The pressure gradient reverses and is now adverse; V_e becomes positive and the flow as a whole starts moving away from the wall, taking the vorticity with it. The shear stress rapidly falls to zero. Finally the vorticity leaves the inner region: U_e falls to zero and the shear layer is now in the outer region under the form of vortices. Downstream of the separation region the pressure fluctuates as the eddies contained in the outer region progress along the wall. However the time-averaged pressure is smooth and almost constant in the wake region.

The behavior that was just described is consistent with what is known of the flow. The comparison between Fig. 35b and Fig. 36 probably explains why the numerical results differ significantly between $Re = 10^4$ and 10^5. Fig. 36 shows that at 10^4 the separating shear layer is much thicker than at 10^5. As a result, its breakdown into circular vortices is slower and occurs farther away from the wall region. Being thicker the shear layer is also better represented by the limited number of vortices that are available. In contrast, at 10^5 it becomes difficult for the vortices to properly model the shear layer; the vortices are seen to linger near the wall while they separate more cleanly at 10^4. Very probably, the vortices cause too much mixing too soon, which creates a situation analogous to a turbulent boundary layer: a layer with strong mixing and a laminar sublayer. This situation is not incorrect physically, but the intense mixing is partly of numerical origin and may not be quantitatively correct.

To support this conjecture the flow at $Re = 10^5$ was simulated with two levels of numerical resolution. At the low level $N_v = 1000$, $N_w = 200$ and $\Delta t = 0.025$ were used. At the high level $N_v = 1600$, $N_w = 300$ and $\Delta t = 0.02$ were used. The results were significantly different: the C_d is 0.8 with low resolution and 1.03 with high resolution (the correct value is 1.2). We can conclude that the regime just below critical and the critical regime itself are the most difficult to simulate, because the shear layers are very thin, and the level of resolution used is not quite sufficient.

Other quantities have been computed to compare with experiments. The average velocity at the edge of the attached boundary layer is shown in Fig. 37. The agreement with the experiments reported in [65] is excellent. This is consistent with the good agreement shown by the pressure in the same region.

The value of the streamwise velocity on the centerline behind the cylinder is shown on Fig. 38 and compared with experiments from [62]. The agreement is good in the near wake but worsens in the far wake. The computations seem to introduce less dissipation than the experiments indicate. This was to be expected since the successive merging of the vortices in the wake tends to concentrate the vorticity whereas in the real flow the turbulent stresses spread it. It seems that the description of the wake is adequate up to approximatively 2 diameters of the back of the cylinder.

In conclusion, the subcritical regime, even though the boundary layers are laminar, appears to be more sensitive to transition in the near wake than was expected. A more accurate description of this region is probably needed. Another possible source of error is the three-dimensional character of the real flow; the consensus seems to be that large scale three-dimensional effects are not very strong in the subcritical regime, but small scale effects like streamwise vortices might play an important role in the transition region.

b) Critical regime.

This regime is the most complex and the most difficult to model. An intense experimental activity to measure and describe the flow accurately is

being carried out [61]. It has long been known that the drag coefficient takes very low values, of the order of 0.25, and that vortex shedding is disrupted [64]. It was also known that this "drag crisis" is associated with transition in the boundary layers [1]. Recent experiments have shown in addition that the decrease in the drag is probably not smooth but occurs in steps instead, and that the flow can be in states with a non-zero average lift [61]. Finally, the span-wise coherence of the real, three-dimensional flow is probably weakest in the critical regime [67].

The numerical method essentially failed to model the critical regime. This is not very surprising; the dramatic changes in the flow pattern are probably associated to reattachment of the boundary layers, or of only one of them. Reattachment is a delicate phenomenon to simulate; it requires a very accurate coupling if a zonal viscous-inviscid approach is used, and in any case a very fine transition and turbulence model [55]. The turbulence model used here was not designed with low Reynolds numbers in mind. Furthermore the transition model was designed for attached boundary layers. It is a "one-dimensional" model in which the whole boundary layer transitions at once. In contrast the results in [55] showed a very non-uniform turbulent energy across the layer.

As mentioned earlier transition was not predicted by the simulations for Reynolds numbers of 3.16×10^5 or less; for Reynolds numbers of 10^6 or more transition always occurred in both boundary layers. In that sense, the critical regime predicted by the computations is between these two values of Re. At $Re = 5.62 \times 10^5$ transition was intermittent; in Fig. 39 transition is seen to occur in only one of the boundary layers, as can be inferred by the sudden rise in the wall shear stress. However the simulation did not stay locked in either position (Fig. 39a and 39b). As a result the stable, asymmetric, lifting situation that was observed in experiments [61] was not obtained. The low drag values were not observed either.

The shear stress distribution at 5.62×10^5 reflects this intermittent transition: it has a plateau between 90° and 110°. The pressure distribution does not compare well with experiments, if only because it is essentially symmetrical.

One feature of the critical regime that is observed is the alteration of the vortex shedding pattern. Fig. 40 shows the drag and lift as function of time in the simulations at $Re = 10^4$, 3.16×10^5 and 3.16×10^6, and Fig.41 shows the spectra of the lift signals. The lift has a fairly well defined oscillation at 10^4 (although strong modulations are evident) and very regular oscillations at 3.16×10^6. At 3.16×10^5 the lift keeps the same sign for much longer periods of time and its behavior is very far from being harmonic. This impression is confirmed by the examination of the spectra: the peak is much broader at $Re = 3.16 \times 10^5$. This might be an indication that a small modification of the conditions could cause the simulation to find the stable asymmetric configuration. However, the samples were too short for the spectra to be entirely reliable. For instance, the peak at a Strouhal number of approximatively 0.08, at $Re = 10^5$, is thought to be spurious.

In conclusion, the correct simulation of the critical regime would probably require a more elaborate transition and turbulence model (the McDonald-Fish model used for the simulations in [55] was quite complex). However it seems that the method should first be improved until it simulates the subcritical regime very accurately before another attempt is made on the critical regime.

c) Supercritical regime.

This regime exists for Reynolds numbers above approximatively 4×10^6. Both boundary layers transition before separating and the flow is similar to the subcritical flow, except that separation occurs much later, which results in a narrower wake, a lower drag coefficient and a higher shedding frequency. The drag coefficient seems to be almost constant again in that range (although the experiments do not exceed 8×10^6, so that the "plateau" is quite narrow, covering only a factor 2 in Reynolds number).

The numerical results show slow variations of drag coefficient, Strouhal number and separation angle up to $Re = 3.16 \times 10^7$. Separation does occur later than in the subcritical regime, and the changes in wake pattern, shedding frequency and drag are all correct qualitatively. The pressure and friction distributions are almost Reynolds number-independent; the transition

point just moves upstream as the Reynolds number increases. The agreement with experiments for the pressure distribution is not excellent and the drag coefficient is lower than the experiments indicate. However there is significant scatter in the experimental results. The agreement in the shear stress is poor; the experiments do not show the steep rise associated with transition.

Numerically the simulations look "healthier" in that range than at lower Reynolds numbers. The separation is frank and the pressure distribution is smooth (Fig. 42 shows a still of the inner flow and Fig. 43 four stills of the outer flow. The non-dimensional time, based on velocity and radius, is indicated and the four stills cover approximatively one period of shedding). The reason is probably that the separating shear layer is thicker again, due to the Reynolds stresses in the inner region. Another sign is that at $Re = 10^6$ the simulations with low and high resolution agree very well (Figs. 33 and 34). This indicates that the resolution is sufficient.

In conclusion, the supercritical regime is easier to simulate from a numerical point of view, and the Baldwin-Lomax turbulence model seems to work well. The accuracy of the drag is not easy to assess since few experiments have been conducted in that range.

This concludes the description of the results obtained from the programs *KPD*1, *KPD*2 and *KPD*3. These results show that the method can reproduce many of the features of separated flows and is generally in fair to good agreement with experimental predictions. There is, however, room for improvement of the quantitative agreement, even in the framework of a two-dimensional method.

V) CONCLUSION.

In this work we have developed a new numerical method for two-dimensional separated flows. It incorporates an improved version of the Vortex Method, to treat the inviscid outer region, and widely used integral or finite difference methods, to treat the viscous inner region.

The numerical method uses a formulation of the equations in terms of the vorticity. This formulation has been shown to be mathematically equivalent to the conventional velocity/pressure formulation and includes cases with solids in non-uniform motion or rotation. It could also treat bodies in a uniform shear flow.

The flow is treated as inviscid away from the solid walls. This is motivated both by physical arguments (in the wake the large structures dominate and are not very sensitive to the viscosity) and by numerical arguments (it is not practical to model structures so fine that the viscosity influences them significantly).

It is shown that the Vortex Method can produce a significant numerical diffusion. This diffusion is present only if velocity gradients are present; this is an advantage, compared to Eulerian methods. However strong gradients are present in most viscous flows, especially near the wall. As a result, the numerical diffusion can have a dominant influence on the simulation.

In the first main version of the algorithm all the vorticity is represented by vortices, but their departure from the wall is delayed, if necessary, so that separation occurs at the proper location. This location is predicted by a boundary layer solution based on an integral method, which is run in parallel with the vortex solution.

In the second main version, a thin region near the wall is treated as viscous, with boundary layer assumptions. This inner region is treated by a Finite Difference method. The key assumption is not the neglect of the streamwise viscous term $\nu\partial^2\omega/\partial s^2$, since centered finite differences are used in the s direction anyhow, it is the neglect of the $\partial v/\partial n$ term in the vorticity (to avoid the solution of an elliptic equation for the velocity) and the coupling with the outer flow by means of a vortex sheet (to simplify the interaction between the two regions). The coupling algorithm is the most delicate element of the algorithm, and can create problems especially if the wall has tight curves. However it is an essential ingredient to make the method versatile and lessen its dependence on empiricism.

The new method conserves the traditional advantages of the Vortex Method for the treatment of the wake: it is grid free and accurate in modeling transport phenomena, it treats the far field in a simple and accurate way It requires much less memory space and possibly less computing effort than comparable Finite Difference methods. In addition the method can now treat arbitrary solid bodies or groups of bodies; conformal mappings are not involved.

Many choices have to be made when designing a practical method. Some of these choices could be made in a systematic way: for instance the design of the merging device. Some choices were made on a more intuitive basis, and therefore could probably be improved: for instance some details of the coupling procedure, and of the implementation of the turbulence model.

In its first version the new method treats bluff bodies reliably and is quite accurate. With separation properly controlled it simulates the stall of airfoils accurately; the comparison with experimental results is very encouraging. Some possible reasons for the remaining disagreement are the three-dimensional character of the real flow, which the method is unable to account for, and the interference with wind-tunnel walls. These wall effects are being added to the method.

The second version has been used for an extensive study of the flow past a circular cylinder at Reynolds numbers ranging from 10^4 to $3. \times 10^7$. The change in wake pattern and decrease in the drag coefficient as the boundary layers switch from laminar to turbulent are clearly observed, even though the pattern in the critical range itself is not correct. In this range, the three-dimensional effects are probably quite strong, and the modeling of transition and turbulence is the most delicate. In the supercritical regime (above $3. \times 10^6$) most of the flow characteristics are essentially constant and agree well with experimental results. In the subcritical regime (from 10^4 to $2. \times 10^5$) the shedding frequency is accurate and the drag is close to the correct value. However the drag coefficient tends to decrease steadily as the Reynolds number increases, which is not correct. This seems to be due to a "transition" of the separating shear layers which is not accurate, physically. This problem could be alleviated significantly, although not suppressed, by refining the discretization. However, a further increase in the computation cost might not be the best answer; it would be preferable to improve the algorithm in some way.

The prospects for the method developed here to be applied to practical cases, at least in its first version, are good. This version already has two active research applications: the Tilt-Rotor Wing study and the Vortex Flowmeter study. Both projects are continuing and a favorable interaction between the numerical work and the experimental work is building up. The second version will probably be used for further investigation of the circular cylinder flow.

For the future many extensions are possible, especially for the second method. They include:

- The introduction of a boundary layer model of higher order, with curvature terms, in the hope of treating bodies with tight curves.

- The refinement of the coupling algorithm in the spirit of the "strong interaction" theories for the separation region. A more mathematical approach could be taken; the improvement of the coupling might involve a more com-

plex model than the single vortex sheet placed at δ^*.

• In the long term the inner region could be of order 1 in thickness and be treated by a full Navier Stokes solver. This should remove all the problems associated with boundary layer assumptions. On the other hand it would probably demand a much more complex coupling procedure, as well as the solution of an elliptic equation in the inner region instead of Eqs. 29 and 30.

• The introduction of a more elaborate model for transition and for the turbulent stresses, in the hope of reproducing the well-known "drag crisis" of the circular cylinder and the recent findings about stable asymmetric states and discontinuous variation of the drag coefficient. However, such a model is not readily available, and in addition it might be that a two-dimensional model will never be able to account for the drag crisis. This question is open.

• It has been proposed to couple the Vortex Method to a finite difference method to treat compressible flows; the finite differences would handle the compressible effects efficiently on a fairly coarse mesh while the vortices would provide a fine description of the thin shear layers in the wake. The theoretical work to support these ideas has not been done yet.

• The extension to three dimensions, to treat wings or cars for instance. The validity of two-dimensional analysis for such cases is very limited, and a relatively crude three-dimensional method might be more useful than a "fine-tuned" two dimensional method. The power of a CRAY should be sufficient for simple cases, and the treatment of the solid should not be very different from the two-dimensional case. What is needed is a new three-dimensional Vortex discretization that would be reliable and more flexible than the present methods, with their connected filaments; such methods are currently being developed.

APPENDIX A

This appendix contains the description of the versions $KPD1$ and $KPD2$ of the program. They differ from $KPD3$ in the way they handle the wall region.

1) Program $KPD1$.

This version is a pure Vortex Method. It is mentioned mostly to clarify some issues about the Vortex Method and its ability to simulate some viscous flows while solving the inviscid equation.

In $KPD1$ even the boundary layer vorticity is represented by vortices that belong to the outer flow. The vorticity is immediately injected into the vortex region instead of transiting through an inner region as in $KPD3$; the new vortices follow the wall until they separate. The treatment of the wall region is thus very simple (Fig. 36). The rest of the algorithm (blob shape, time integration, merging, etc.) is the same as in the outer region of $KPD3$ (see Chapter IV).

Fig. 37 is a flow chart of $KPD1$; it is quite a simple program and a listing of it is included in Appendix B.

2) Program $KPD2$.

In this version, the premature separation of the vortices that often occurs with $KPD1$ (see Results), is artificially prevented on the basis of a boundary layer computation. The boundary layer is computed by an integral method.

The integral method is chosen for its simplicity and low cost. The solvers used are taken from Ref. [68]: Thwaites' method for the laminar part of the boundary layer and Head's method for the turbulent part. Both methods use a small number of integral quantities in the boundary layer as degrees of freedom and compute the boundary layer by marching in the stream direction, using empirical laws for the evolution of the integral quantities. Neither

method can be used downstream of the separation point. Both methods were designed for steady boundary layers; the unsteady effects on the boundary layer were neglected. Finer integral methods exist that include the unsteady effects; however these are probably weak compared to the interaction with the outer flow when massive separation occurs. Transition was modeled by the Schlichting-Granville criterion as in $KPD3$.

The coupling between the vortex flow and the boundary layer is done as follows: the vortex flow determines the instantaneous pressure distribution, and the boundary layer determines the separation points. Fig. 38 is a flow chart of $KPD2$.

At each time step, the pressure distribution is computed from the outer flow solution, using Equation 13. This pressure is then used as the forcing function to solve the boundary layer equation (this is upstream of separation and Bernoulli's theorem applies). The upper and lower boundary layers are computed, from the attachment point to their first separation point.

Experience with $KPD1$ shows that the vortices, if they are left free, always separate too soon. Therefore making them separate at the proper location is simply a matter of delaying their natural separation. To achieve this, all the vortices that were created upstream of the desired separation point are marked as "temporary" and after one time step are removed and replaced by a fresh layer of vortices. This prevents the vorticity layer from thickening prematurely. The vortices that are created downstream of the separation point are marked as "permanent" and treated as in $KPD1$; being in an adverse pressure gradient, near the separation point, they leave the vicinity of the wall quite promptly. Thus the vorticity layer is effectively released into the outer flow a short distance downstream of the separation that was predicted by the boundary layer solver.

```
      PROGRAM KPD1(INPUT,OUTPUT,TAPE1,TAPE8,TAPE9,
     > TAPE5=INPUT, TAPE6=OUTPUT)
C
C       2D VORTEX TRACING SIMULATION PROGRAM.
C
C       PROGRAM WRITTEN BY PHILIPPE R. SPALART
C
C     IN COLLABORATION WITH ANTHONY LEONARD.
C
C           SEE AIAA PAPER 81-1246.
C
C      NASA AMES RESEARCH CENTER, NOVEMBER 1982.
C
C  INCOMPRESSIBLE FLUID.  UNIFORM VELOCITY UINF
C  AT INFINITY, UINF IS COMPLEX (MAGNITUDE: ABSUIN,
C  INCIDENCE IN DEGREES: ALPHA).
C  THE PROGRAM COMPUTES THE UNSTEADY FLOW,
C  STARTING FROM POTENTIAL FLOW.
C  THE SOLID SHAPE IS ARBITRARY, GIVEN BY THE ROUTINE SOLID.
C  IT CAN BE MADE OF SEVERAL SEPARATE BODIES.
C  THIS VERSION OF THE PROGRAM IS SIMPLIFIED
C  AND MORE ROBUST (COMPARED TO THE ONE USED
C  FOR THE PAPER) AND DOES NOT HAVE ANY
C  REYNOLDS NUMBER EFFECTS.
C  THEREFORE IT IS SUITED FOR SHAPES THAT DO NOT
C  HAVE A STRONG REYNOLDS NUMBER DEPENDENCE,
C  ESPECIALLY SHAPES WITH SHARP CORNERS.
C  FOR OTHER SHAPES, CIRCLES FOR EXAMPLE,
C  THIS PROGRAM GENERALLY GIVES RESULTS
C  CLOSE TO LAMINAR RESULTS (RE=10**5 OR SO).
C
C  THIS MAIN PROGRAM CALLS
C  READPR, GMTRY, INIT, MERGE, BCBODY ,MOVE.
C  WRITING RESULTS ON TAPE8, THEN READING THEM
C  FROM TAPE9 ALLOWS RUNS TO CONTINUE EACH OTHER.
C
      COMPLEX Z,V,FORCE(2),HUB,Z0,WALL,ZCR,VM,UINF,AVFO
      REAL MOM(2),DPDS(215,1),CP(215,1),CPAV(215)
C
      COMMON/VORTEX/NVORT,Z(2000),V(2000),VM(2000),
     > GAMMA(2000)
      COMMON/SOLID/NBDIES,NWALL(2),WALL(215,1),
     > ZCR(215,1),HUB(2),Z0(2),THETA(215,1),NINC(2)
     > ,INC(15,2),XMAX(2)
```

```
      COMMON/SYSTEM/NDIM,A(215,215),X(215),IPVT(215)
C
C  READ AND PRINT THE PARAMETERS.
      CALL READPR(ISTART,NDES,NSTEP,N2,ABSUIN,ALPHA,
     > DELT,D0,GAMMA0)
C
C                SET UP THE GEOMETRY
C  DEFINE THE SOLID AND THE CREATION POINTS ON ITS SURFACE.
C  COMPUTE AND GAUSS ELIMINATE MATRIX OF INFLUENCE
C  COEFFICIENTS BETWEEN WALL POINTS, AND DO OTHER
C  THINGS THAT DEPEND ONLY ON THE SOLID.
      CALL GMTRY(SIGMA2,CHARD)
C
C  INITIALIZE THE TIME-DEPENDENT VARIABLES.
      CALL INIT(ISTART,NSTART,T,V0,ABSUIN,CHARD,D0)
C
      UINF=ABSUIN*CEXP(CMPLX(0.,ALPHA*ATAN(1.)/45.))
      AVFO=0
C
C  MAIN LOOP; ADVANCE FLOW TIME STEP BY TIME STEP.
      WRITE (6,104)
104   FORMAT(//,"  STEP BY STEP EVOLUTION OF THE FLOW:",//)
C
      NEND=NSTART+NSTEP-1
      DO1 N=NSTART,NEND
C
C  MERGE VORTICES TO KEEP THEIR NUMBER REASONABLE.
      CALL MERGE(D0,V0,NDES,N)
C
C  TREAT BOUNDARY CONDITION AT THE BODY BY AN
C  EXCHANGE OF VORTICITY.
      CALL BCBODY(FORCE,MOM,GAMMA0,N,T,UINF,
     > CHARD,NOLD,CP,DELT,SIGMA2)
      AVFO=AVFO+FORCE(1)
C
C  MOVE VORTICES.
1     CALL MOVE(UINF,SIGMA2,NOLD,DELT)
C
C  END OF MAIN LOOP.
C
C  STORE RESULTS IN CASE WE WANT A FOLLOW UP TO
C  THIS RUN.
      WRITE(8) N,T,NVORT,Z,GAMMA,VM,V0
C
```

```
C  OUTPUT AVERAGE LOADS.
      AVFO=AVFO/NSTEP
      WRITE (6,100)REAL(AVFO),AIMAG(AVFO)
100   FORMAT(/,24H AVERAGE DRAG AND LIFT: ,2F8.4)
C
C  END OF RUN.
      STOP
      END
      SUBROUTINE READPR(ISTART,NDES,NSTEP,N2,
     > ABSUIN,ALPHA,DELT,D0,GAMMA0)
C
C  READ PARAMETERS.
C  ISTART=1 IF RUN IS FROM TIME 0.
C  ISTART=0 IF IT IS A FOLLOW-UP.
C  NDES DESIRED NUMBER OF VORTICES.
C  THE PROGRAM WILL ROUGHLY MAINTAIN
C  THE NUMBER OF VORTICES AT NDES. NSTEP NUMBER OF STEPS.
C  ABSUIN MODULUS OF UINF, ALPHA INCIDENCE
C  IN DEGREES. DELT TIME STEP.
C  D0 PARAMETER IN MERGING DEVICE. D0 SMALLER PUTS MORE
C  VORTICES  NEAR THE SOLID AND LESS FAR FROM IT.
C  GAMMA0 ALLOWS THE USER TO DISTURB THE FLOW TO
C  MAKE IT REACH THE SHEDDING REGIME FASTER.
C  GAMMA0=0 LEAVES IT UNDISTURBED.
C  GAMMA0.NE.0 ARTIFICIALLY ADDS A CIRCULATION
C  GAMMA0 AT THE BEGINNING OF THE RUN.
C  (GAMMA0 IS IGNORED IF ISTART=0).
      READ (5,200)ISTART,NDES,NSTEP,N2
200   FORMAT(I1,3I5)
      READ (5,201)ABSUIN,ALPHA,DELT,D0,GAMMA0
201   FORMAT(5F8.5)
C
C  PRINT THE PARAMETERS.
      WRITE(6,100)
100   FORMAT(//," VORTEX SIMULATION OF BLUFF BODY FLOW",//)
      IF(ISTART.NE.0)WRITE(6,101)GAMMA0
101   FORMAT(" THIS RUN STARTED WITH CIRCULATION: ",E8.2)
      WRITE (6,102)NDES
102   FORMAT(/," APPROXIMATE NUMBER OF VORTICES: ",I6)
      WRITE (6,103)ABSUIN,ALPHA
103   FORMAT(/,
     >" FREESTREAM VELOCITY MAGNITUDE AND INCIDENCE ",2F7.4)
      WRITE (6,111)DELT
111   FORMAT(/,11H TIME STEP ,F7.4)
```

```
      WRITE (6,113)D0
113   FORMAT(/,
     >" CHARACTERISTIC DIMENSION IN MERGING DEVICE ",F7.4)
C
      RETURN
      END
      SUBROUTINE GMTRY(SIGMA2,CHARD,LA,KA,LB,KB)
C
C  OBTAIN SOLID SHAPE, COMPUTE SOLID-RELATED ARRAYS,
C  GAUSS ELIMINATE THE MATRIX, +MISCELLANEOUS.
C  NBDIES NUMBER OF BODIES.
C  NWALL NUMBER OF WALL POINTS ON EACH OF THEM.
C  WALL ARRAY OF WALL POINTS. ZCR ARRAY OF CREATION POINTS.
C  THETA POLAR ANGLE OF ZCR POINTS.
C  THETA IS USED TO FIND IF VORTICES ARE
C  INSIDE SOLID. Z0 USED ALONG WITH THETA.
C  HUB(L) IS THE HUB OF THE BODY "L". INC WILL
C  HELP FIND OVER WHICH WALL POINT THE VORTEX IS,
C  BY BISECTION. THE FIRST DIMENSION
C  OF INC MUST BE AT LEAST LOG2(NWALL).
C  A IS THE MATRIX OF INFLUENCE COEFFICIENTS FROM
C  CREATION POINTS TO WALL POINTS.
C
      INTEGER FIRST,NEXT(215)
      COMPLEX WALL,ZCR,Z0,HUB,INTSEC,ZZ
      COMMON/SOLID/NBDIES,NWALL(2),WALL(215,1),
     >ZCR(215,1),HUB(2),Z0(2),THETA(215,1),NINC(2),
     >INC(15,2),XMAX(2)
      COMMON/SYSTEM/NDIM,A(215,215),X(215),IPVT(215)
C
C  DEFINE SOLID.
      CALL SOLID(NBDIES,NWALL,WALL,CHARD)
C
C  COMPUTE ARCLENGTH.
      ARCL=0
      NDIM=0
      DO 9 L=1,NBDIES
        NDIM=NDIM+NWALL(L)
        DO 9 K=1,NWALL(L)
9         ARCL=ARCL+CABS(WALL(K,L)-WALL(1+MOD(K,NWALL(L)),L))
C
C  COMPUTE CORE RADIUS.
      R0=ARCL/NDIM/2.
```

```
      SIGMA=R0/3
      WRITE(6,104)SIGMA
104   FORMAT(/," THE CORE RADIUS WAS CHOSEN AS: ",F8.4,/)
      SIGMA2=SIGMA**2
C
C  DEFINE CREATION POINTS.
      DO6 L=1,NBDIES
        DO7 K=1,NWALL(L)
          ZZ=WALL(1+MOD(K+NWALL(L)-2,NWALL(L)),L)
     >     -WALL(1+MOD(K,NWALL(L)),L)
7         ZCR(K,L)=WALL(K,L)+CMPLX(0.,R0/CABS(ZZ))*ZZ
C  CHECK THAT WALL AND CREATION POINTS ARE NOT
C  CROSSED DUE TO TOO SHARP A CONCAVE KINK OR AN
C  ERROR IN DEFINING THE BODY.
        XMAX(L)=REAL(ZCR(1,L))
        DO6 K=1,NWALL(L)
          XMAX(L)=AMAX1(XMAX(L),REAL(ZCR(K,L)))
          KP=1+MOD(K,NWALL(L))
          IF(REAL((ZCR(KP,L)-ZCR(K,L))*
     >     CONJG(WALL(KP,L)-WALL(K,L))).GT.0.)GO TO 6
          WRITE (6,102)L,K
102   FORMAT(
     >" ON BODY NUMBER ",I3," YOU HAVE TOO SHARP A",
     >" KINK NEAR POINT ",I4)
          STOP
6         CONTINUE
C
C                    COMPUTE MATRIX.
C  EXCEPT FOR THE LAST ONE ON EACH BODY, EACH LINE
C  WILL REPRESENT: PSI(WALL(NWALL))-PSI(WALL(I))
C  WHERE PSI CORRESPONDS TO THE NEW VORTICES TO BE
C  CREATED AND WILL HAVE TO CANCEL THE PSI DUE TO
C  THE FREESTREAM + OLD VORTICES.
C  THE LAST LINE IS ALL 0, EXCEPT ON COLUMNS
C  BELONGING TO THE SAME BODY, THEN IT IS 1.
C  IT WILL CONTROL THE TOTAL STRENGTH OF ALL THE NEW
C  VORTICES EMANATING FROM THAT BODY, AS WELL AS
C  PREVENTING THE MATRIX A FROM BEING SINGULAR.
      PI=4*ATAN(1.)
      I0=0
      DO2 L1=1,NBDIES
        J0=0
        DO4 L2=1,NBDIES
          KRON=0
```

```
      IF(L1.EQ.L2)KRON=1
      DO3 J=1,NWALL(L2)
       A(I0+NWALL(L1),J0+J)=KRON
       DO3 I=1,NWALL(L1)-1
3       A(I0+I,J0+J)=-.25/PI*ALOG(
     >      (SIGMA2+CABS(WALL(I+1,L1)-ZCR(J,L2))**2)
     >      /(SIGMA2+CABS(WALL(I,L1)-ZCR(J,L2))**2))
4      J0=J0+NWALL(L2)
2     I0=I0+NWALL(L1)
C
C  GAUSS ELIMINATION.
C  SGECO IS THE LINPACK ROUTINE.
C  X IS USED AS A DUMMY HERE.
     CALL SGECO(A,215,NDIM,IPVT,COND,X)
     COND=1/COND
     WRITE (6,103)COND
103   FORMAT(/," CONDITION NUMBER ",E8.2)
C
C  MISCELLANEOUS; BISECTION DEVICE.
     DO1 L=1,NBDIES
C  FIND A HUB FOR THE RAYS OF THE BISECTION DEVICE.
       HUB(L)=0
       NPTS=0
       FIRST=0
       DO 20 I=1,NWALL(L)
        IP=1+MOD(I,NWALL(L))
        IM=1+MOD(I+NWALL(L)-2,NWALL(L))
        IF(1.+AIMAG((ZCR(IP,L)-ZCR(I,L))*
     >    CONJG(ZCR(IM,L)-ZCR(I,L))).EQ.1.)GO TO 20
       NEXT(I)=FIRST
       FIRST=I
20      CONTINUE
C
      I=FIRST
21     IF(I.EQ.0)GO TO 22
       IP=1+MOD(I,NWALL(L))
       K=NEXT(I)
24      IF(K.EQ.0)GO TO 23
        KP=1+MOD(K,NWALL(L))
        AA=AIMAG( (ZCR(IP,L)-ZCR(I,L)) *
     >     CONJG (ZCR(KP,L)-ZCR(K,L)) )
        IF(AA.EQ.0.)GO TO 10
        INTSEC=ZCR(I,L)+AIMAG((ZCR(K,L)-ZCR(I,L))*
     >     CONJG(ZCR(KP,L)-ZCR(K,L)))*
```

```
     >      (ZCR(IP,L)-ZCR(I,L))/AA
            DO 11 J=1,NWALL(L)
11           IF(1.+AIMAG ( (INTSEC-ZCR(J,L)) *
     >       CONJG(ZCR(1+MOD(J,NWALL(L)),L)-ZCR(J,L))
     >       ) .LT. 1.)GO TO 10
            HUB(L)=HUB(L)+INTSEC
            NPTS=NPTS+1
10           K=NEXT(K)
            GO TO 24
23          I=NEXT(I)
           GO TO 21
22         IF(NPTS.GE.1)GO TO 12
          WRITE(6,100)L
100       FORMAT(
     >" THERE IS A PROBLEM WITH BODY NUMBER ",I4,/,
     >" ITS SHAPE IS PROBABLY TOO COMPLEX AND THE "
     >,PROGRAM WAS UNABLE TO DEFINE A HUB. ",
     >"OR ELSE YOUR POINTS ARE NOT COUNTERCLOCKWISE")
          STOP
12         HUB(L)=HUB(L)/NPTS
         WRITE (6,101)L,REAL(HUB(L)),AIMAG(HUB(L))
101      FORMAT(/," THE HUB FOR BODY ",I4," IS AT: ",2F8.3)
C  NOW COMPUTE THE POLAR ANGLE OF ALL THE POINTS.
          Z0(L)=CONJG(ZCR(NWALL(L),L)-HUB(L))
          DO8 I=1,NWALL(L)
8           THETA(I,L)=
     >     AIMAG(CLOG(-Z0(L)*(ZCR(I,L)-HUB(L))))
C
C  NOW COMPUTE THE INCREMENTS FOR THE BISECTION.
          INC(1,L)=NWALL(L)/2
          K=NWALL(L)-INC(1,L)
          DO5 II=2,15
           IF(K.EQ.1)GO TO 1
           INC(II,L)=MAX0(1,INC(II-1,L)/2)
5           K=K-INC(II,L)
1          NINC(L)=II-1
C
         RETURN
         END
         SUBROUTINE SOLID(NBDIES,NWALL,WALL,CHARD)
C
C  ALLOWS THE USER TO INPUT THE SHAPE OF THE SOLID.
C  IT CAN BE 1 BODY (NBDIES=1), OR SEVERAL.
C  NWALL(L) NUMBER OF POINTS ON SOLID L (L=1,NBDIES).
```

```
C  WALL(K,L) COMPLEX POSITIONS OF THESE POINTS
C  (K=1,NWALL(L)).
C  THEY MUST RUN COUNTER-CLOCKWISE!!
C  CHARD IS THE CHARACTERISTIC DIMENSION
C
      COMPLEX WALL(215,1)
      INTEGER NWALL(2)
C
      NBDIES=1
C  FIRST BODY.
      NWALL(1)=200
      DO 1 K=1,100
      Y=-1+.02*K
      WALL(K,1)=CMPLX(.2*(1-Y*Y),Y)
1     WALL(K+100,1)=CMPLX(0.,-Y)
      CHARD=2
C
      WRITE(6,100)
100   FORMAT(/," THE SOLID IS A CAMBERED FLAT PLATE")
C
      RETURN
      END
      SUBROUTINE INIT(ISTART,NSTART,T,V0,ABSUIN,
     > CHARD,D0)
C
C  INITIALIZE TIME-DEPENDENT VARIABLES.
C
      COMPLEX Z,V,VM
      COMMON/VORTEX/NVORT,Z(2000),V(2000),VM(2000)
     > ,GAMMA(2000)
      IF(ISTART.EQ.0)GO TO 8
C  CASE OF A START FROM POTENTIAL FLOW.
C  START AT STEP 1 WITH T=0 AND NO VORTICES.
      NSTART=1
      T=0
      NVORT=0
C  GIVE PHONY VALUES TO THE VORTEX POSITIONS AND
C  CIRCULATIONS.
      DO7 I=1,2000
        Z(I)=10.
        VM(I)=0.
7       GAMMA(I)=0.
C  A TENTATIVE VALUE FOR V0, WHICH WILL BE
C  ADJUSTED LATER.
```

```
      V0=1.E-5*ABSUIN*(CHARD/D0)**3
      RETURN
C
C  CASE OF A START FROM A PREVIOUS RUN.
8     READ (9) NSTART,T,NVORT,Z,GAMMA,VM,V0
C
      RETURN
      END
      SUBROUTINE MERGE(D0,V0,NDES,N)
C
C  THIS ROUTINE MERGES PAIRS OF VORTICES INTO ONE
C  WHENEVER THE PENALTY FOR DOING SO
C  IS UNDER A TOLERANCE (V0).
C  ALSO ADJUSTS V0 TO ACHIEVE DESIRED
C  NUMBER OF VORTICES.
C
      REAL B(2000),MERTST(2000)
      COMPLEX HUB,Z,ZI,V,ZCR,Z0,WALL,VM
      COMMON/VORTEX/NVORT,Z(2000),V(2000),VM(2000)
     > ,GAMMA(2000)
      COMMON/SOLID/NBDIES,NWALL(2),WALL(215,1),
     > ZCR(215,1),HUB(2),Z0(2),THETA(215,1),NINC(2)
     > ,INC(15,2),XMAX(2)
C
C  RETURN IF THERE ARE NO VORTICES YET.
      IF(NVORT.LE.5)RETURN
C
C  FEEDBACK NUMBER OF VORTICES TO THE TOLERANCE.
      V0=V0*EXP(AMAX1(-.1,.002*(NVORT-NDES)))
      SQV0=SQRT(V0)
C
C  PREPARE VORTICES FOR MERGING;
C  FIND THEIR DISTANCE TO THE WALL.
      DO 7 I=1,NVORT
        D=1.E+30
        DO1 L=1,NBDIES
C  FIND THE PROJECTION ON EACH WALL BY BISECTION
C  OF THE POLAR ANGLE.
          TTA=AIMAG(CLOG(-Z0(L)*(Z(I)-HUB(L))))
          K=NWALL(L)
          DO5 II=1,NINC(L)
5           IF(TTA.LT.THETA(K-INC(II,L),L))
     >        K=K-INC(II,L)
          KM=1+MOD(K+NWALL(L)-2,NWALL(L))
C  D IS THE DISTANCE TO THE WALL. B(I) IS STORED
```

```
C  TO REDUCE THE WORK IN THE INNER LOOP
C  (LABEL 4, SEE FURTHER DOWN) TO A MINIMUM.
1       D=AMIN1(D,AIMAG(CONJG(Z(I)-ZCR(K,L))*
     >    (ZCR(K,L)-ZCR(KM,L)))/CABS(ZCR(K,L)-ZCR(KM,L)))
        B(I)=ABS(GAMMA(I))*(ABS(D+D0))**(-1.5)/SQV0
7       CONTINUE
C
C  TAKE THE VORTICES ONE BY ONE, STARTING WITH
C  THE LAST ONE.
      NVORT0=NVORT
      DO 3 I=NVORT0,2,-1
C
C  TEST ALL THE OTHER VORTICES AGAINST IT.
        DO 4 J=1,I-1
4         MERTST(J)=(REAL(Z(J)-Z(I))**2+AIMAG(Z(J)-Z(I))**2)*
     >     B(J)*B(I)-ABS(GAMMA(J)+GAMMA(I))

C  IS THE MERGING TOLERANCE SATISFIED?
C  (ISMIN IS A CRAY FUNCTION USED HERE TO FIND THE
C  MINIMUM OF "MERTST"
C  FROM 1 TO IM WITH INCREMENT 1.)
        J=ISMIN(I-1,MERTST,1)
C  IF NOT SO GO TO NEXT INDEX I.
        IF(MERTST(J).GT.0.)GO TO 3
C  IF SO, PROCEED WITH THE MERGING:
C
C  PUT THE NEW VORTEX IN J'S PLACE.
        Z(J)=  (Z(I)*GAMMA(I)+ Z(J)*GAMMA(J))/
     >  (GAMMA(I)+GAMMA(J))
        VM(J)=(VM(I)*GAMMA(I)+VM(J)*GAMMA(J))/
     >  (GAMMA(I)+GAMMA(J))
        GAMMA(J)=GAMMA(I)+GAMMA(J)
        B(J)=B(I)*ABS(GAMMA(J)/GAMMA(I))
C
C  PUT LAST VORTEX (INDEX: NVORT) IN Ith PLACE.
        Z(I)=Z(NVORT)
        VM(I)=VM(NVORT)
        GAMMA(I)=GAMMA(NVORT)
        B(I)=B(NVORT)
        NVORT=NVORT-1
C
C  TAKE NEXT VORTEX ON THE LIST.
3       CONTINUE
C
      END
```

```
      SUBROUTINE BCBODY(FORCE,MOM,GAMMA0,N,T,UINF,
     > CHARD,NOLD,CP,DELT,SIGMA2)
      COMPLEX FORCE(2),UINF
      REAL MOM(2),DPDS(215,1),CP(215,1)
C
C  THE BODY ABSORBS VORTICES AND EMITS NEW VORTICES
C  TO ACCOUNT FOR IT, PLUS SOME NEW VORTICITY WHICH
C  WILL ALLOW THE VELOCITY FIELD
C  TO SATISFY THE BOUNDARY CONDITION U=V=0.
C
C  DETECT AND ABSORB VORTICES THAT CRASHED INTO WALL.
C  START COMPUTING PRESSURE AND FORCE.
      CALL ABSORB(DPDS,FORCE,MOM,GAMMA0,N)
C
C  EMIT NEW VORTICES TO SATISFY BOUNDARY CONDITION,
C  AND FINISH COMPUTING PRESSURE, FORCE, ETC.
      CALL EMIT(N,T,UINF,CHARD,NOLD,FORCE,MOM,DPDS,
     > CP,DELT,SIGMA2)
C
      RETURN
      END
      SUBROUTINE ABSORB(DPDS,FORCE,MOM,GAMMA0,N)
      REAL DPDS(215,1),MOM(2)
      COMPLEX FORCE(2),Z,V,VM,WALL,ZCR,HUB,Z0
      COMMON/VORTEX/NVORT,Z(2000),V(2000),VM(2000)
     > ,GAMMA(2000)
      COMMON/SOLID/NBDIES,NWALL(2),WALL(215,1),
     >ZCR(215,1),HUB(2),Z0(2),THETA(215,1),NINC(2)
     >,INC(15,2),XMAX(2)
      COMMON/SYSTEM/NDIM,A(215,215),X(215),IPVT(215)
C
C  KILL THE VORTICES THAT ARE TOO CLOSE TO A WALL.
C  (LOST VORTICITY WILL BE REINTRODUCED IMMEDIATELY.)
C
C  TAKE THE SEPARATE BODIES ONE BY ONE.
      I0=0
      DO9 L=1,NBDIES
C  GET READY TO COMPUTE THE FORCE, MOMENT, AND WALL
C  PRESSURE ON BODY "L".
        FORCE(L)=0
        MOM(L)=0
        DO 3 K=1,NWALL(L)
3         DPDS(K,L)=0
        I0=I0+NWALL(L)
C
```

```
C  X(I0) IN THE SECOND MEMBER WILL BE THE CIRCULATION
C  DEFECT TO BE FILLED UP BY THE NEW VORTICES
C  EMANATING FROM THIS BODY.
      X(I0)=0
C  IF THIS IS THE FIRST STEP, INTRODUCE THE DESIRED
C  CIRCULATION AROUND THE FIRST BODY.
      IF(N.EQ.1.AND.L.EQ.1)X(I0)=GAMMA0
C
C  LOOK AT THE VORTICES ONE BY ONE.
      I=1
6       IF(I.GT.NVORT)GO TO 9
        IF(REAL(Z(I)).GT.XMAX(L))GO TO 5
C  OVER WHICH WALL SEGMENT IS THE VORTEX?
C  FIND IT BY BISECTION OF THE POLAR ANGLE.
        TTA=AIMAG(CLOG(-Z0(L)*(Z(I)-HUB(L))))
        K=NWALL(L)
        DO 7 II=1,NINC(L)
7         IF(TTA.LT.THETA(K-INC(II,L),L))
     >      K=K-INC(II,L)
C  MAKE SURE OF WHERE THE PROJECTION OF THE VORTEX
C  IS ON THE WALL.
2       KM=1+MOD(K-2+NWALL(L),NWALL(L))
        IF(REAL((Z(I)-ZCR(KM,L))*CONJG(ZCR(K,L)-
     >    ZCR(1+MOD(K+NWALL(L)-3,NWALL(L)),L))).GE.0.)GO TO 1
        K=KM
        GO TO 2
1       KP=1+MOD(K,NWALL(L))
        IF(REAL((Z(I)-ZCR(K,L))*CONJG(ZCR(KP,L)
     >    -ZCR(KM,L))).LE.0.)GO TO 4
        KM=K
        K=KP
        GO TO 1
C
C  IS THE VORTEX INSIDE THE SOLID?
4       KM=1+MOD(K-2+NWALL(L),NWALL(L))
        D=AIMAG(CONJG(Z(I)-ZCR(K,L))*(ZCR(K,L)-ZCR(KM,L)))
C
C  IF IT IS NOT, LEAVE IT ALONE.
        IF(D.GT.0.)GO TO 5
C  IF IT IS, KILL IT (FIRST RECORD THE LOSS OF
C  CIRCULATION, AND LINEAR AND ANGULAR MOMENTUM)
        X(I0)=X(I0)+GAMMA(I)
        FORCE(L)=FORCE(L)-GAMMA(I)*Z(I)
```

```
      MOM(L)=MOM(L)-GAMMA(I)*(REAL(Z(I)-HUB(L))
     >    **2+AIMAG(Z(I)-HUB(L))**2)
C  ALSO RECORD VORTICITY ABSORPTION FOR THE PRESSURE
C  GRADIENT. LINEAR DEPOSITION.
      D=REAL((Z(I)-ZCR(KM,L))*
     >   CONJG(ZCR(K,L)-ZCR(KM,L)))
      DM=REAL((ZCR(K,L)-Z(I))*
     >   CONJG(ZCR(K,L)-ZCR(KM,L)))
      DPDS(K,L)=DPDS(K,L)+GAMMA(I)*D/(D+DM)
      DPDS(KM,L)=DPDS(KM,L)+GAMMA(I)*DM/(D+DM)
C
C  NOW PUT LAST VORTEX IN THE Ith PLACE IN THE ARRAY.
      Z(I)=Z(NVORT)
      GAMMA(I)=GAMMA(NVORT)
      VM(I)=VM(NVORT)
      NVORT=NVORT-1
      GO TO 6
C
C  GO TO NEXT VORTEX.
5     I=I+1
      GO TO 6
9     CONTINUE
C
      RETURN
      END
      SUBROUTINE EMIT(N,T,UINF,CHARD,NOLD,FORCE,
     > MOM,DPDS,CP,DELT,SIGMA2)
      COMPLEX Z,V,VM,WALL,ZCR,HUB,Z0,FORCE(2),UINF
      REAL MOM(2),DPDS(215,1),CP(215,1),PSI(215,1)
     > ,PS(2000)
      COMMON/VORTEX/NVORT,Z(2000),V(2000),VM(2000)
     > ,GAMMA(2000)
      COMMON/SOLID/NBDIES,NWALL(2),WALL(215,1),
     > ZCR(215,1),HUB(2),Z0(2),THETA(215,1),NINC(2)
     > ,INC(15,2),XMAX(2)
      COMMON/SYSTEM/NDIM,A(215,215),X(215),IPVT(215)
C
      PI=4*ATAN(1.)
      I0=0
      DO5 L   1,NBDIES
C  STREAM FUNCTION AT THE WALL; CONTRIBUTION OF...
        DO 16 K=1,NWALL(L)
C  ...THE FREESTREAM...
C  ...AND OF THE OLD VORTICES.
        DO4 I=1,NVORT
```

```
4         PS(I)=GAMMA(I)*
     >     ALOG(REAL(Z(I)-WALL(K,L))**2+
     >     AIMAG(Z(I)-WALL(K,L))**2+SIGMA2)
16      PSI(K,L)=AIMAG(WALL(K,L)*CONJG(UINF))
     >  -SSUM(NVORT,PS,1)*.25/PI
C
C  THE NEW VORTICES MUST CANCEL THE STREAM FUNCTION
C  AT THE WALL.
C  THIS GIVES A LINEAR SYSTEM FOR THEIR CIRCULATIONS.
C  COMPUTE ITS SECOND MEMBER.
      DO18 K=1,NWALL(L)-1
18      X(I0+K)=-PSI(K,L)-PSI(K+1,L)
5     I0=I0+NWALL(L)
C
C  SOLVE SYSTEM.
C  SGESL IS THE LINPACK ROUTINE.
C  X IS THE RIGHT HAND SIDE, AND
C  THE SOLUTION IS WRITTEN OVER IT.
     CALL SGESL(A,215,NBODY,IPVT,X,0)
C
C  CREATE NEW VORTICES.
C  REMEMBER WHICH VORTICES ARE OLD ENOUGH TO USE
C  ADAMS-BASHFORTH.
     NOLD=NVORT
     I0=0
     DO17 L=1,NBDIES
      DO 3 K=1,NWALL(L)
C  PUT THE NEW VORTEX AT THE END OF THE ARRAY.
        NVORT=NVORT+1
        Z(NVORT)=ZCR(K,L)
        GAMMA(NVORT)=X(I0+K)
C  RECORD THE GAIN OF LINEAR AND ANGULAR MOMENTUM.
        FORCE(L)=FORCE(L)+GAMMA(NVORT)*Z(NVORT)
        MOM(L)=MOM(L)+GAMMA(NVORT)*(REAL(Z(NVORT)
     >   -HUB(L))**2+AIMAG(Z(NVORT)-HUB(L))**2)
C  ALSO RECORD VORTICITY CREATION FOR THE PRESSURE
C  GRADIENT.
3       DPDS(K,L)=DPDS(K,L)-X(I0+K)
C
C  FILTER PRESSURE GRADIENT AND INTEGRATE IT TO GET
C  PRESSURE.
      CP(1,L)=0
      DO14 K=2,NWALL(L)
```

```
14      CP(K,L)=CP(K-1,L)+(3*(DPDS(K,L)+DPDS(K-1,L))
     >   +DPDS(1+MOD(K+NWALL(L)-3,NWALL(L)),L)+
     >   DPDS(1+MOD(K,NWALL(L)),L))/
     >   (4*DELT*CABS(UINF)**2)
C     )RMALIZE PRESSURE.
      CPMAX=CP(ISMAX(NWALL(L),CP(1,L),1),L)
      DO22 K=1,NWALL(L)
22      CP(K,L)=CP(K,L)-CPMAX
C
C  FINISH COMPUTING FORCE AND MOMENT AND
C  NON-DIMENSIONALIZE THEM.
      FORCE(L)=FORCE(L)*
     >  CMPLX(0.,2./(DELT*CHARD*CABS(UINF)**2))
      MOM(L)=MOM(L)*2/(DELT*(CHARD*CABS(UINF))**2)
17     I0=I0+NW
C
C  PRINT INSTANTANEOUS DATA.
     T=T+DELT
     IF(MOD(N,5).EQ.0)
     > WRITE (6,105)N,T,NVORT,REAL(FORCE(1)),
     > AIMAG(FORCE(1)),MOM(1)
105   FORMAT(/,6H STEP ,I4,6H TIME ,F8.4,7H NVORT ,
    >I4,3H CD,F7.4,3H CL,
    >F7.4,4H MOM,F7.4)
     IF(MOD(N,5).EQ.0.AND.NBDIES.GE.2)
     > WRITE(6,106)REAL(FORCE(2)),AIMAG(FORCE(2))
     > ,MOM(2)
106   FORMAT("   CD, CL, AND MOM ON SECOND BODY:"
    >,2F10.4,F11.4)
     RETURN
     END
     SUBROUTINE MOVE(UINF,SIGMA2,NOLD,DELT)
C
C          MOTION OF THE VORTICES.
C  OLD VORTICES USE ADAMS-BASHFORTH-2,
C  NEW ONES USE EULER EXPLICIT.
C
     COMPLEX Z,V,VM,UINF
     COMMON/VORTEX/NVORT,Z(2000),V(2000),VM(2000)
     > ,GAMMA(2000)
C
C  COMPUTE VELOCITIES OF THE VORTICES.
     CALL VELOCT(UINF,SIGMA2)
C
C  MOVE VORTICES.
C  ADAMS-BASHFORTH-2 FOR THE OLD VORTICES.
```

```
      DO13 I=1,NOLD
        Z(I)=Z(I)+DELT*(1.5*V(I)-.5*VM(I))
13      VM(I)=V(I)
C  EULER EXPLICIT FOR THE NEW VORTICES.
      DO 2 I=NOLD+1,NVORT
        Z(I)=Z(I)+DELT*V(I)
2       VM(I)=V(I)
C
      RETURN
      END
      SUBROUTINE VELOCT(UINF,RC2)
C
C  BIOT SAVART INTERACTION OF VORTICES, POSITIONS Z(I),
C   CIRCULATION GAMMA(I). VELOCITY AT INFINITY=UINF.
C     RC IS THE CHARACTERISTIC RADIUS IN THE CUT-OFF:
C          U(R) IS= (GAMMA/2PI)*R/(R**2+RC**2)
C
      REAL VX(2000),VY(2000)
      COMPLEX Z,V,DELZ,VM,UINF
      COMMON/VORTEX/NVORT,Z(2000),V(2000),VM(2000)
     > ,GAMMA(2000)
C
C  FREESTREAM VELOCITY.
      PI=4*ATAN(1.)
      DO 3 I=1,NVORT
3       V(I)=CMPLX(0.,-2*PI)*UINF
C
C  COMPUTE INTERACTIONS.
C  LOOP ON FIRST VORTEX.
      DO1 I=2,NVORT
C  LOOP ON SECOND VORTEX.
        DO4 J=1,I-1
          DELZ=Z(I)-Z(J)
          DELZ=DELZ/(RC2+REAL(DELZ)**2+AIMAG(DELZ)**2)
          VX(J)=REAL(DELZ)*GAMMA(J)
          VY(J)=AIMAG(DELZ)*GAMMA(J)
4         V(J)=V(J)-GAMMA(I)*DELZ
C  (THE CRAY FUNCTION SSUM IS USED TO SUM UP A VECTOR
C  LIKE VX, FROM 1 TO I-1 WITH INCREMENT 1.)
C  (NOTE THAT THE CSUM FUNCTION WOULD HAVE BEEN THE
C  LOGICAL CHOICE HERE; BUT IT SEEMS TO HAVE A BUG...)
1       V(I)=V(I)+CMPLX(SSUM(I-1,VX,1),SSUM(I-1,VY,1))
C
C  MULTIPLY BY I/2PI.
      DO2 I=1,NVORT
2       V(I)=V(I)*CMPLX(0.,.5/PI)
C
      RETURN
      END
```

FIGURES.

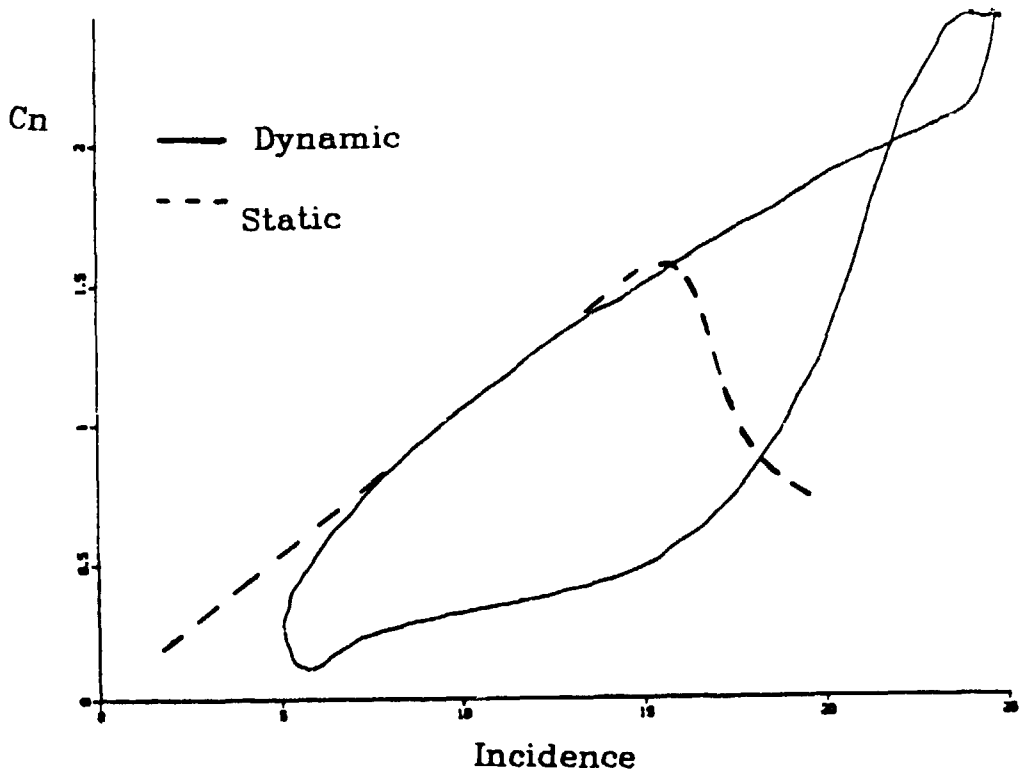

Fig. 1 Normal Force Coefficient on an Airfoil during Dynamic Stall.

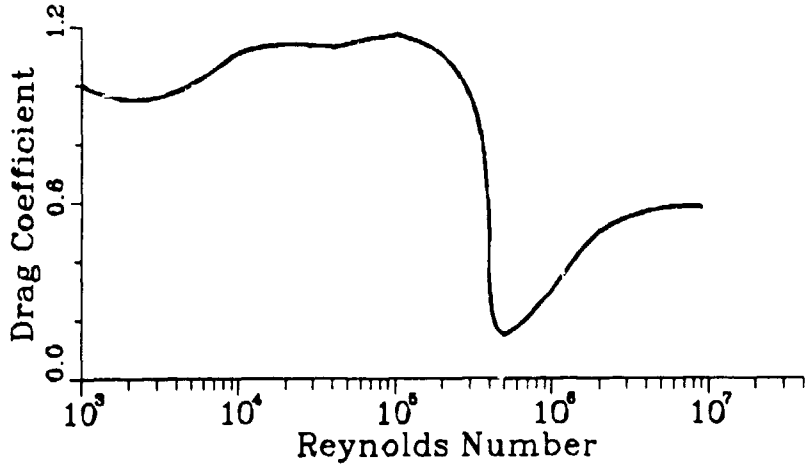

Fig. 2. Drag Coefficient of a Circular cylinder

——Average of Experiments [1],[61],[62],[63],[64]

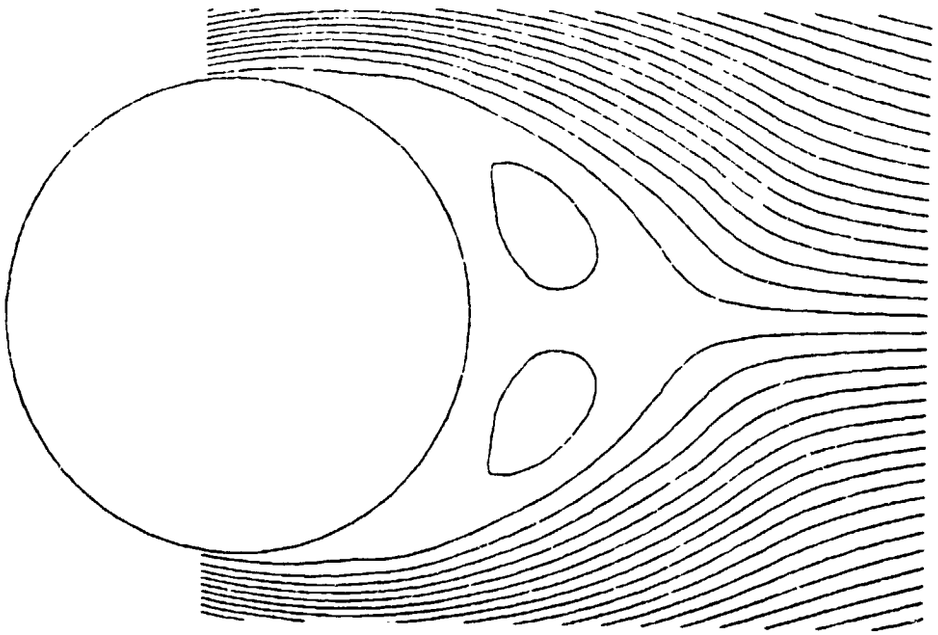

Fig. 3a. Flow Pattern at Re = 10^4

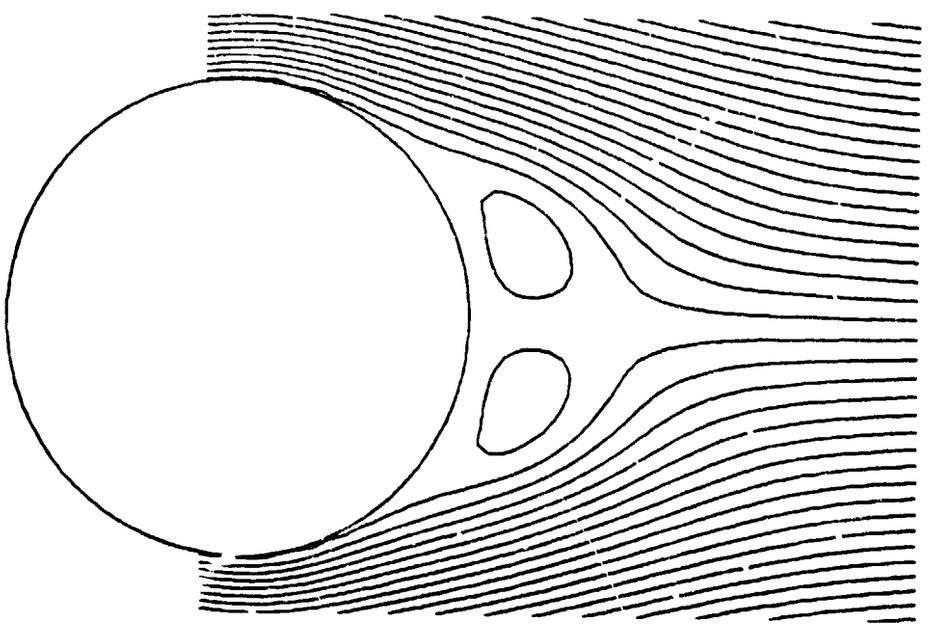

Fig. 3b. Flow Pattern at Re = 10^6

Fig 4a.

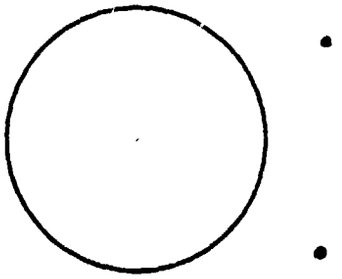

Fig 4b.

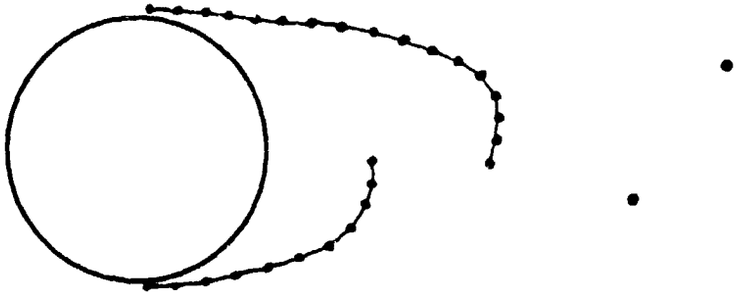

Fig. 4c.

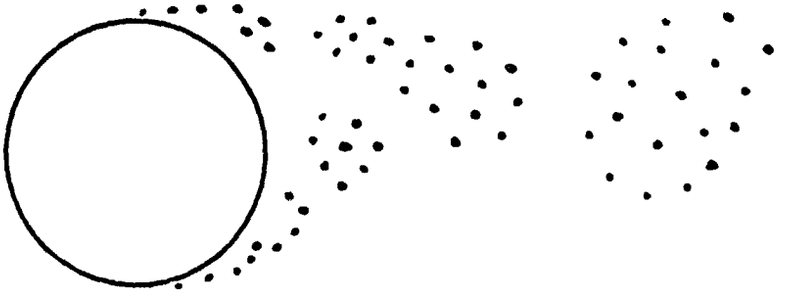

Fig 4d.

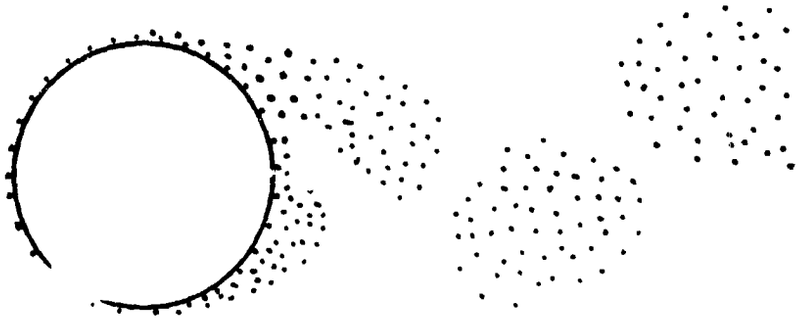

Fig 4. Schematic of successive versions of the Vortex Method

Inviscid Region. ($\frac{D\omega}{Dt} = 0$)

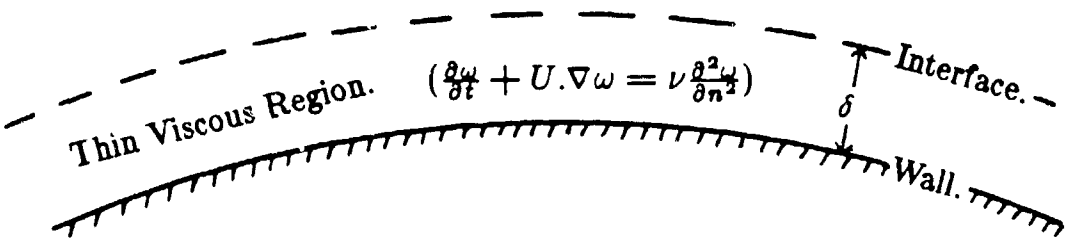

Fig. 5. Division of the flow field into an inviscid and a viscous domain

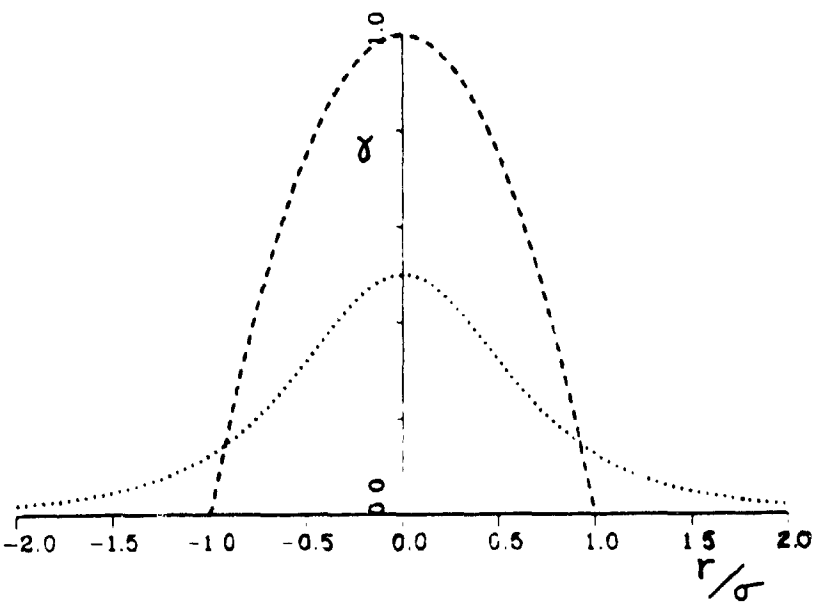

Fig. 6a. Core Vorticity.– – Core 1, ··· Core 2

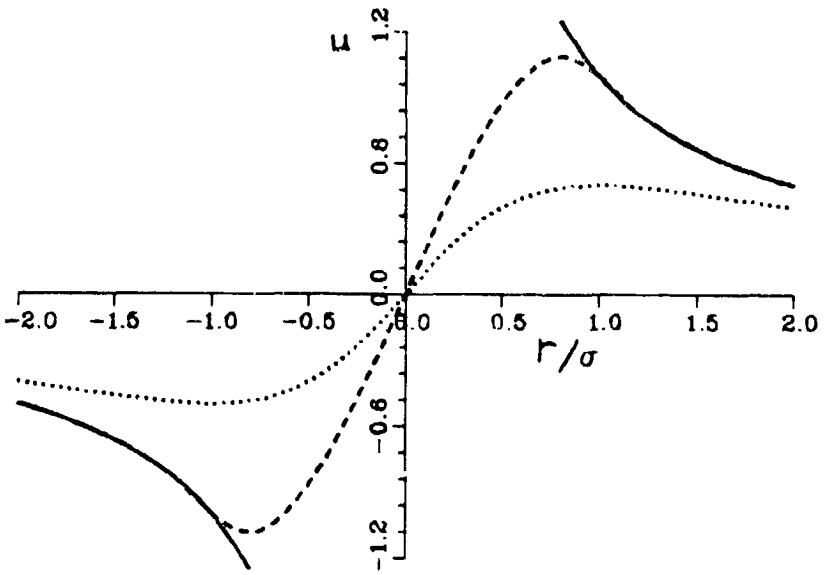

Fig. 6b. Core Velocity.—— Point Vortex, – – Core 1, ····Core 2

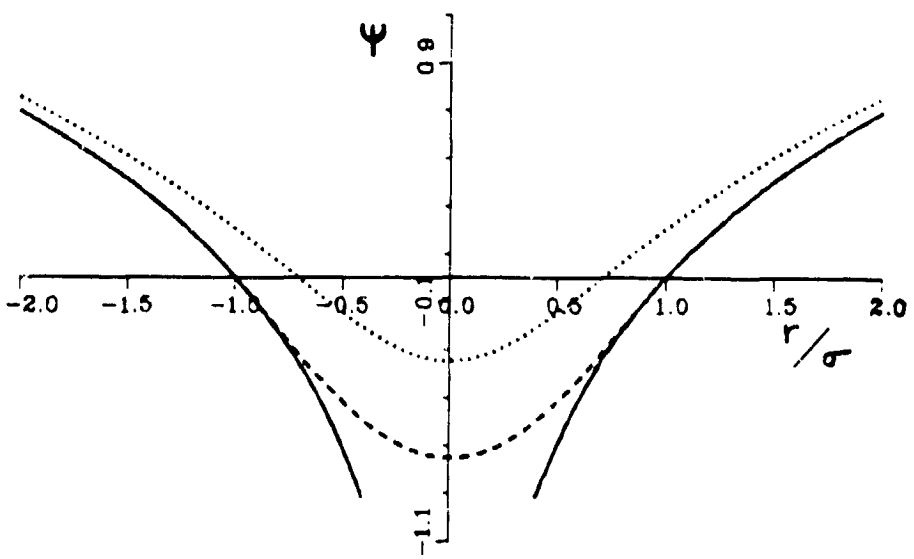

Fig. 6c. Core Stream Function.—— Point Vortex, – – Core 1, ····Core 2

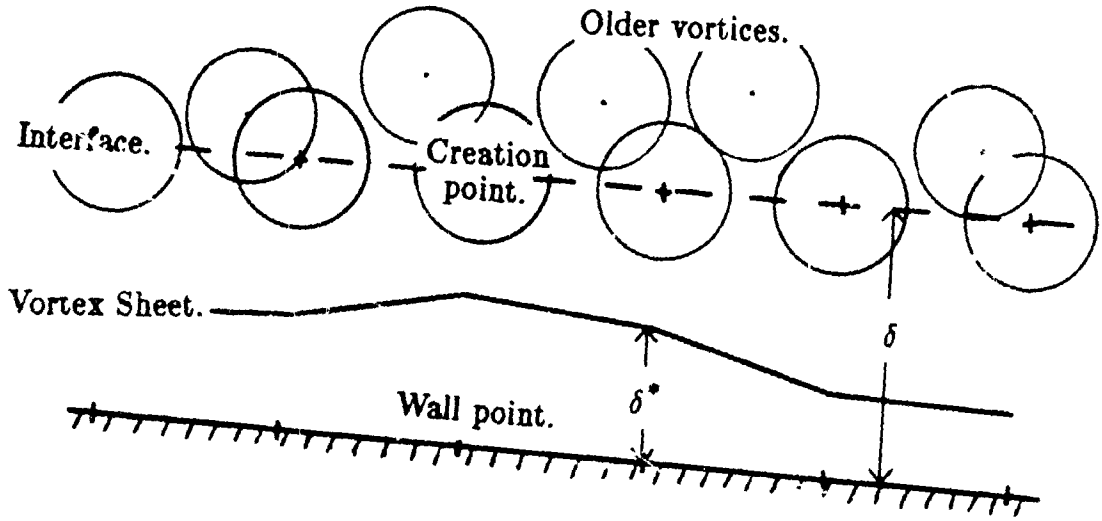

Fig. 7. Detail near wall in program $KPD3$.

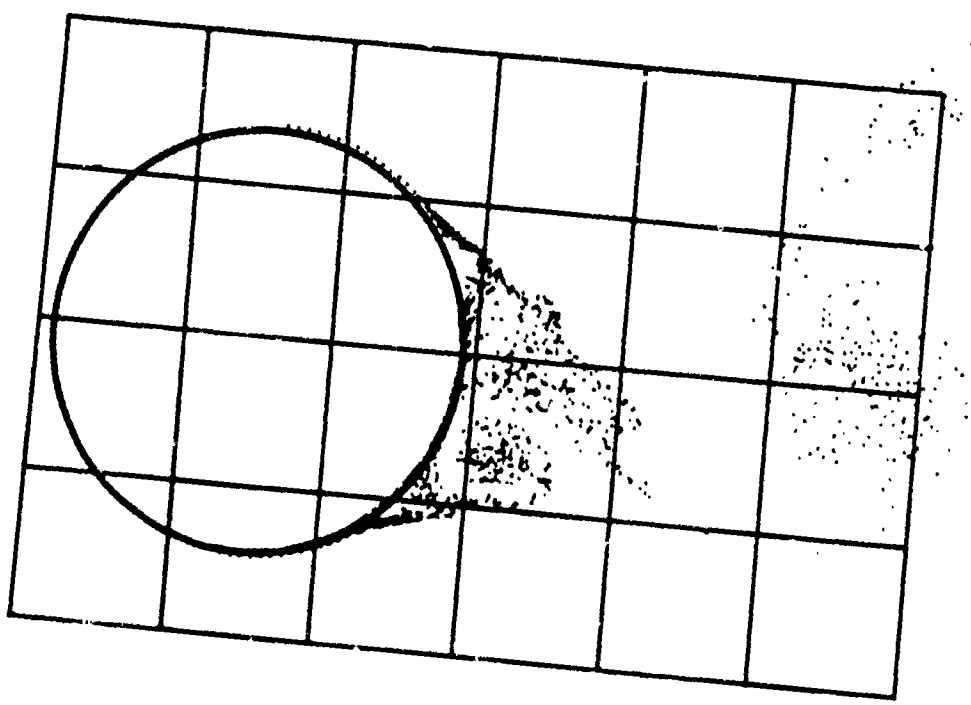

Fig. 8. Cells used for the Taylor expansions

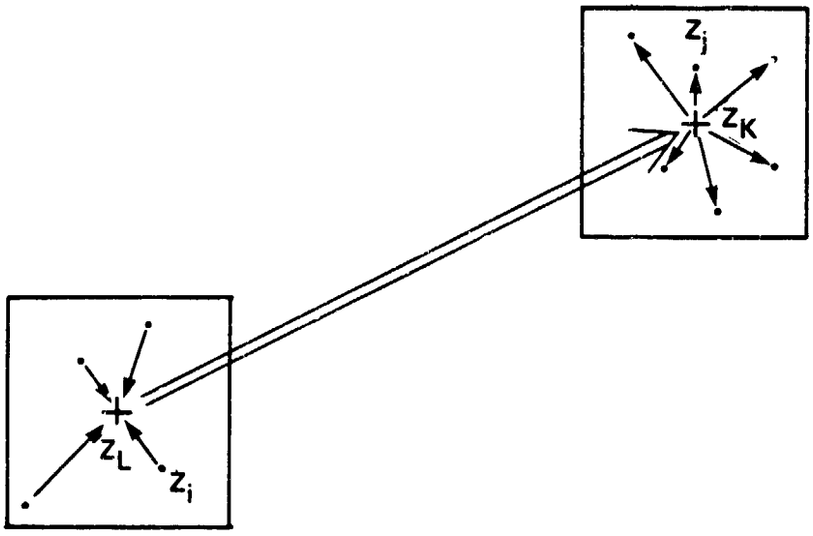

Fig. 9. Schematic of cell–to–cell interactions

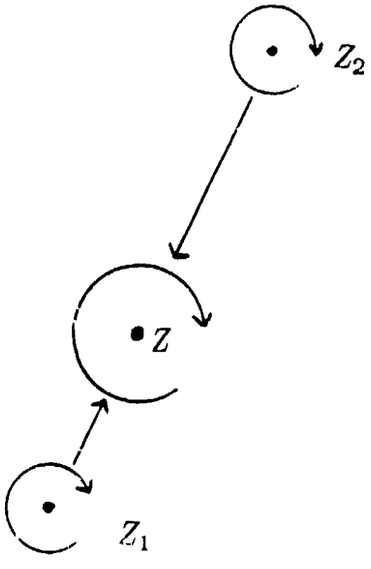

Fig. 10a. Same sign.

Fig. 10b. Opposite signs.

Fig. 10. Schematic of two cases of merging

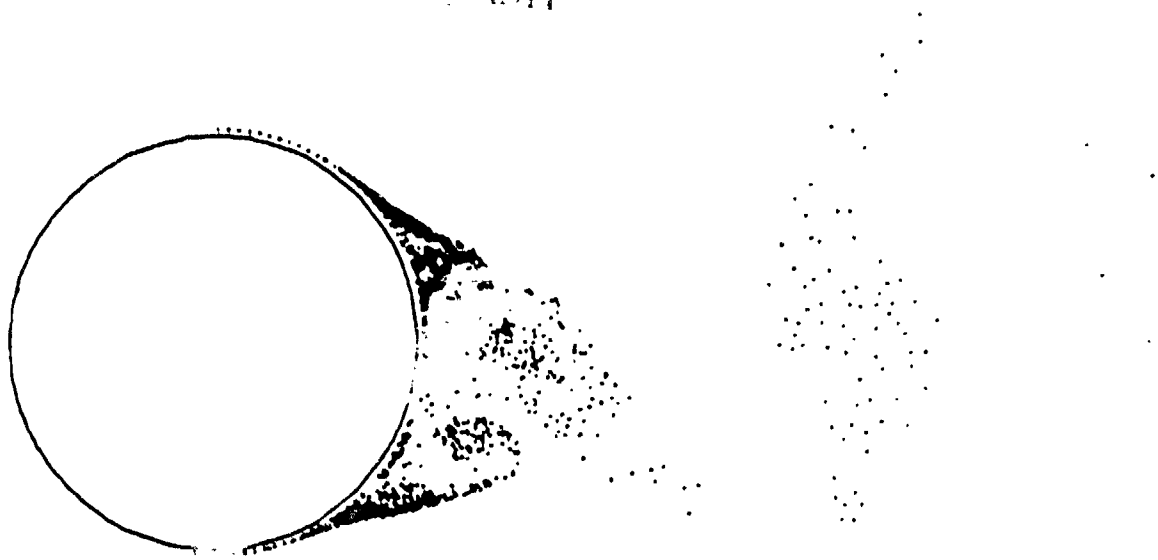

Fig. 11a. Simulation with $D_o=0.1$

Fig. 11b. Simulation with D_o 1

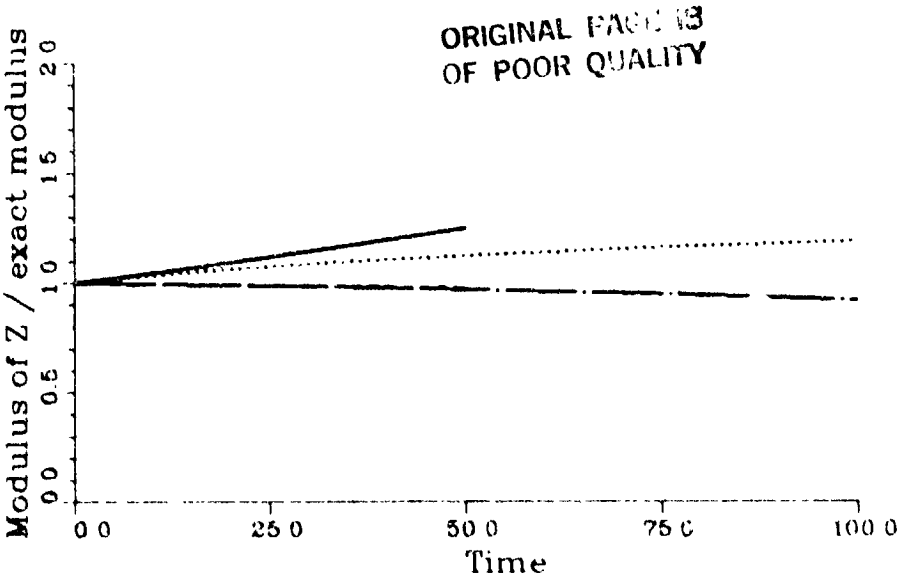

Fig. 12a Model Equations. $\Omega_0\Delta t = .25$——Linear, AB2
– – Linear, Lomax···Non - Linear, AB2 —•—Non - Linear, Lomax

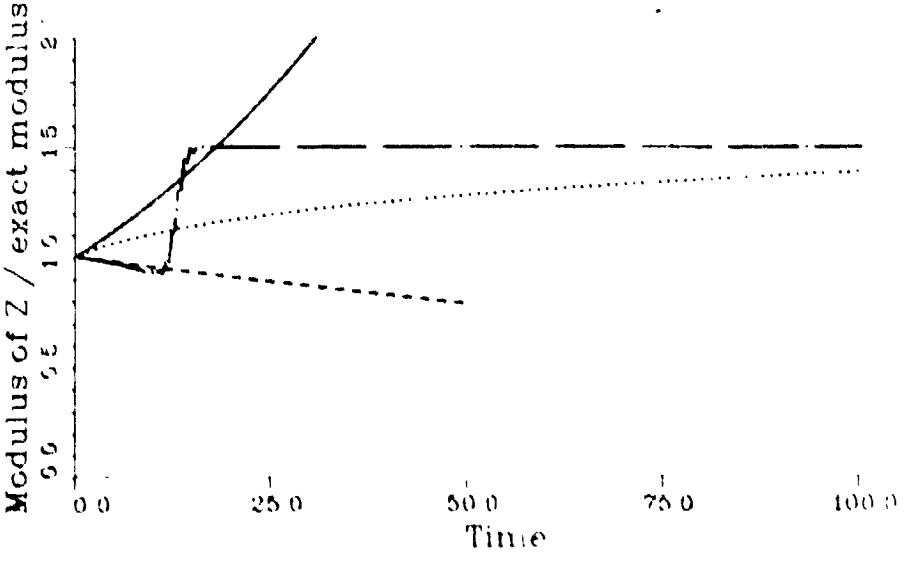

Fig. 12b Model Equations $\Omega_0\Delta t = .4$——Linear, AB2
– – Linear, Lomax···Non - Linear, AB2 —•—Non - Linear, Lomax

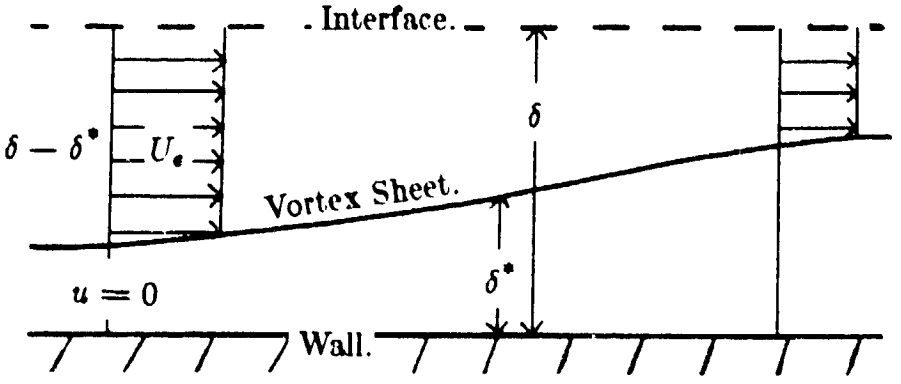

Fig. 13. Displacement of the outer flow by the Vortex Sheet.

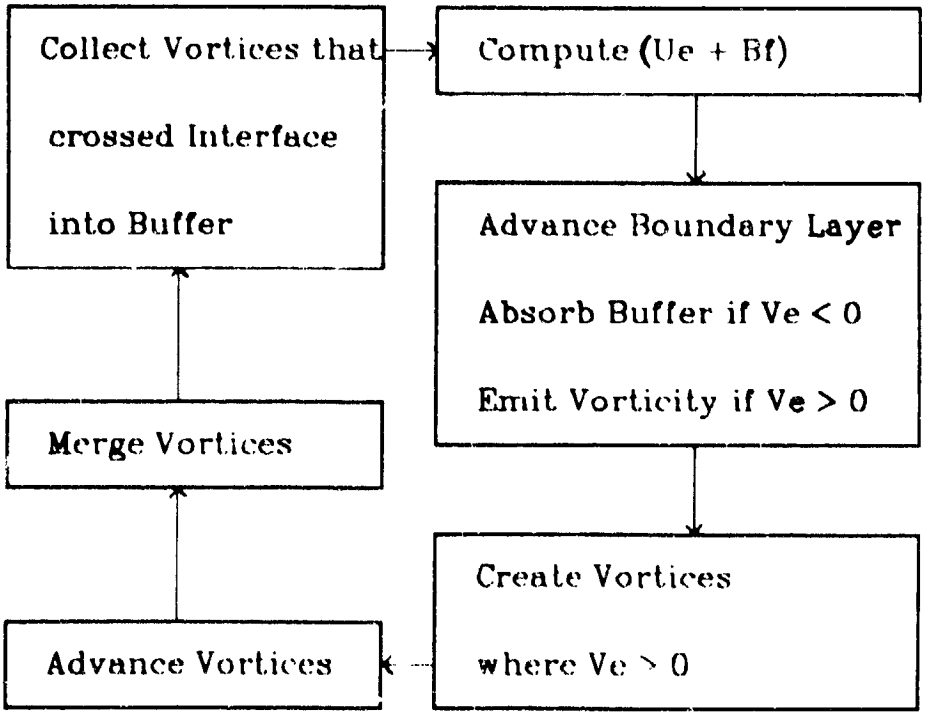

Fig. 14. Flow Chart of Program KPD3

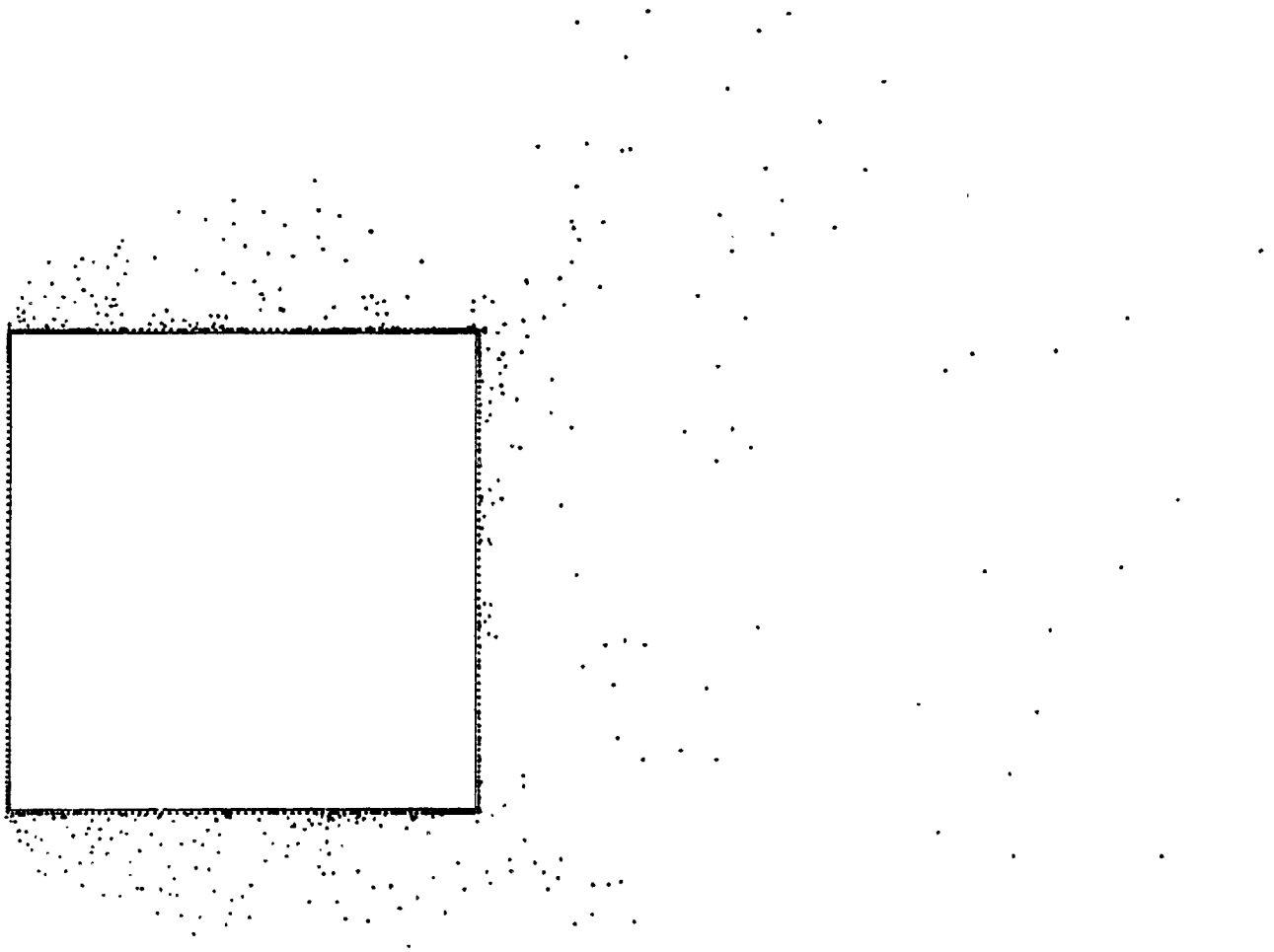

Fig. 15a. Simulation with 800 vortices

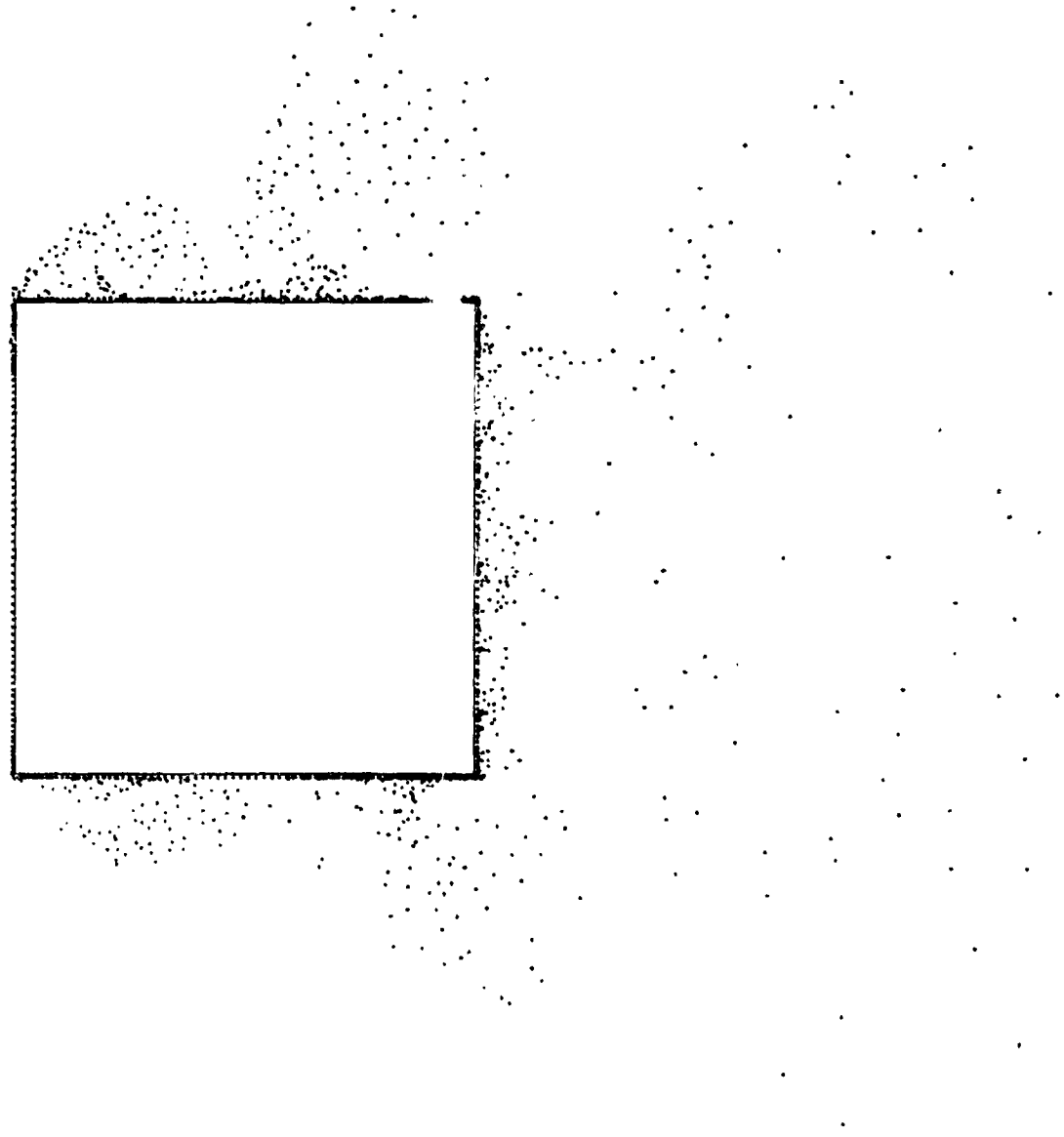

Fig. 15b. Simulation with 1200 vortices

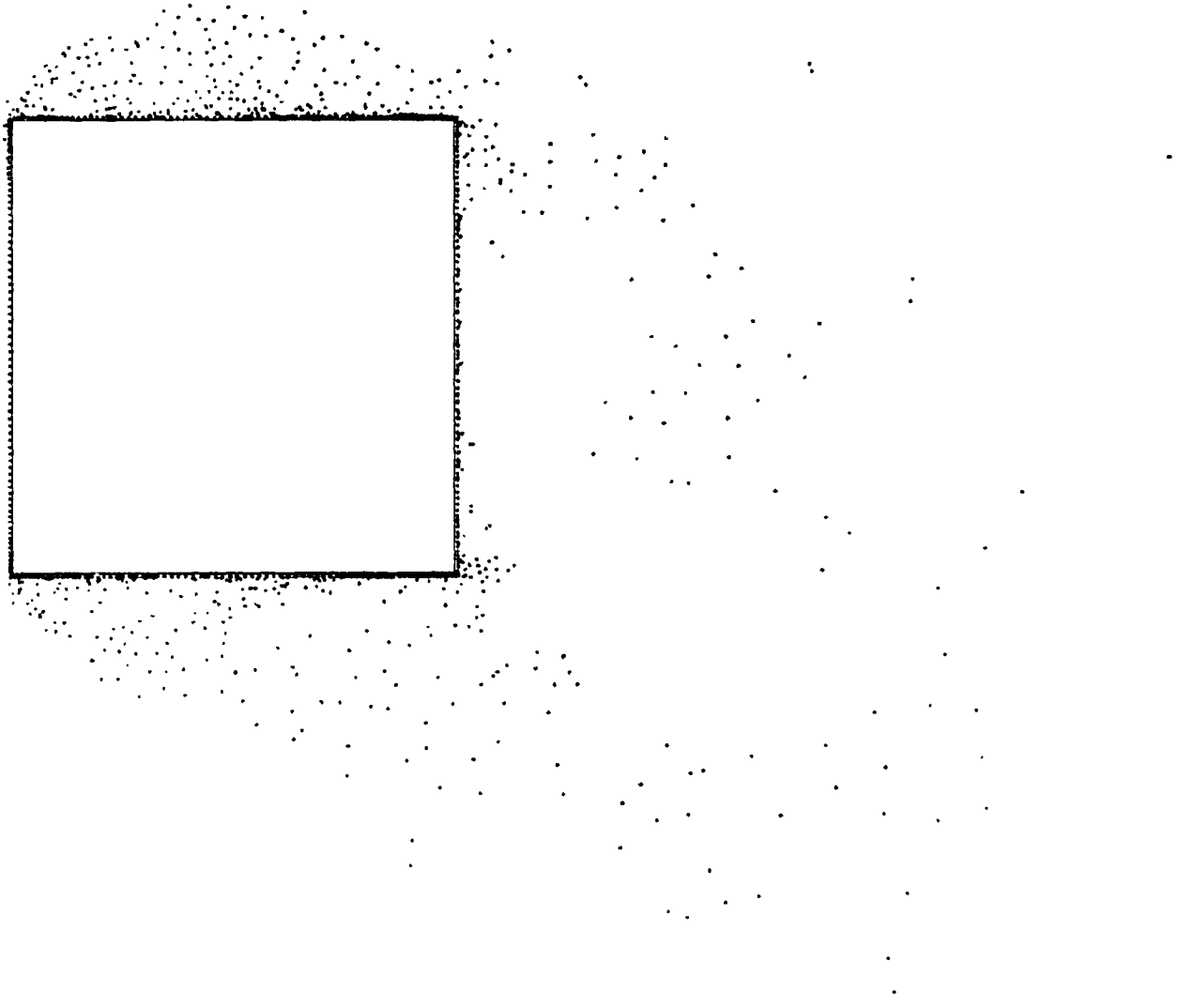

Fig. 16a. Simulation with σ=0.005

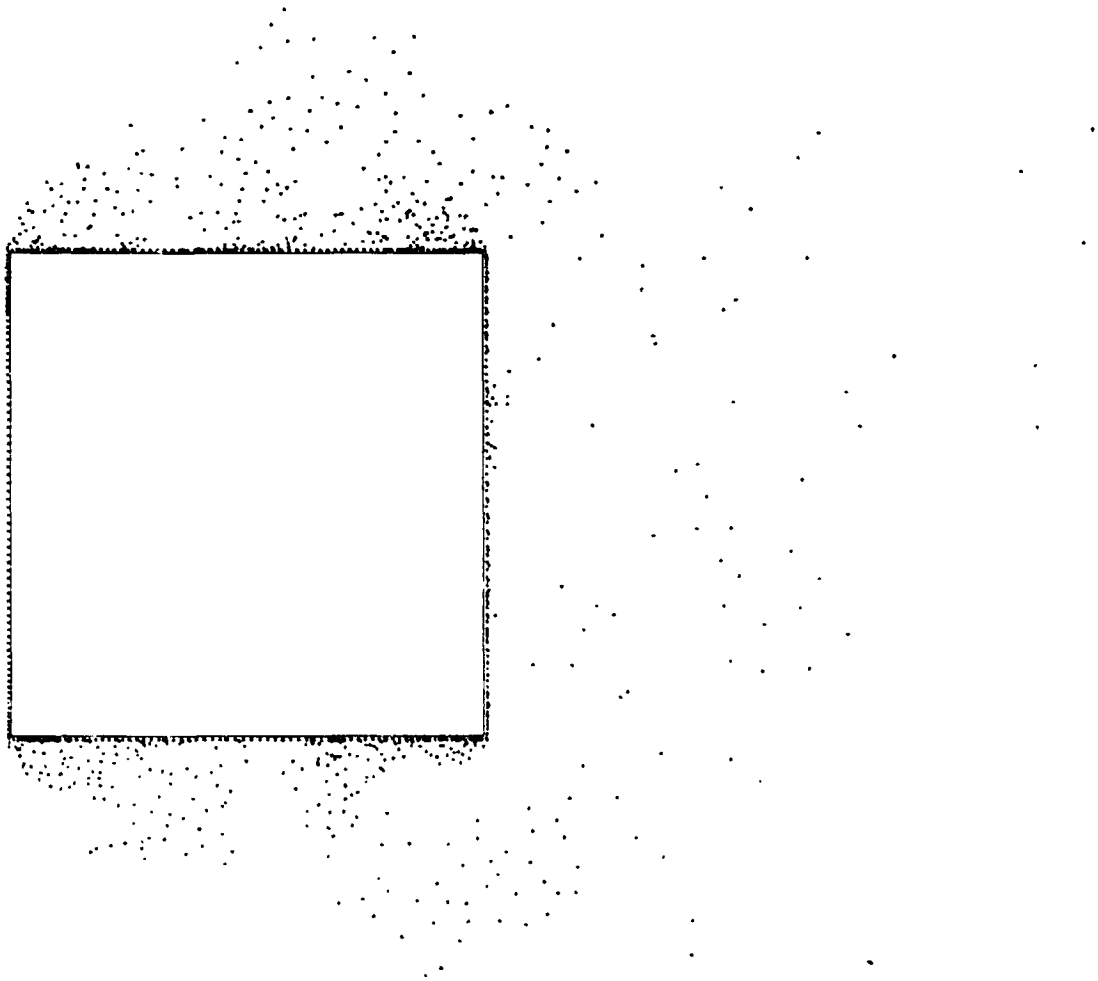

Fig. 16b. Simulation with σ=0.05

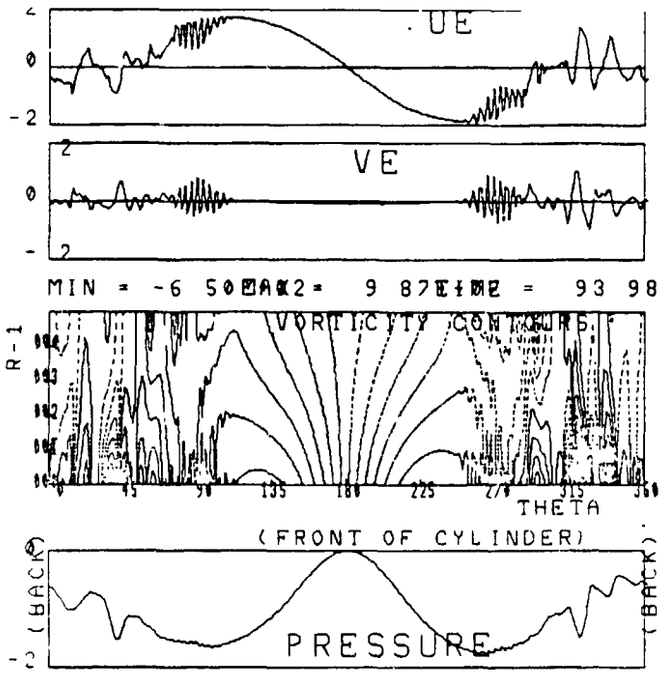

Fig. 17a. Simulation with δ=.005

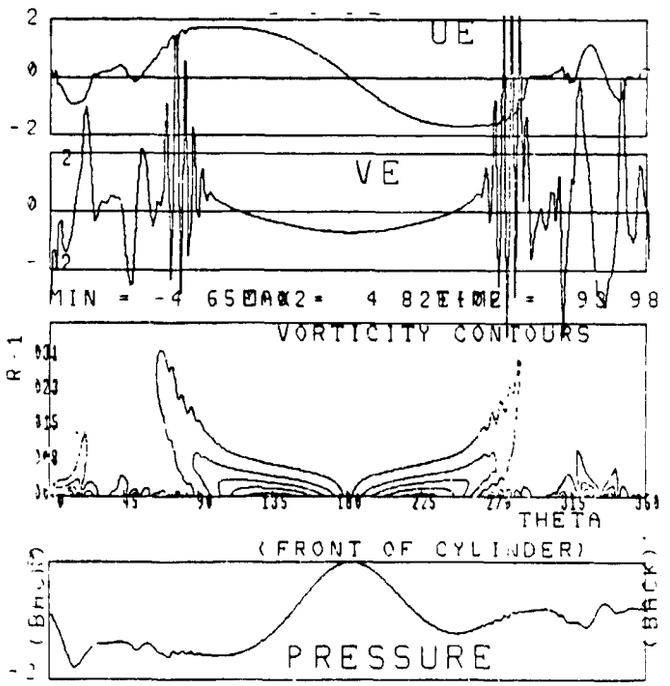

Fig. 17b. Simulation with δ =.04

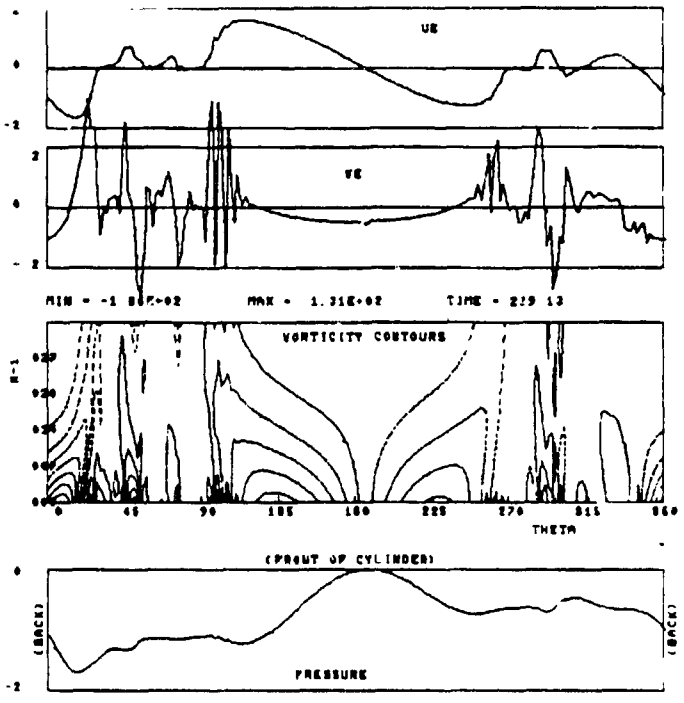

Fig. 18a. Simulation with $\varepsilon=0$

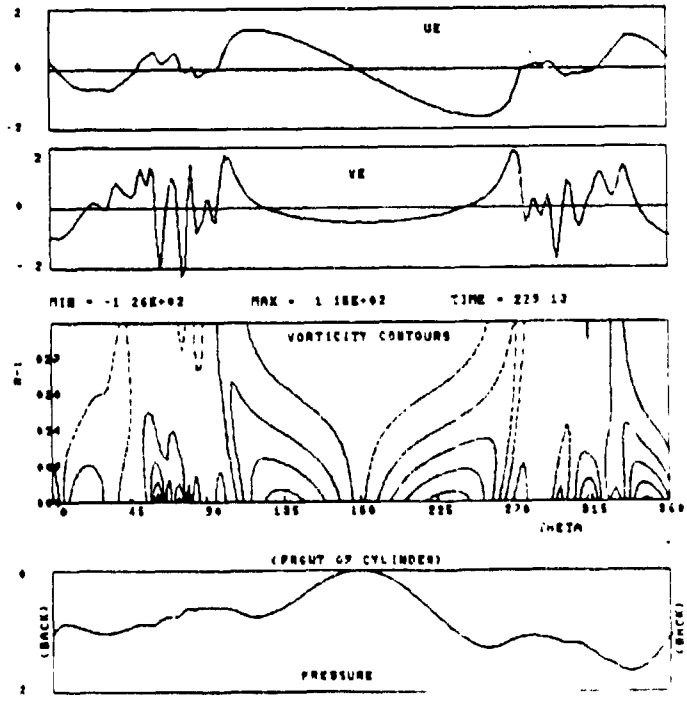

Fig. 18b. Simulation with $\varepsilon = 0.8\ 10^{-6}$

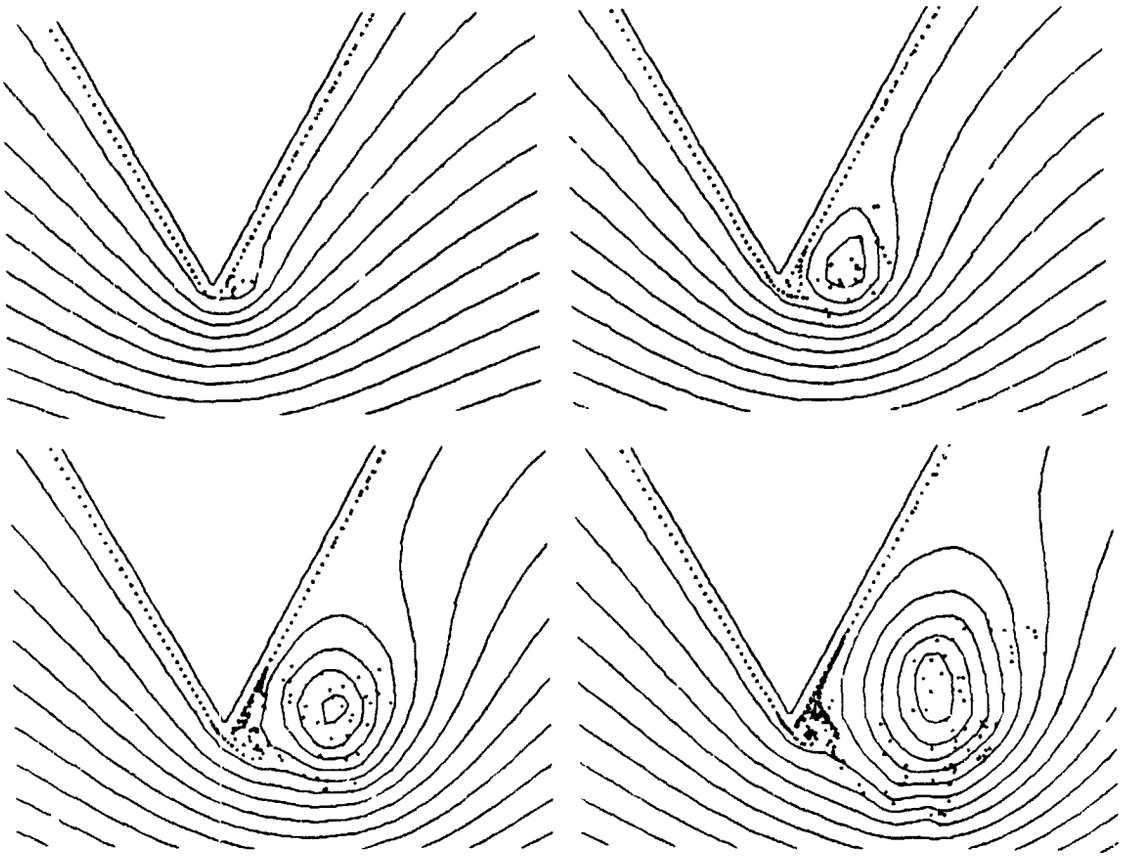

Fig. 19a. Starting Vortex at a Sharp Corner

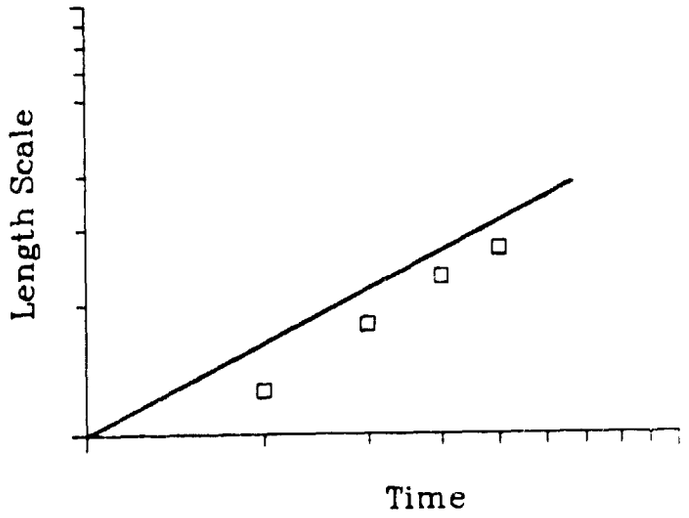

Fig. 19b. Length Scale in Starting Vortex

(Log–Log plot) —slope 5/7, □ Comp.

Fig. 20a. Computation of an Airfoil Flow by KPD1.
(Pure Vortex Method)

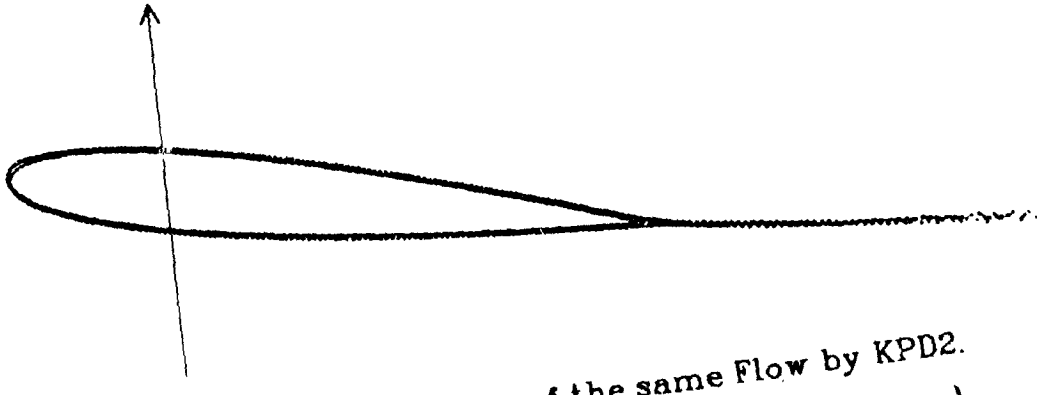

Fig. 20b. Computation of the same Flow by KPD2.
(With Control of Separation)

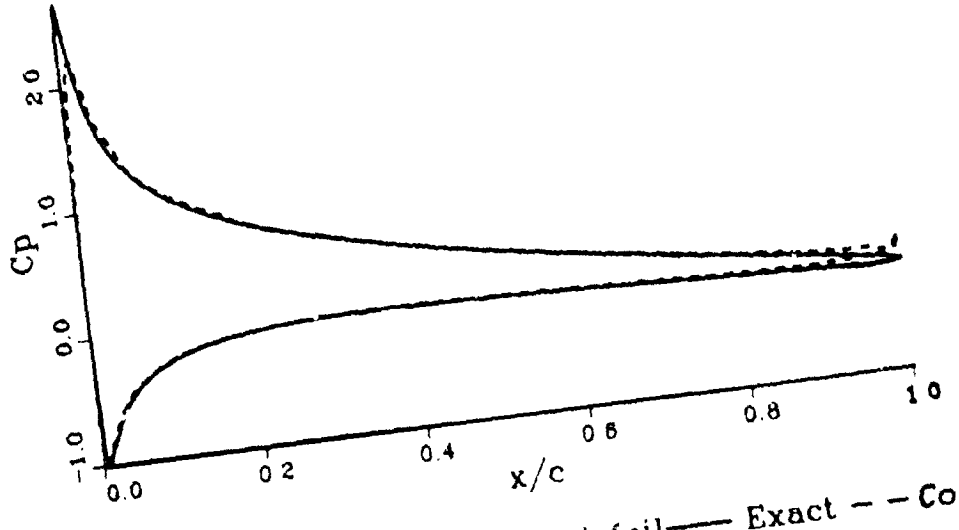

Fig. 21. Pressure on Joukovsky airfoil—— Exact – – Comp.

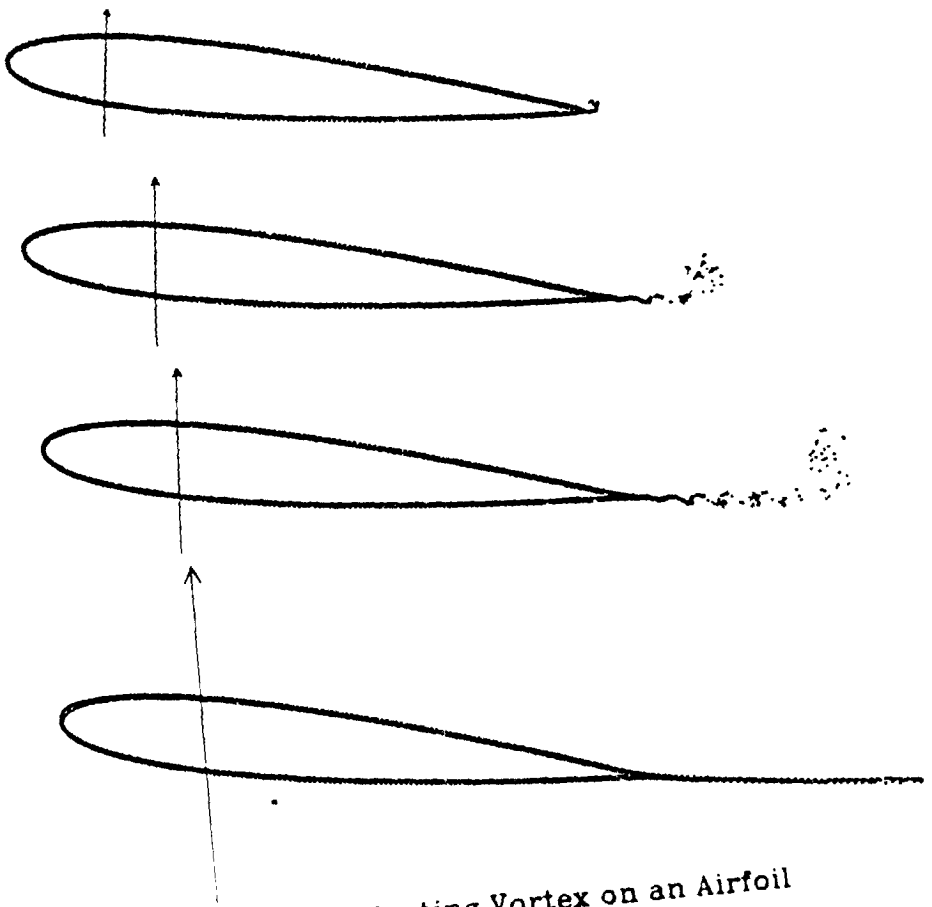

Fig. 22. Starting Vortex on an Airfoil

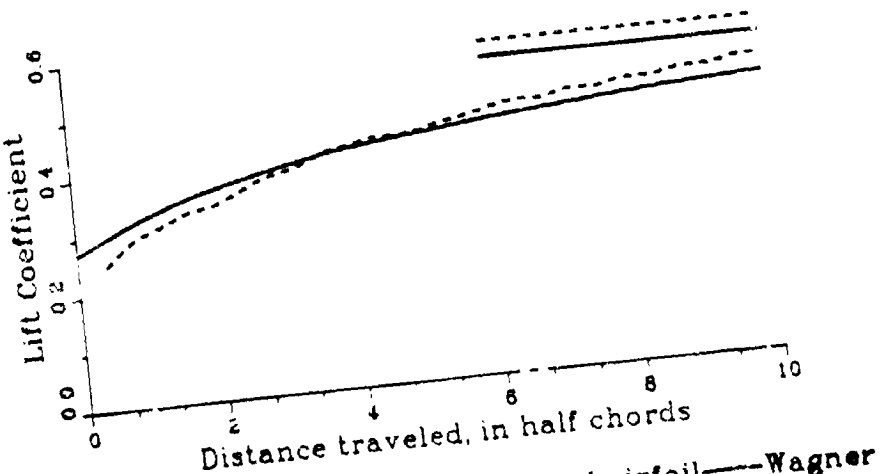

Fig. 23. Lift of an impulsively started airfoil——Wagner
– – Comp. (The Asymptotes are also shown)

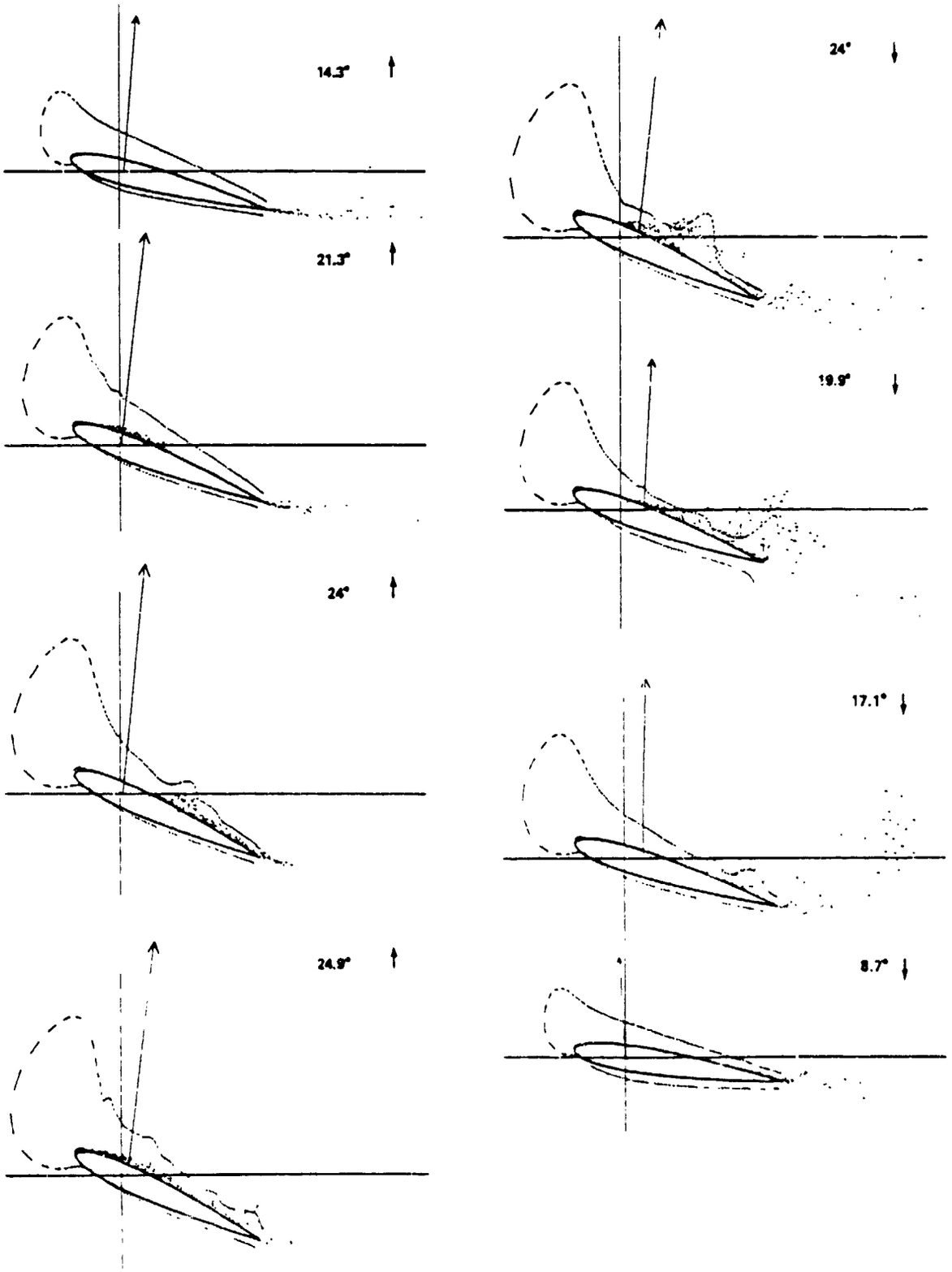

Fig. 24. Stills of the Dynamic Stall Simulation

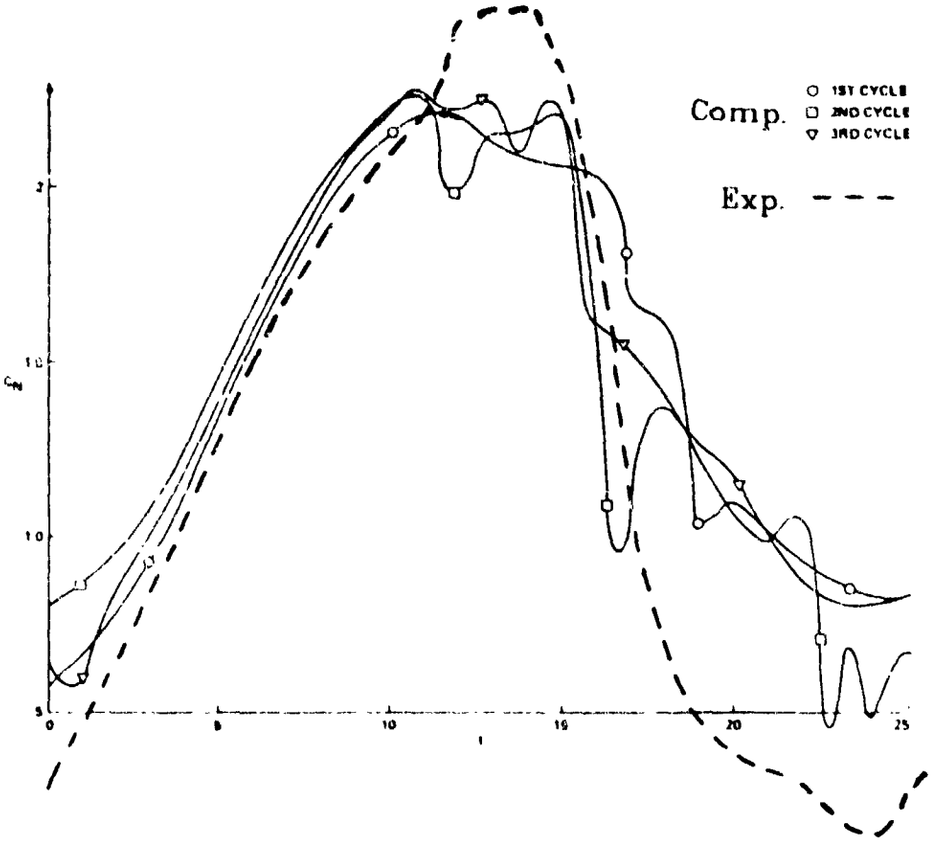

Fig. 25a. Normal Force Coefficient during Dynamic Stall.

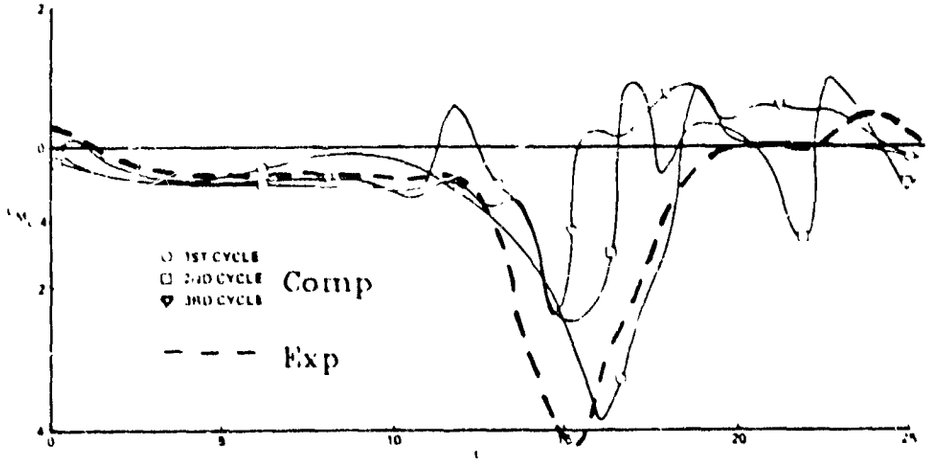

Fig. 25b Moment Coefficient during Dynamic Stall

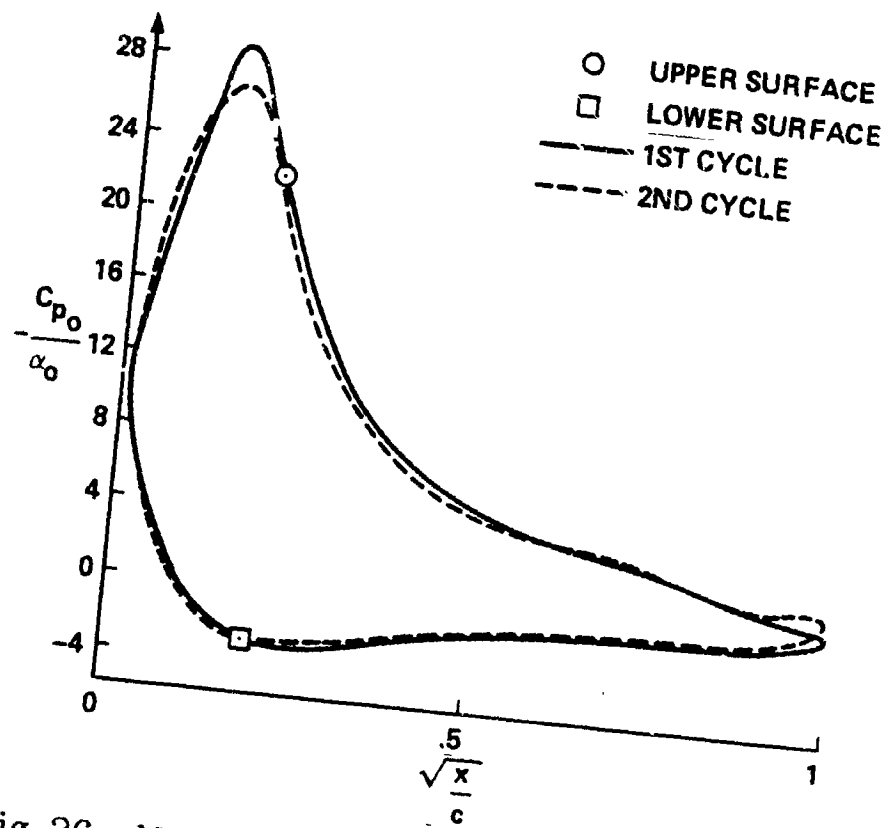

Fig. 26a. Mean pressure during dynamic stall

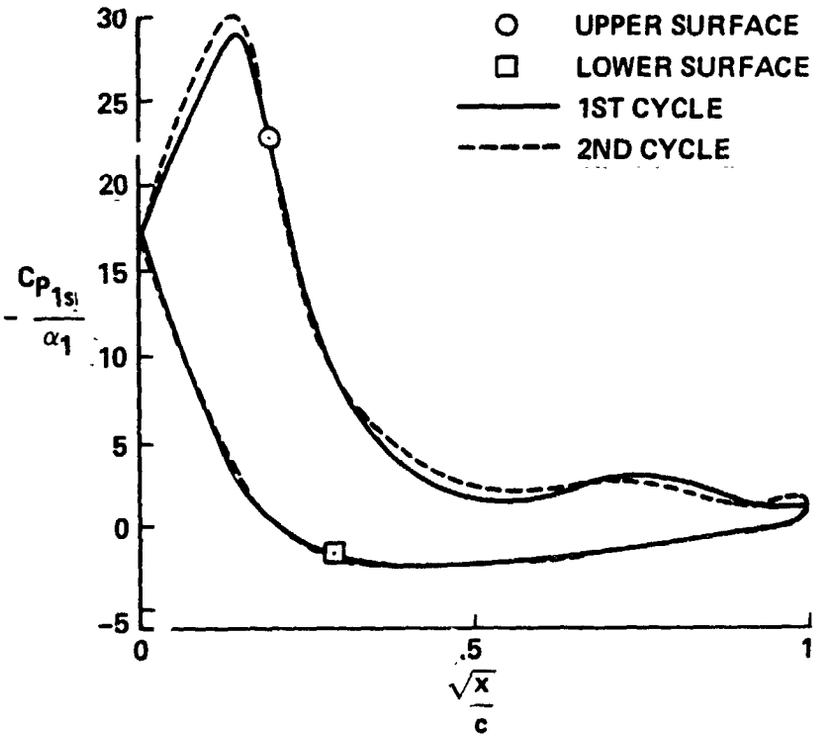

Fig. 26b. In–phase pressure

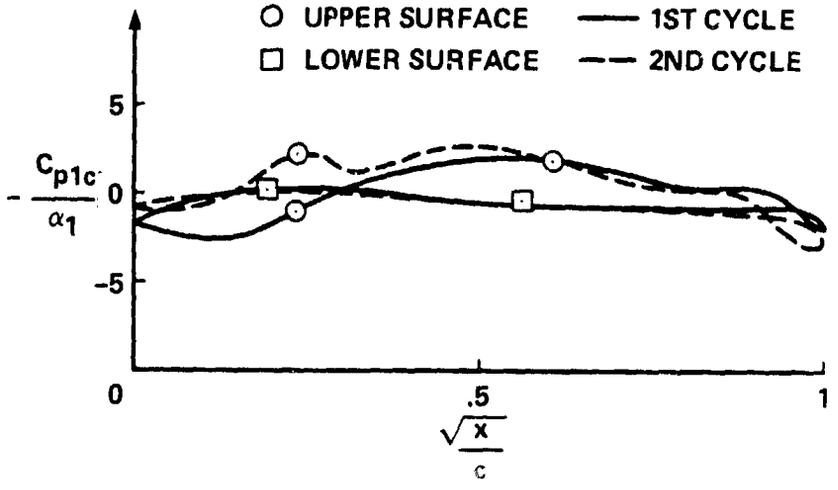

Fig. 26c. Out–of–phase pressure

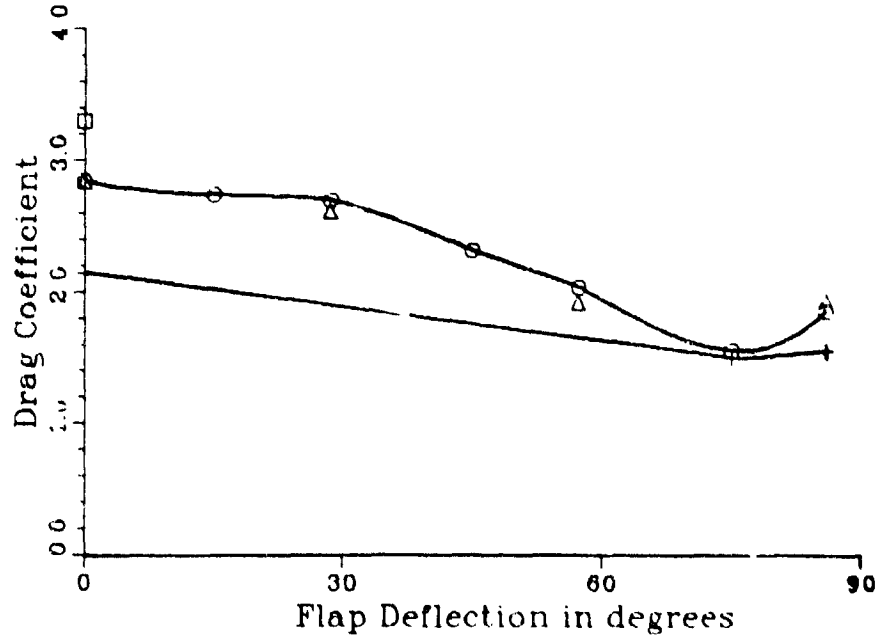

Fig. 27. Results of the tilt-rotor study.

□ = Flat Plate
○ = Large Radius Flap
△ = Small Radius Flap
\+ = Flap and Modified Leading Edge

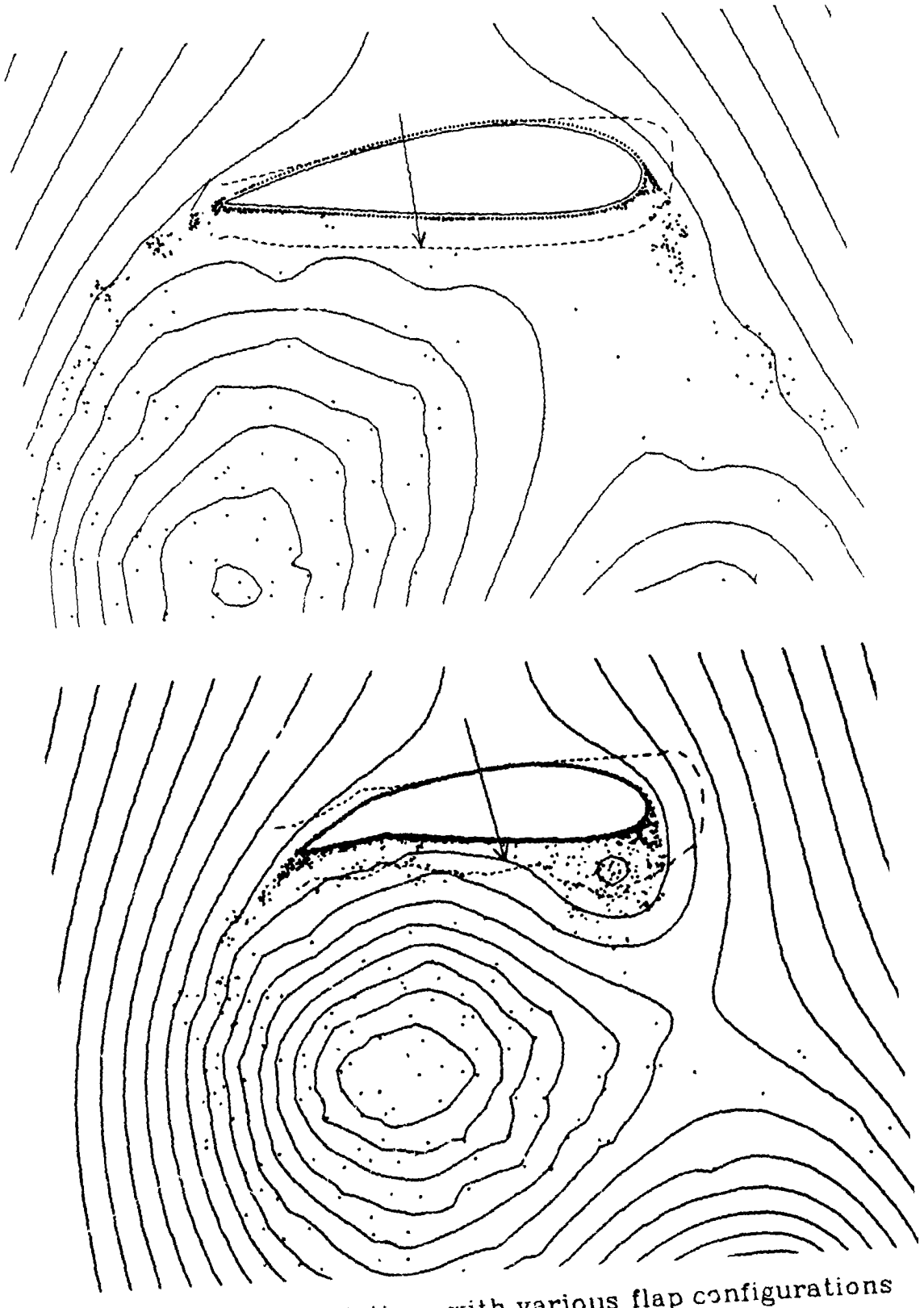

Fig. 28. Simulations with various flap configurations

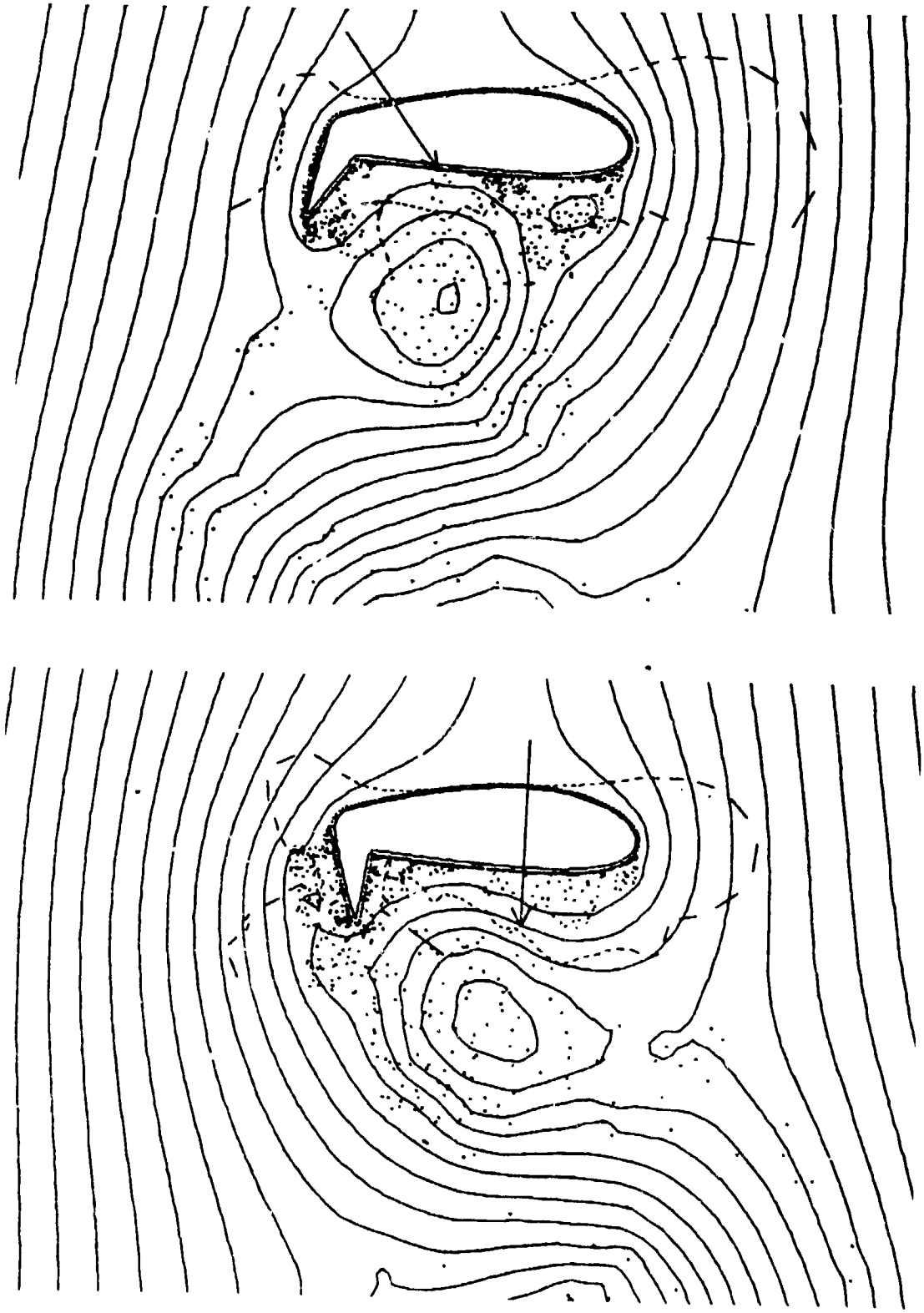

Fig. 28. Simulations with various flap configurations

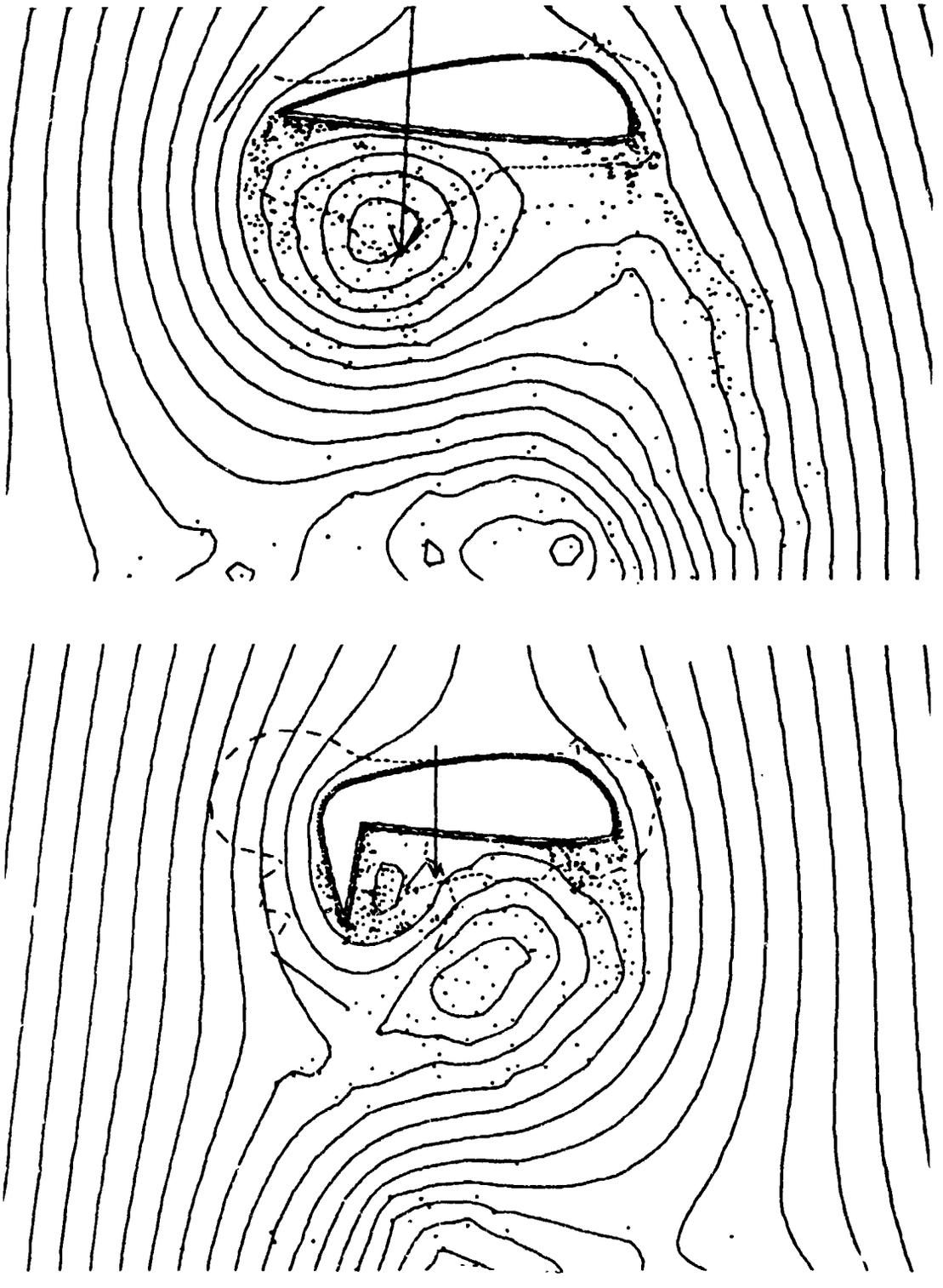

Fig. 29. Simulations with leading edge modification

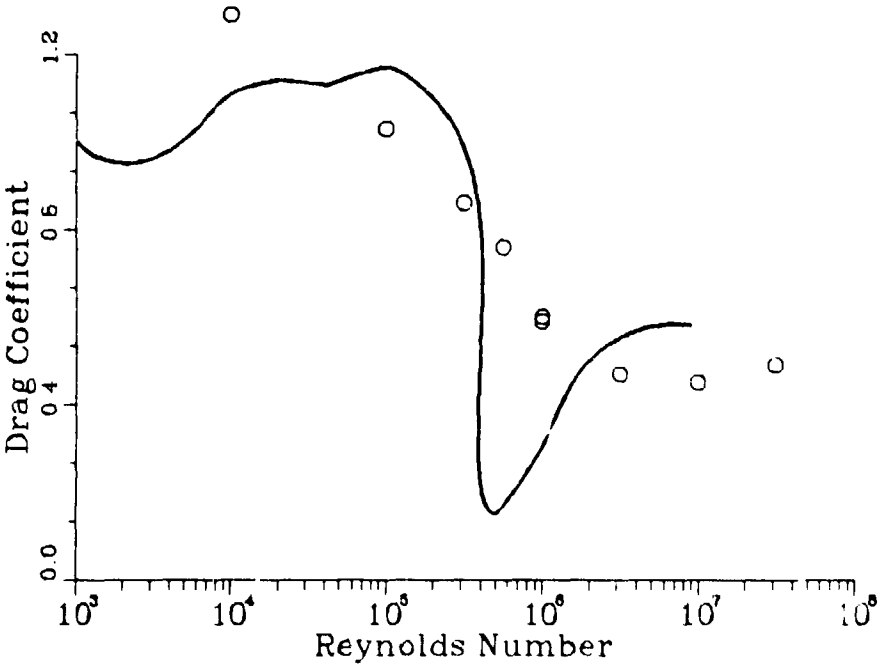

Fig. 30. Drag Coefficient of a Circular cylinder

——Average of Experiments [1],[61],[62],[63],[64] o **Comp.**

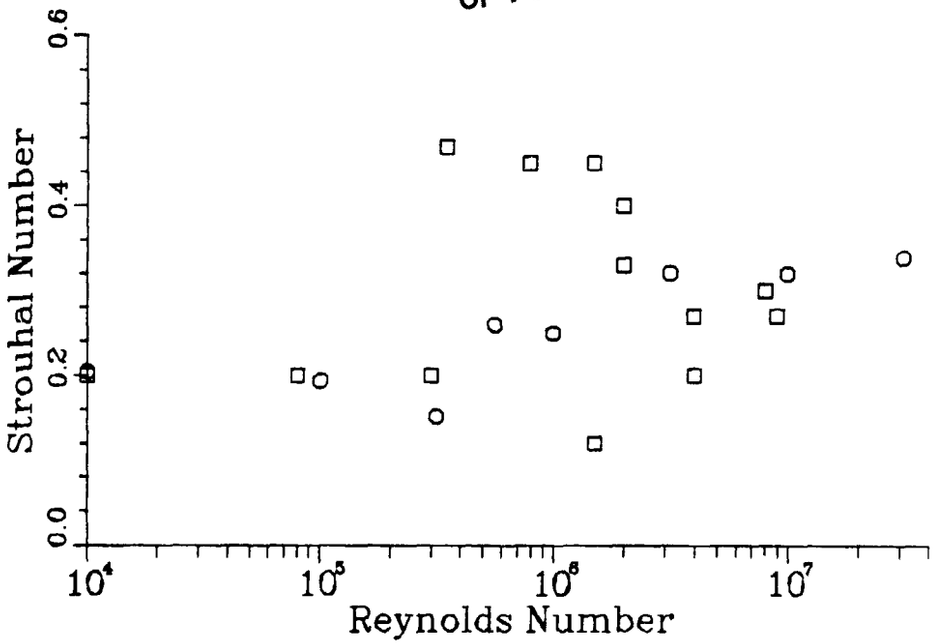

Fig. 31. Shedding frequency of circular cylinder.

▫ Exp. [1],[61],[62],[63],[64], ∘ Comp.

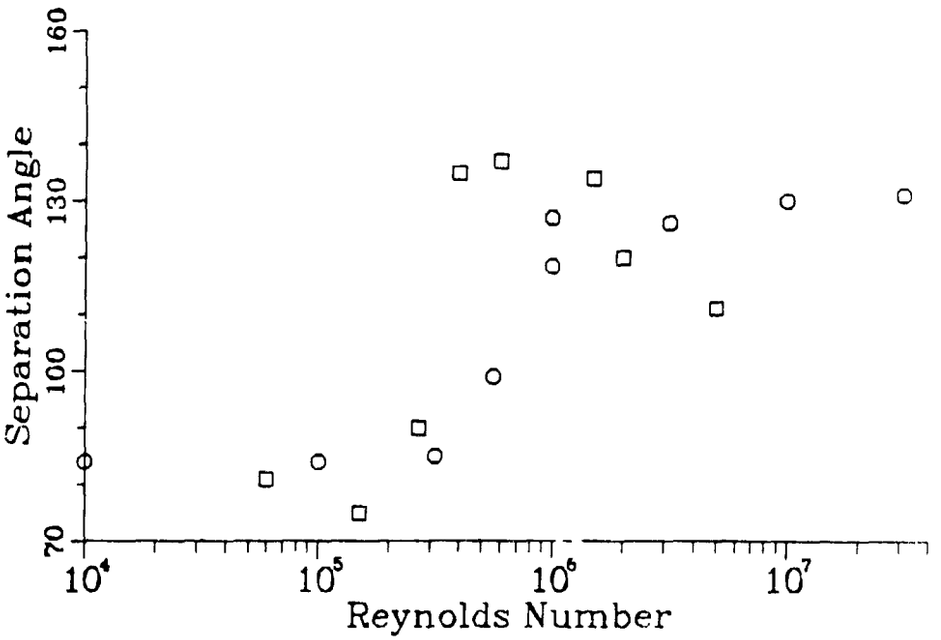

Fig. 32. Separation angle on circular cylinder.

▫ Exp. [63], ∘ Comp.

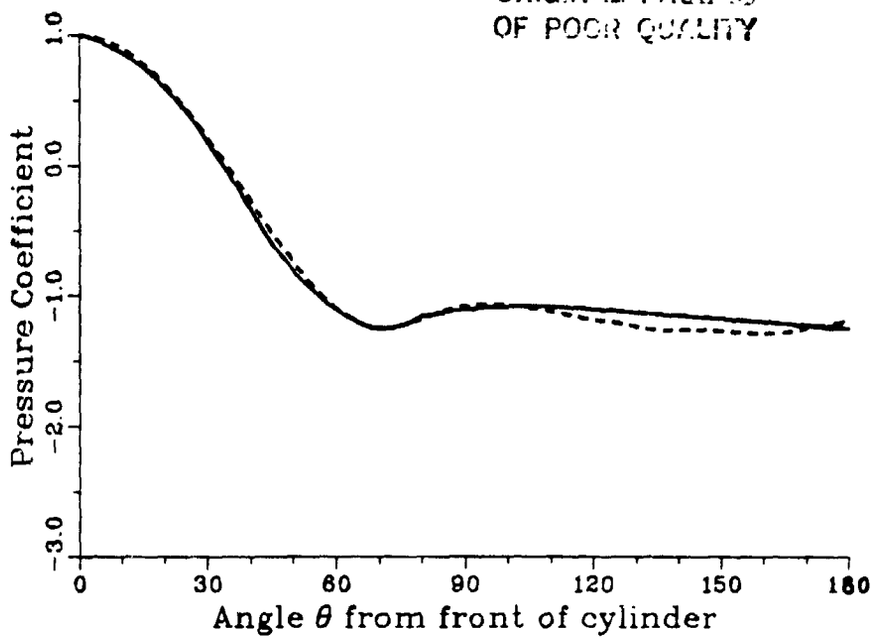

Fig. 33a. Pressure Distribution. ——Exp. , Re=10^6 [62]
– – Comp. , Re=10^4

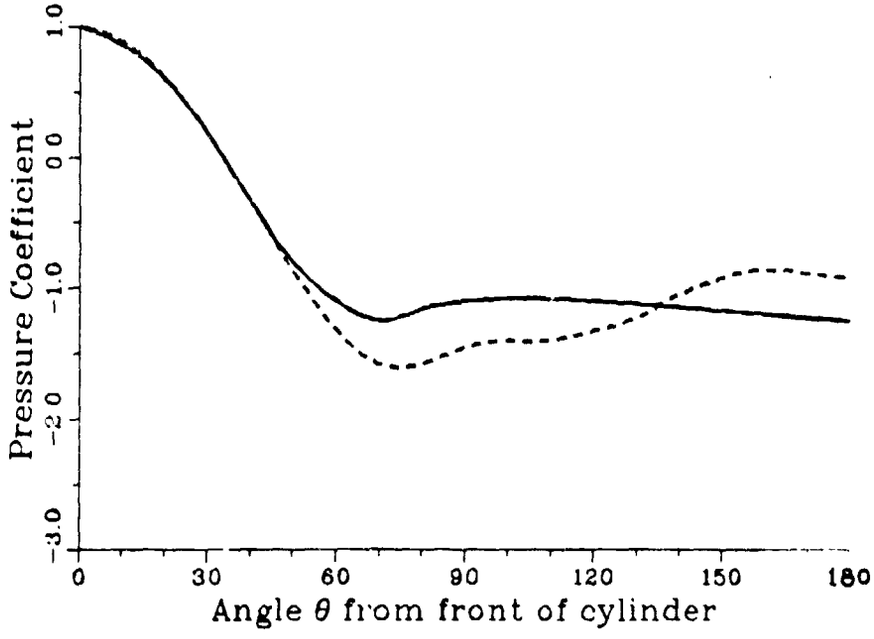

Fig. 33b. Pressure distribution. ——Exp., Re=10^5 [62]
– – Comp., Re=10^5

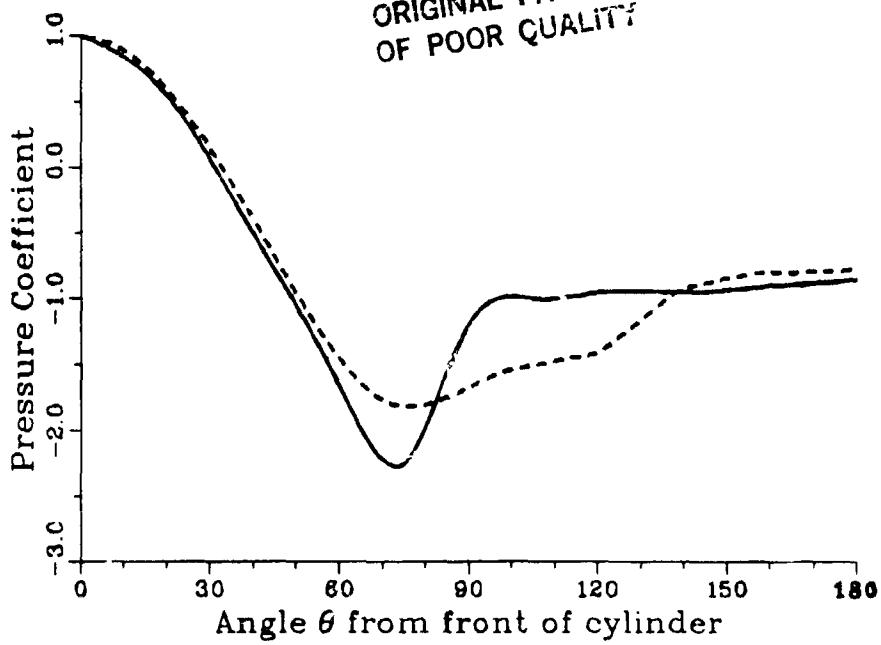

Fig. 33c. Pressure Distribution. ——Exp., Re=2.6 10^6 [63]
– – Comp., Re=3.16 10^6

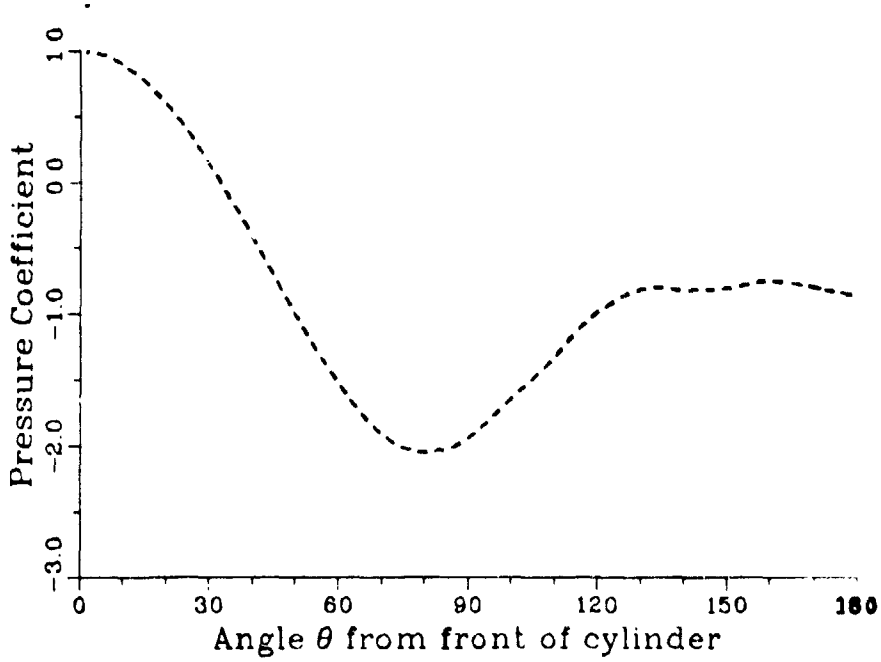

Fig. 33d. Pressure Distribution. – – Comp., Re=5.62 10^6

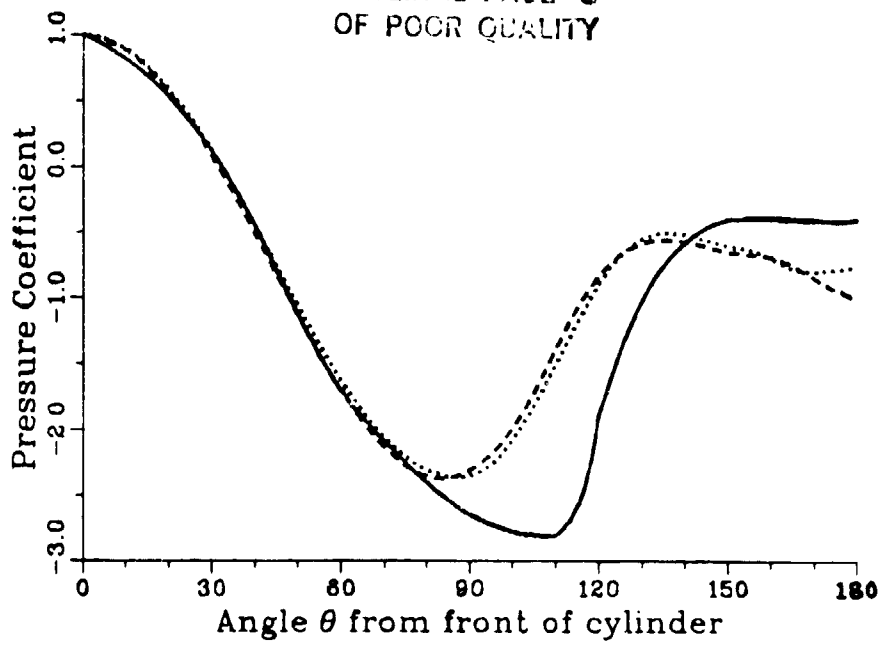

Fig. 33e. Pressure Distribution. ——Exp., Re=8.5 10^6 [63]

– – Low resolution, Re=10^6 ····High resolution, Re=10^6

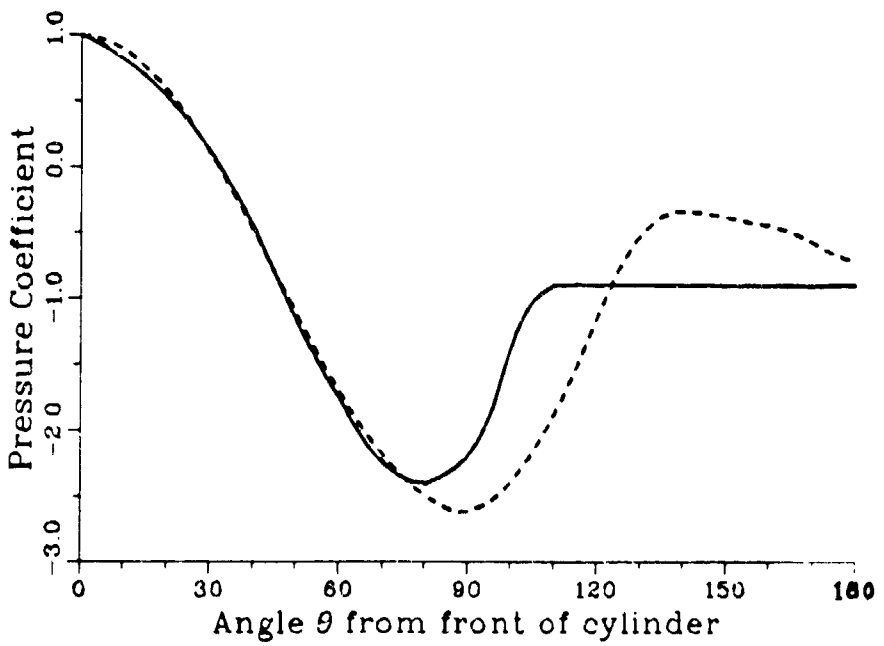

Fig. 33f. Pressure Distribution. ——Exp., Re=3.6 10^6 [63]

– – Comp., Re=3.16 10^6

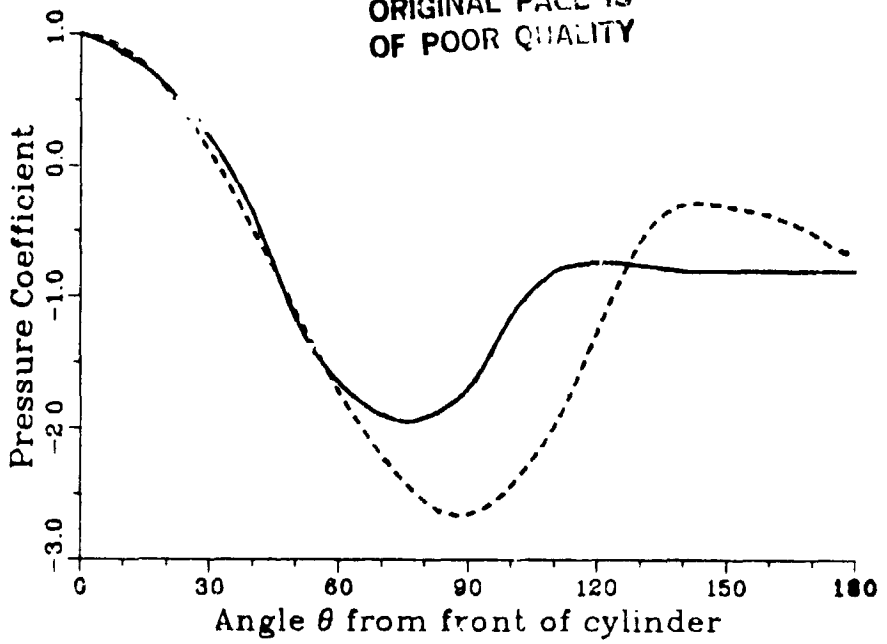

Fig. 33g. Pressure Distribution. ——Exp., Re=8.5 10^6 [64]
– – Comp., Re=10^7

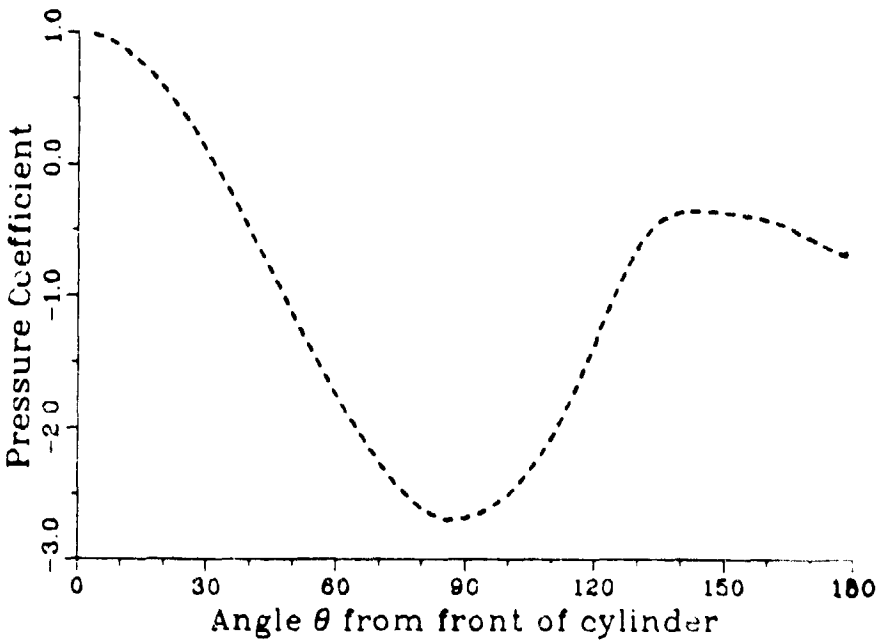

Fig. 33h. Pressure Distribution. – – Comp., Re=3.16 10^7

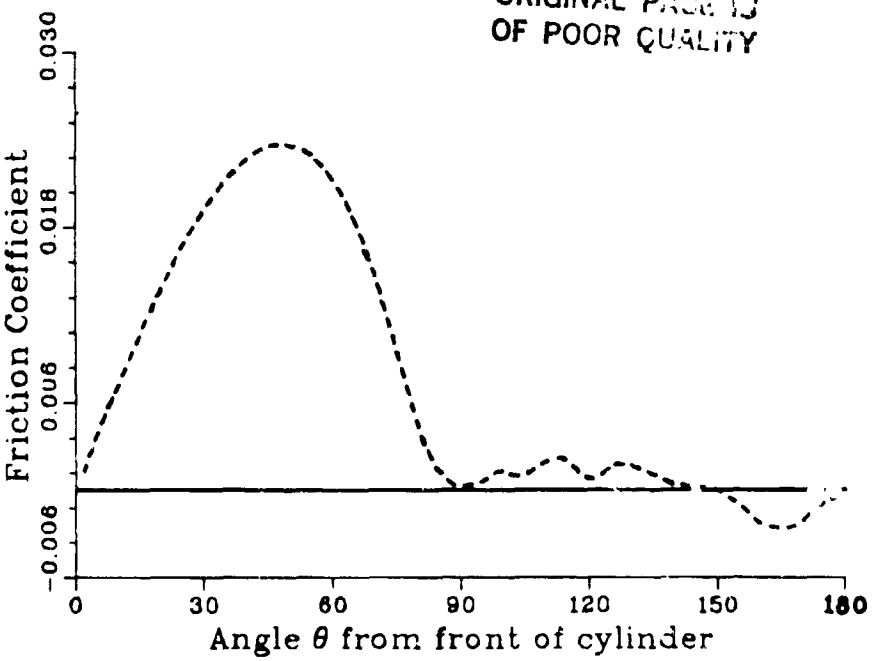

Fig. 34a. Friction Distribution. — — Comp., Re=10^4

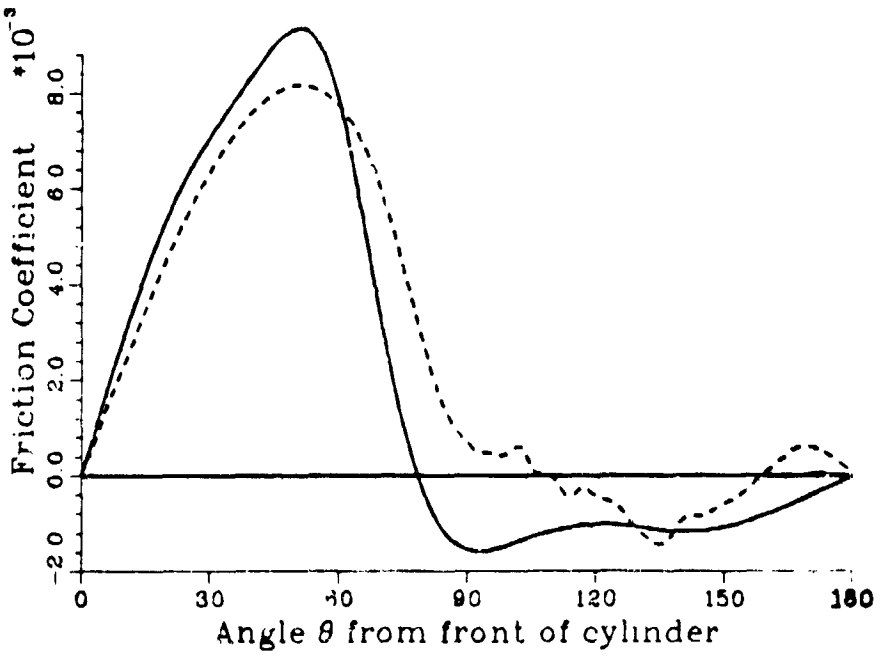

Fig. 34b. Friction Distribution. ——Exp., Re=10^5[63]
– – Comp., Re=10^5

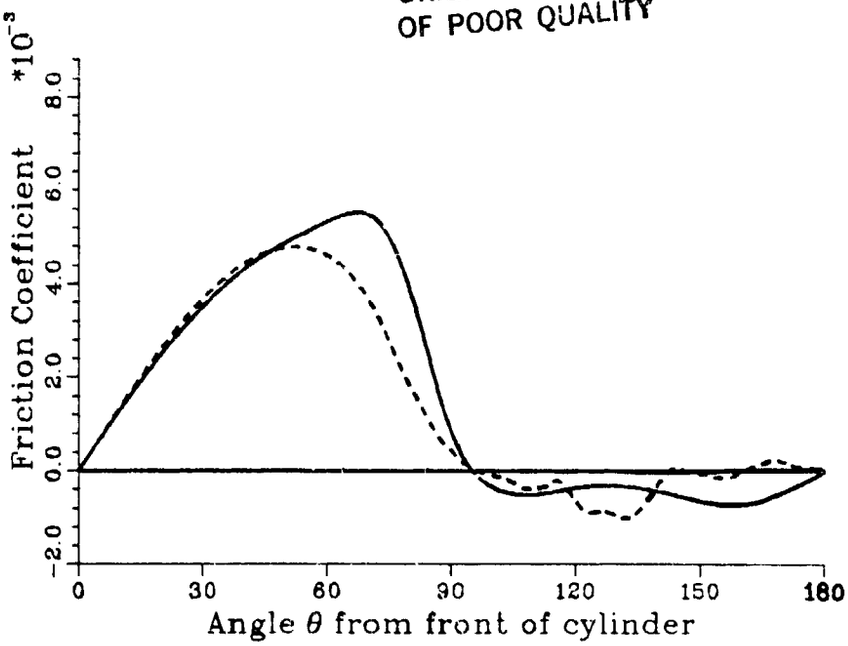

Fig. 34c. Friction Distribution. ——Exp., Re=2.6 10^5[63]
– – Comp., Re=3 16 10^5

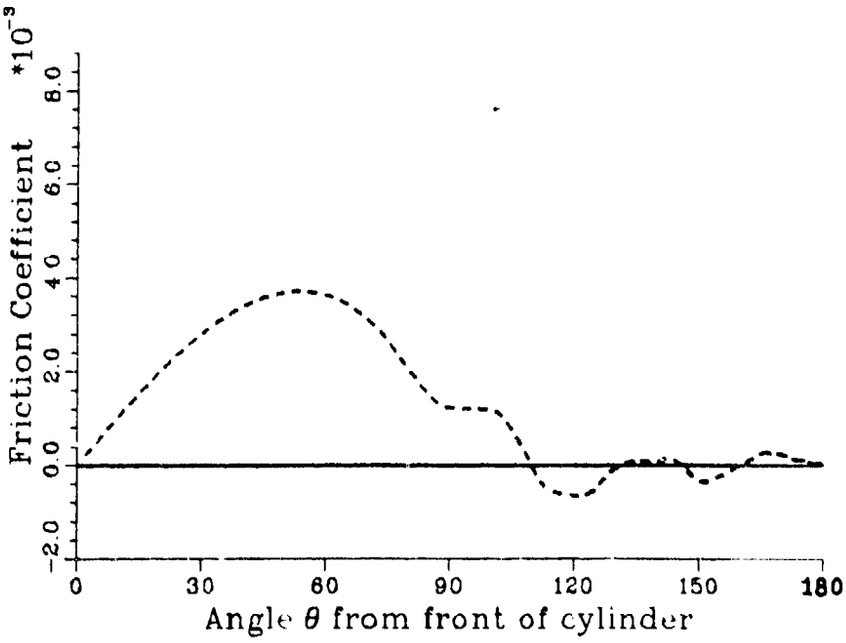

Fig. 34d. Friction Distribution. – – Comp., Re=5.62 10^5

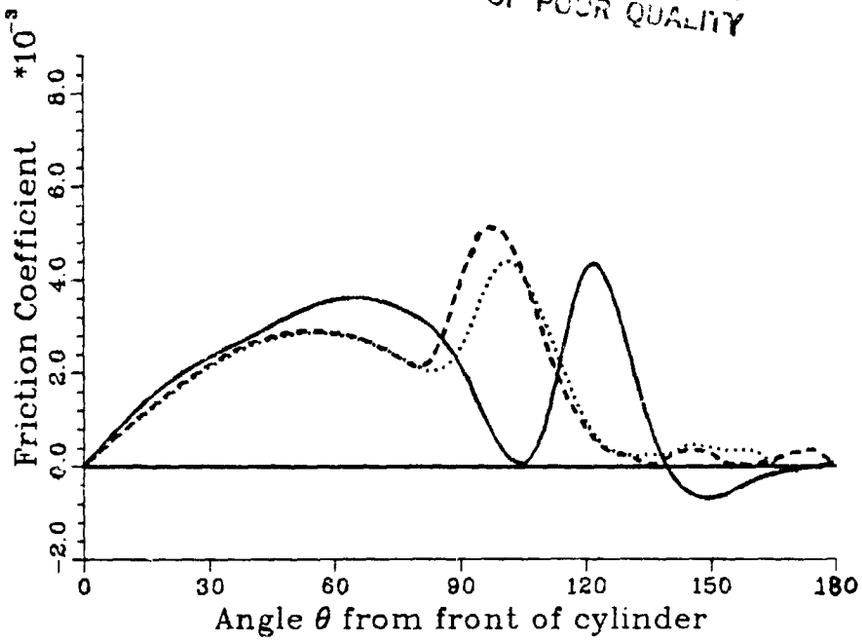

Fig. 34e. Friction Distribution. ——Exp., Re=8.5 10^5[63]
– – Low resolution, Re=10^6 High resolution, Re=10^6

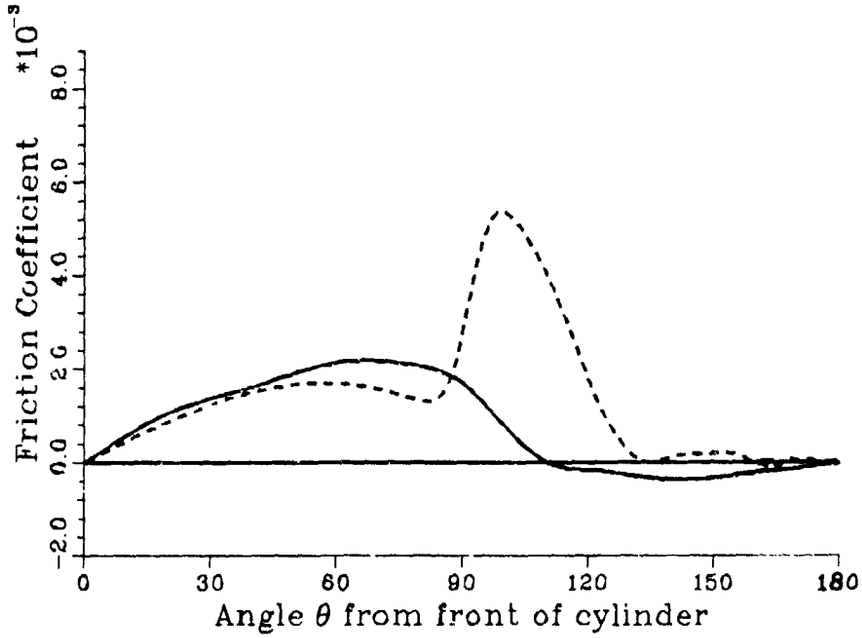

Fig. 34f. Friction Distribution. ——Exp., Re=3.6 10^6[63]
– —Comp., Re=3.16 10^6

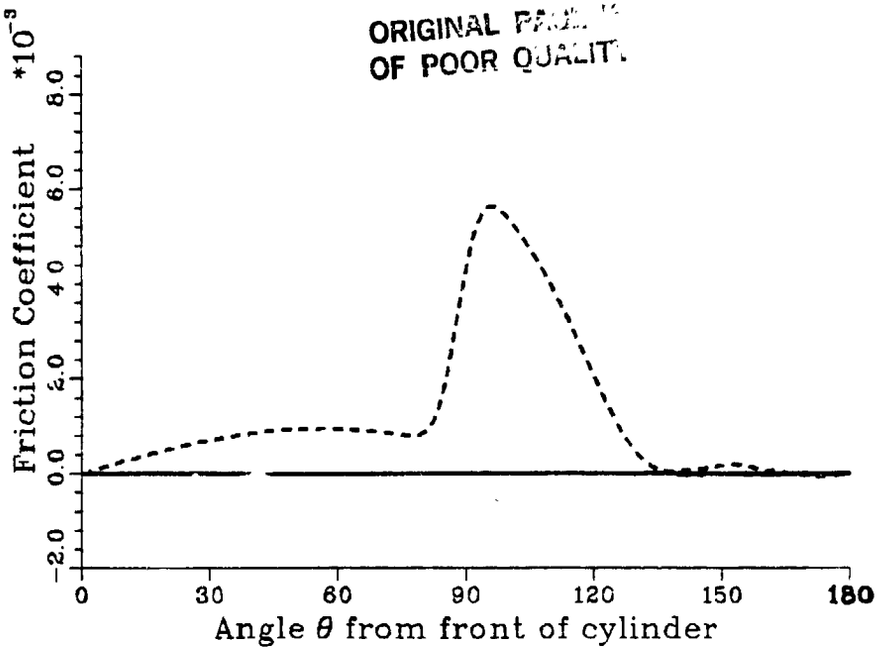

Fig. 34g. Friction Distribution. – —Comp., Re=10^7

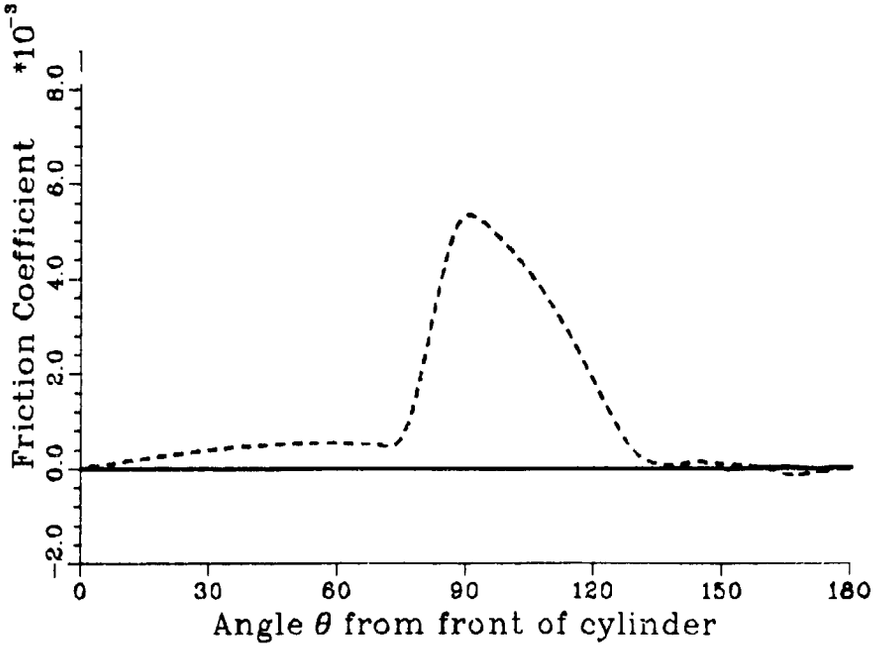

Fig. 34h. Friction Distribution. – – Comp., Re=3.16 10^7

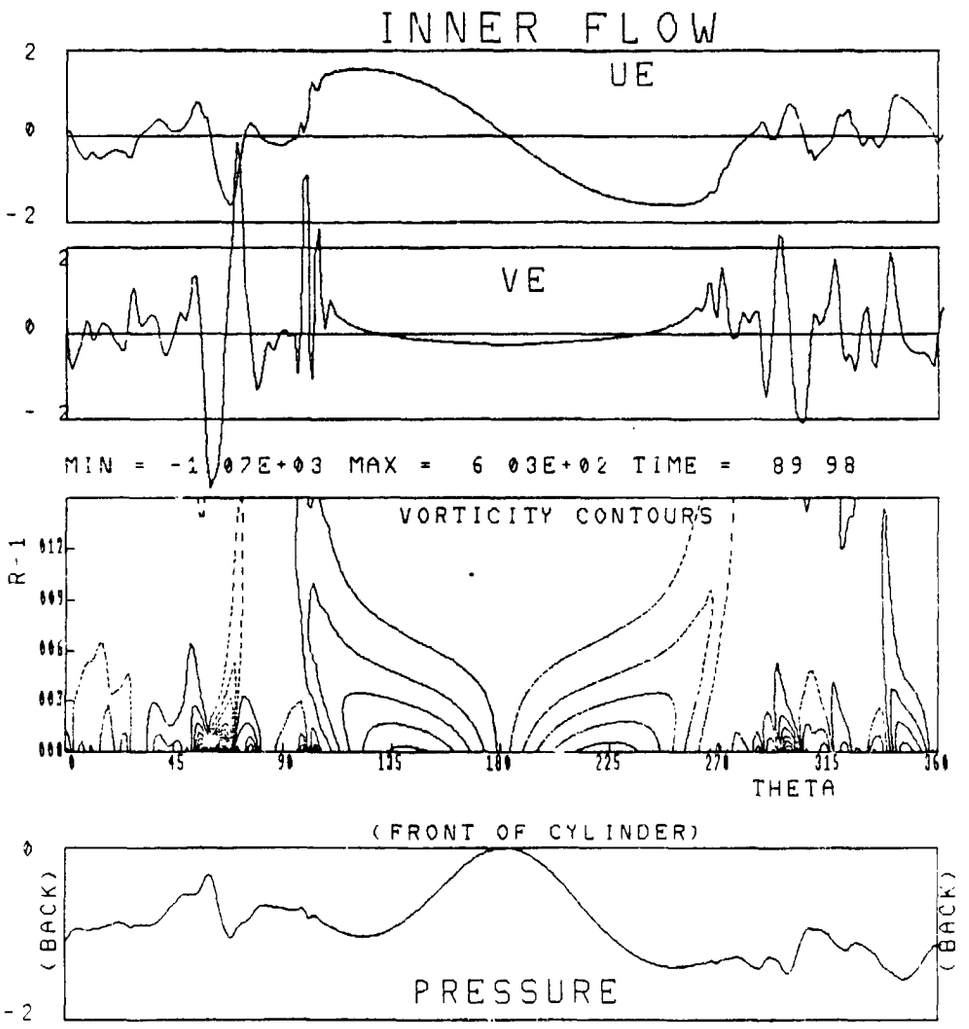

Fig. 35a. Simulation at Re=10^5 Inner Flow.

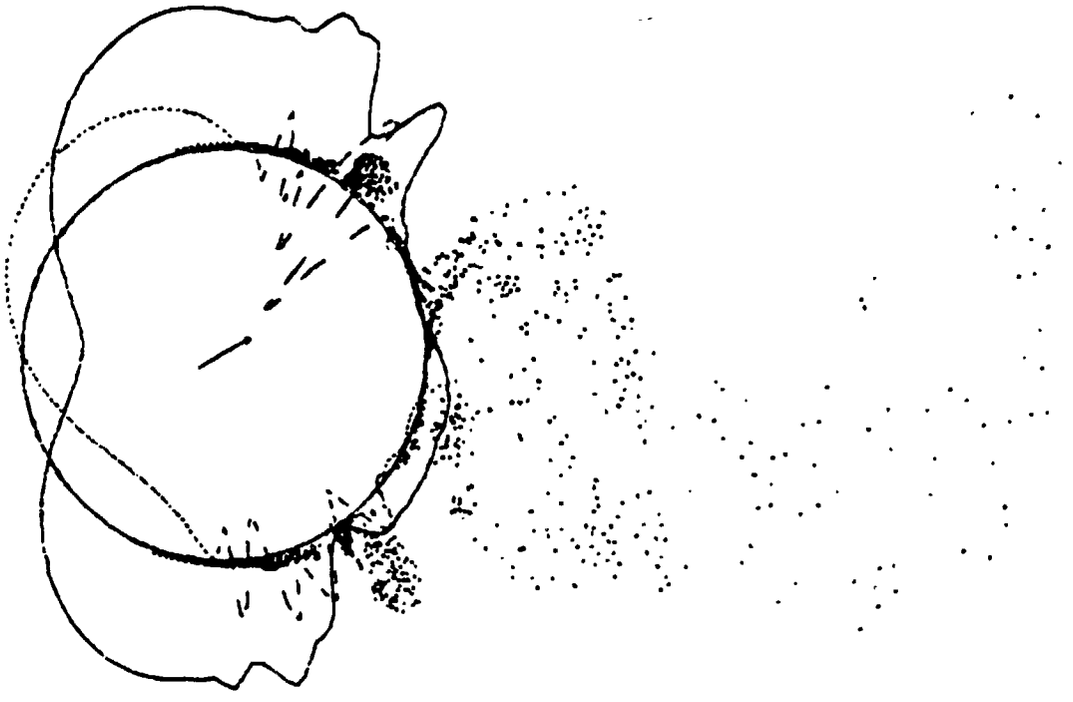

Fig. 35b. Simulation at $Re=10^6$

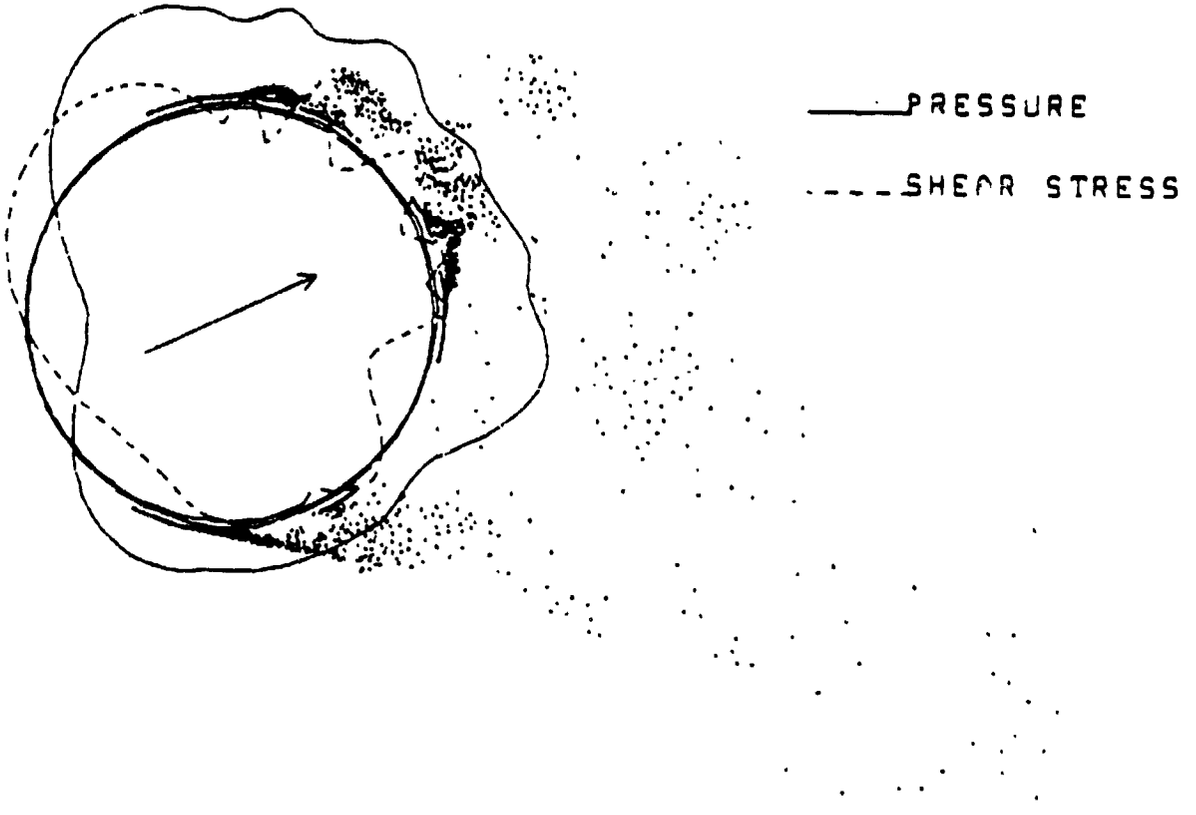

Fig. 36. Simulation at $Re=10^4$

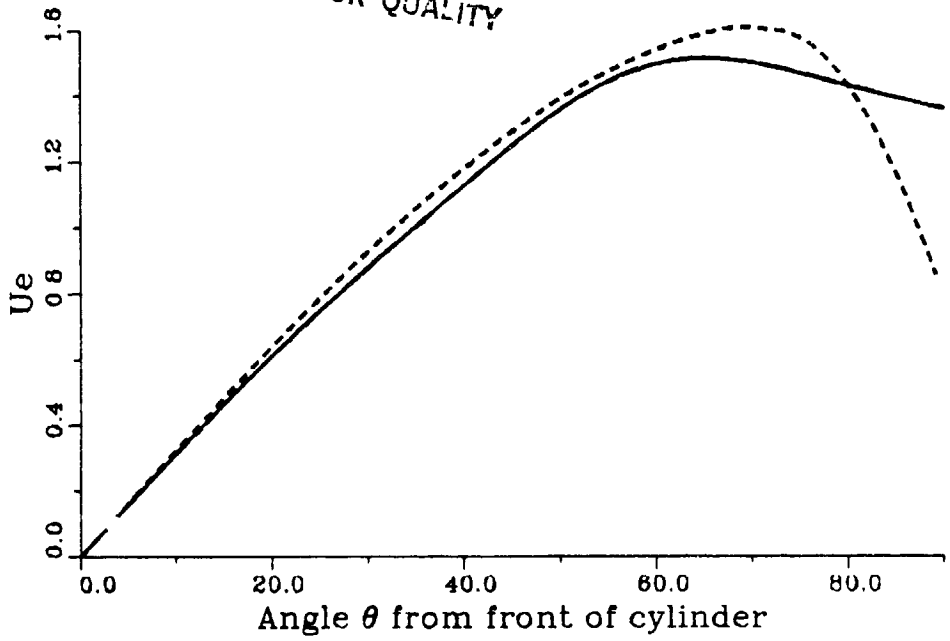

Fig. 37. Velocity at edge of boundary layer——Exp., Re=1.06 10^5[65]

– –Comp., Re=10^5

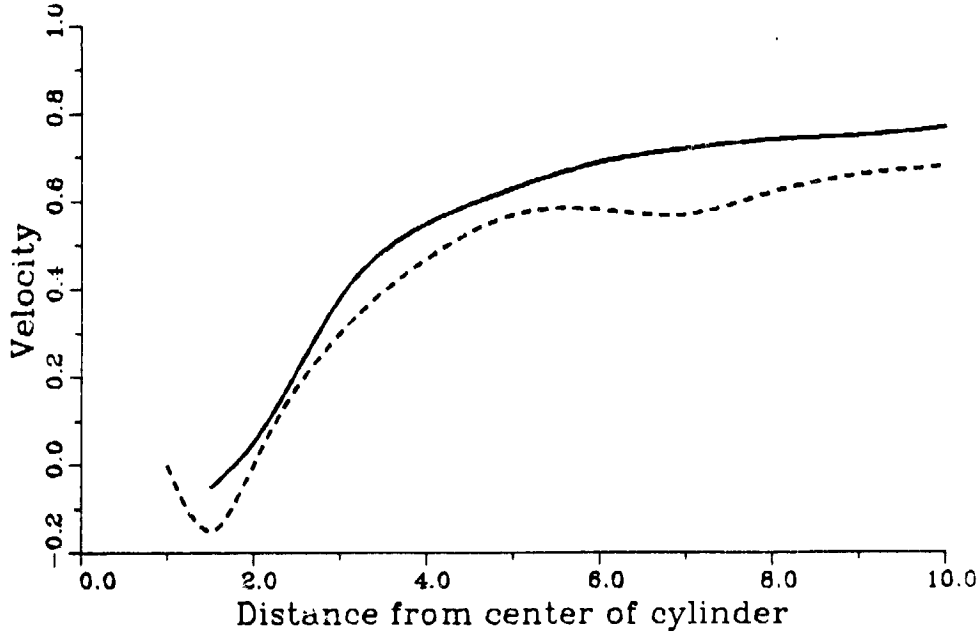

Fig. 38. Velocity on centerline——Exp., Re=1.4 10^5[62]

– –Computations, Re=10^5

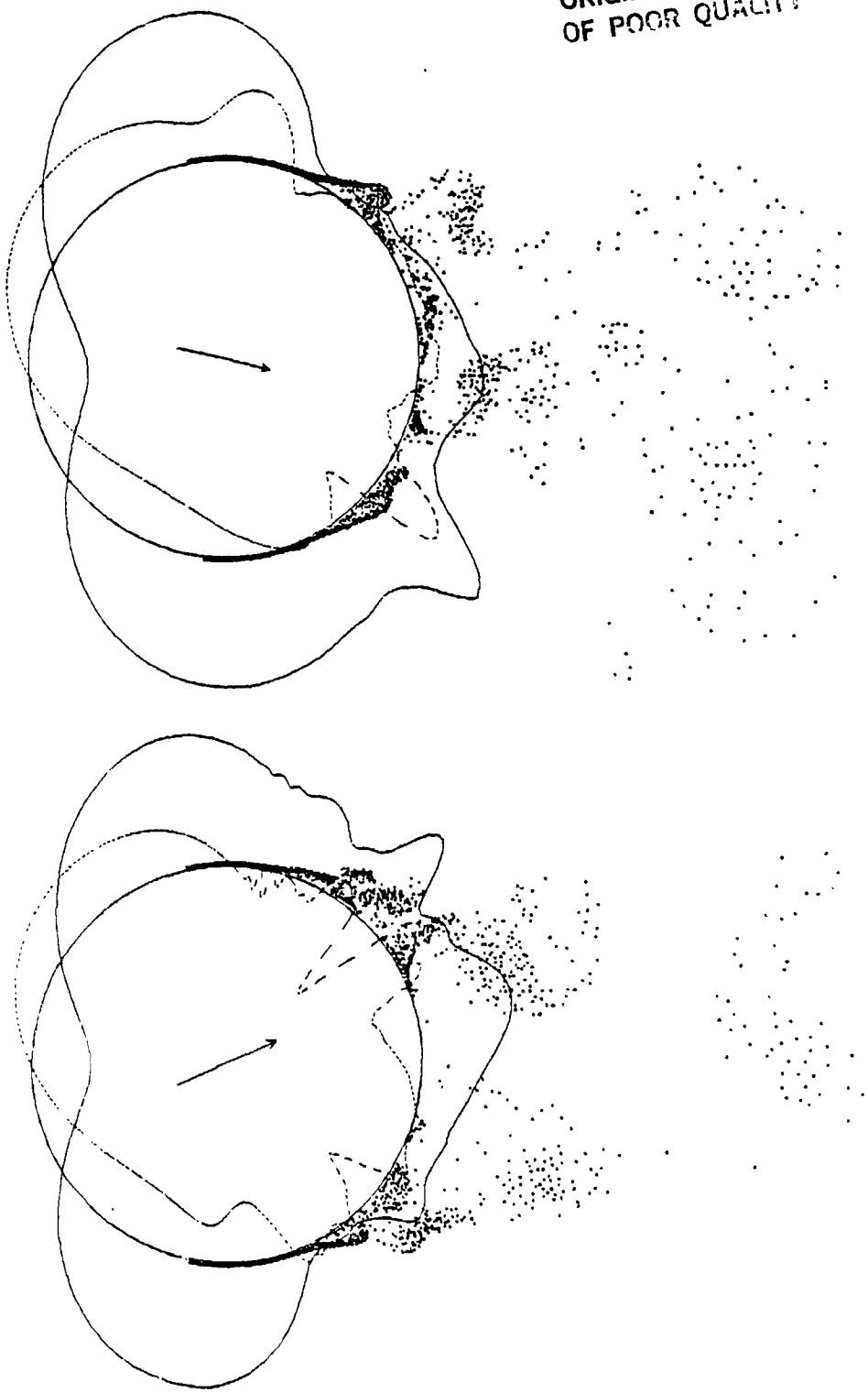

Fig. 39. Stills of the Simulation at Re=5.62 10^3

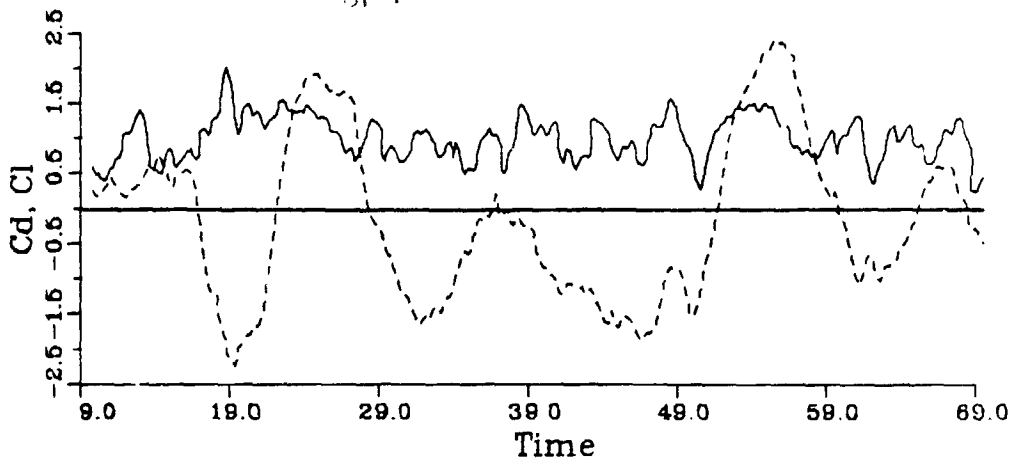

Fig. 40a. Re=10^5, —— Cd, – – Cl

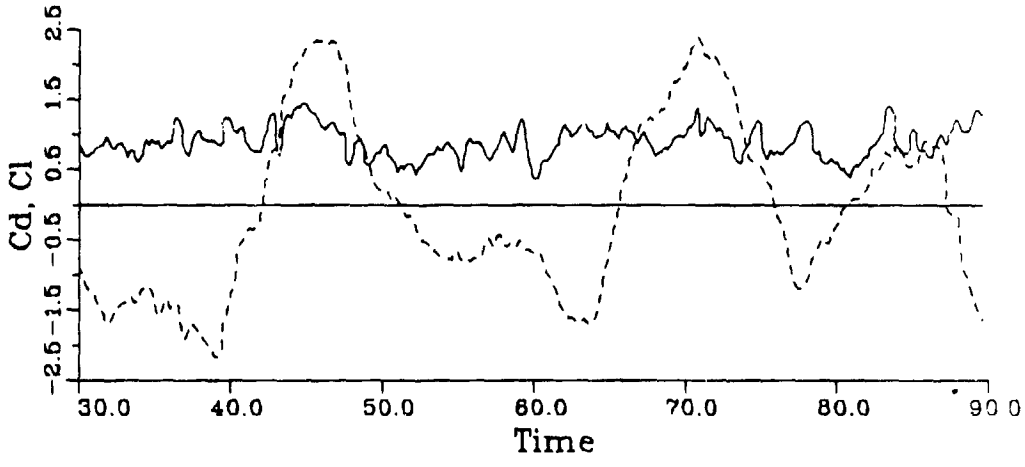

Fig. 40b. Re=3.16 10^5, —— Cd, – – Cl

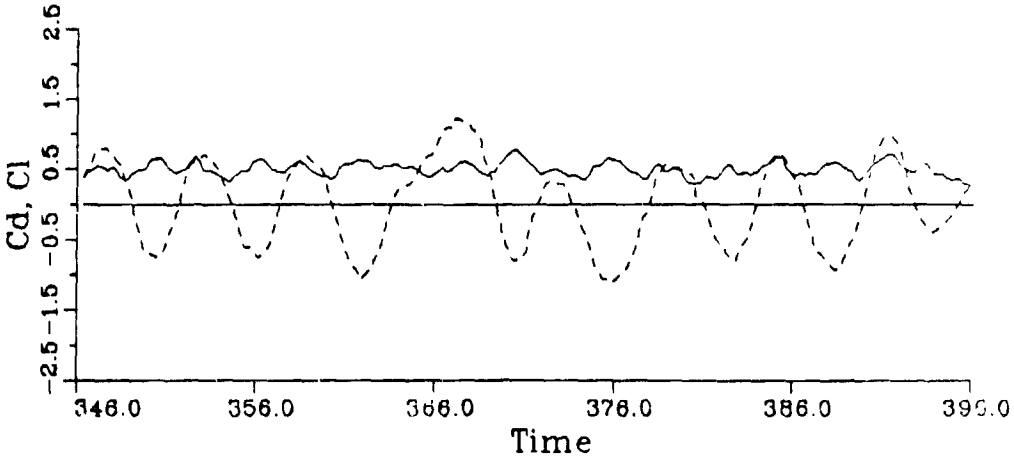

Fig. 40c. Re=3.16 10^6, —— Cd, – – Cl

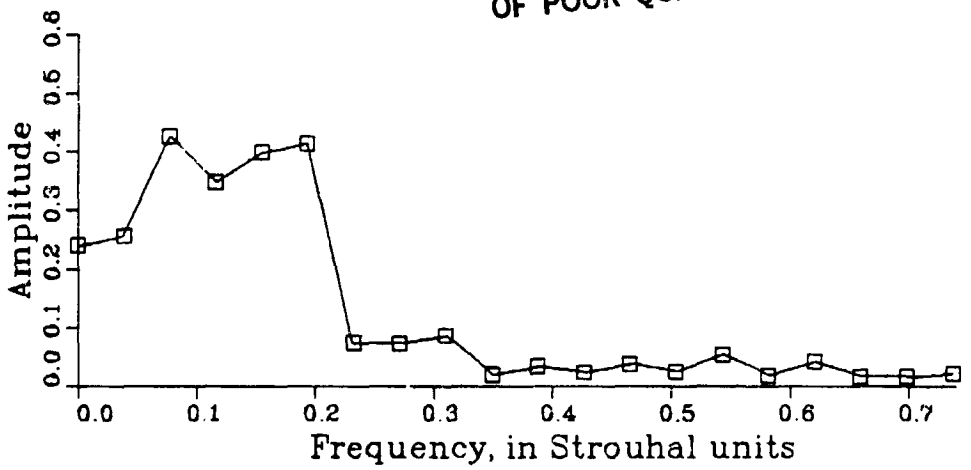

Fig. 41a. Re=10^6

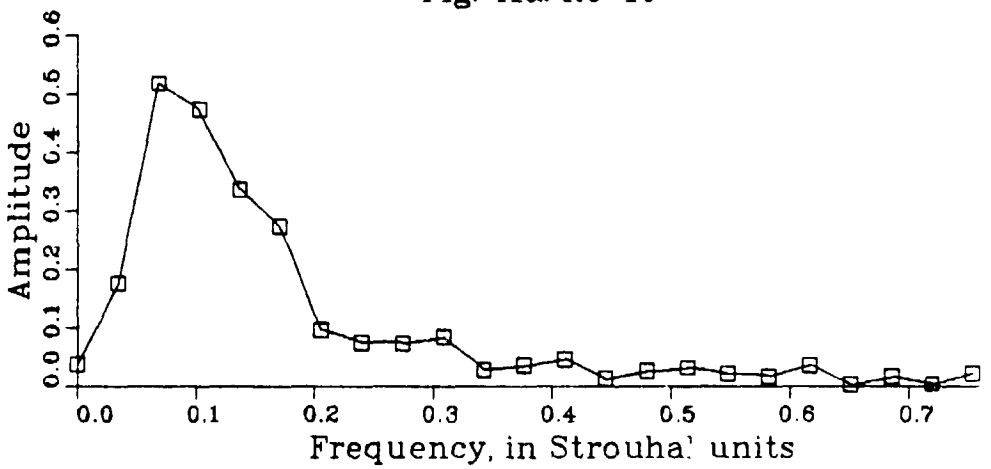

Fig. 41b. Re=3.16 10^6

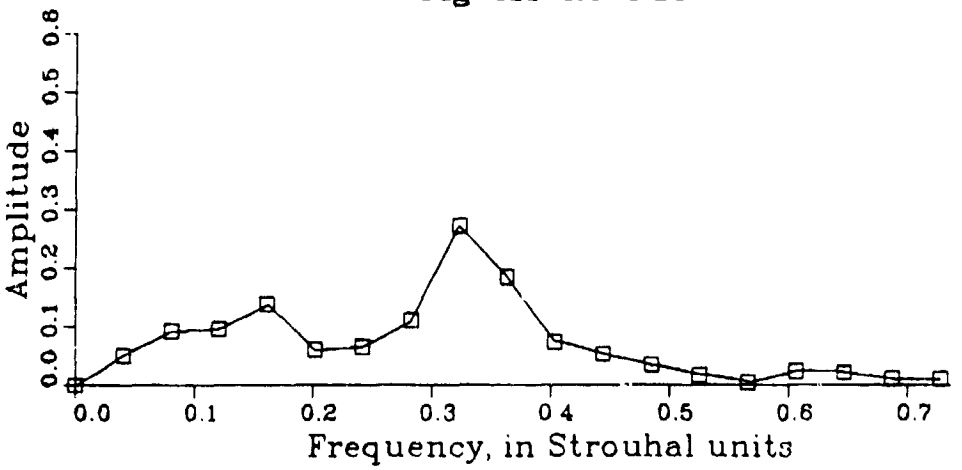

Fig. 41c. Re=3.16 10^6

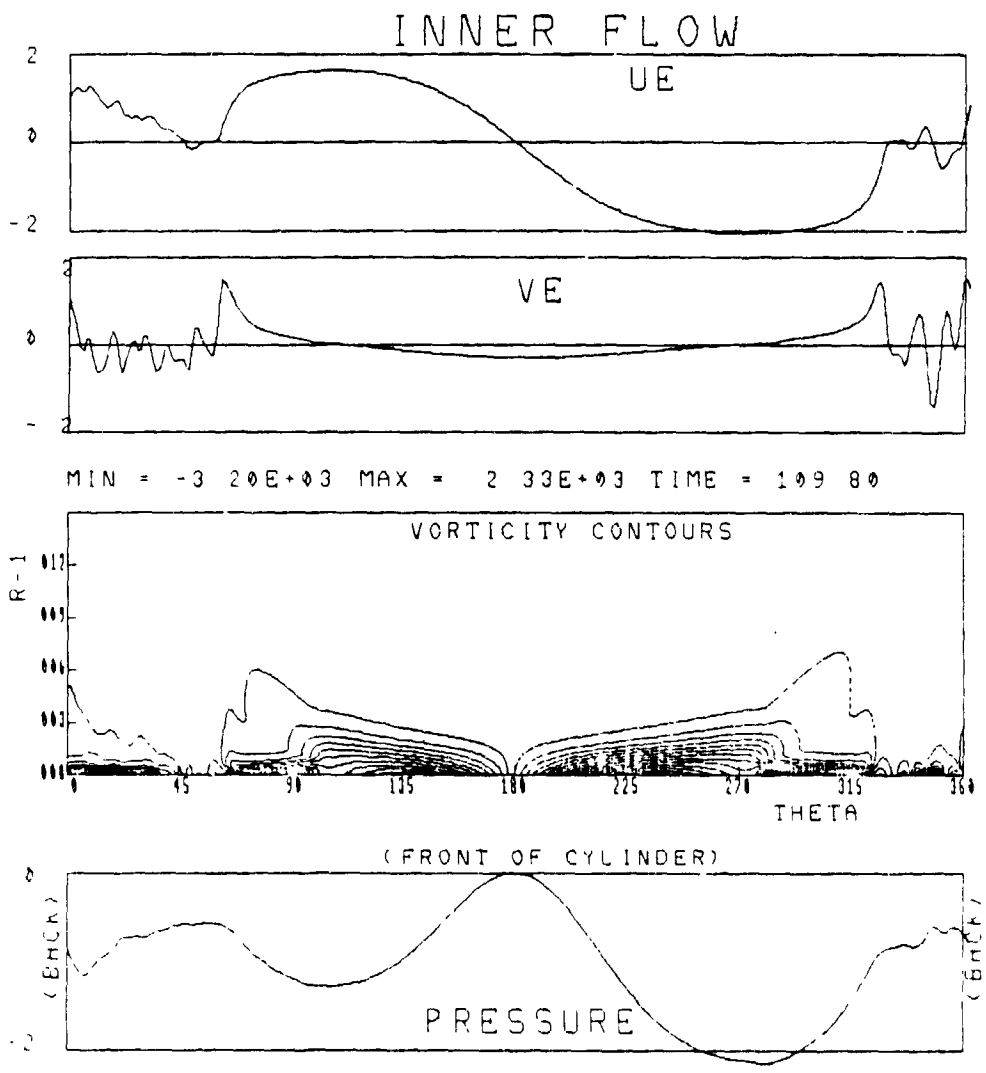

Fig. 42. Still of the simulation at Re=10^6, inner flow.

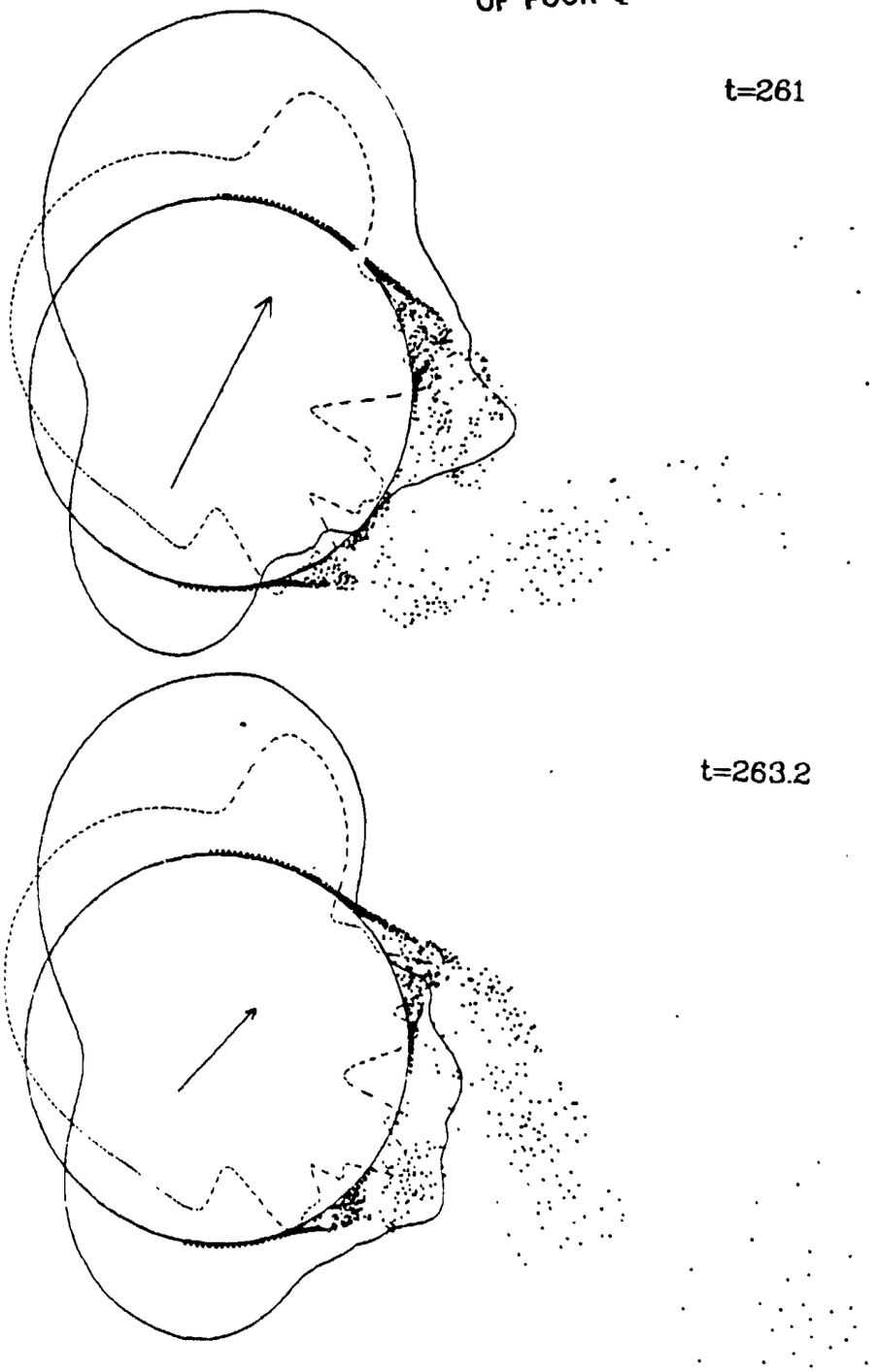

Fig. 43. Stills of the Simulation at Re=10^6

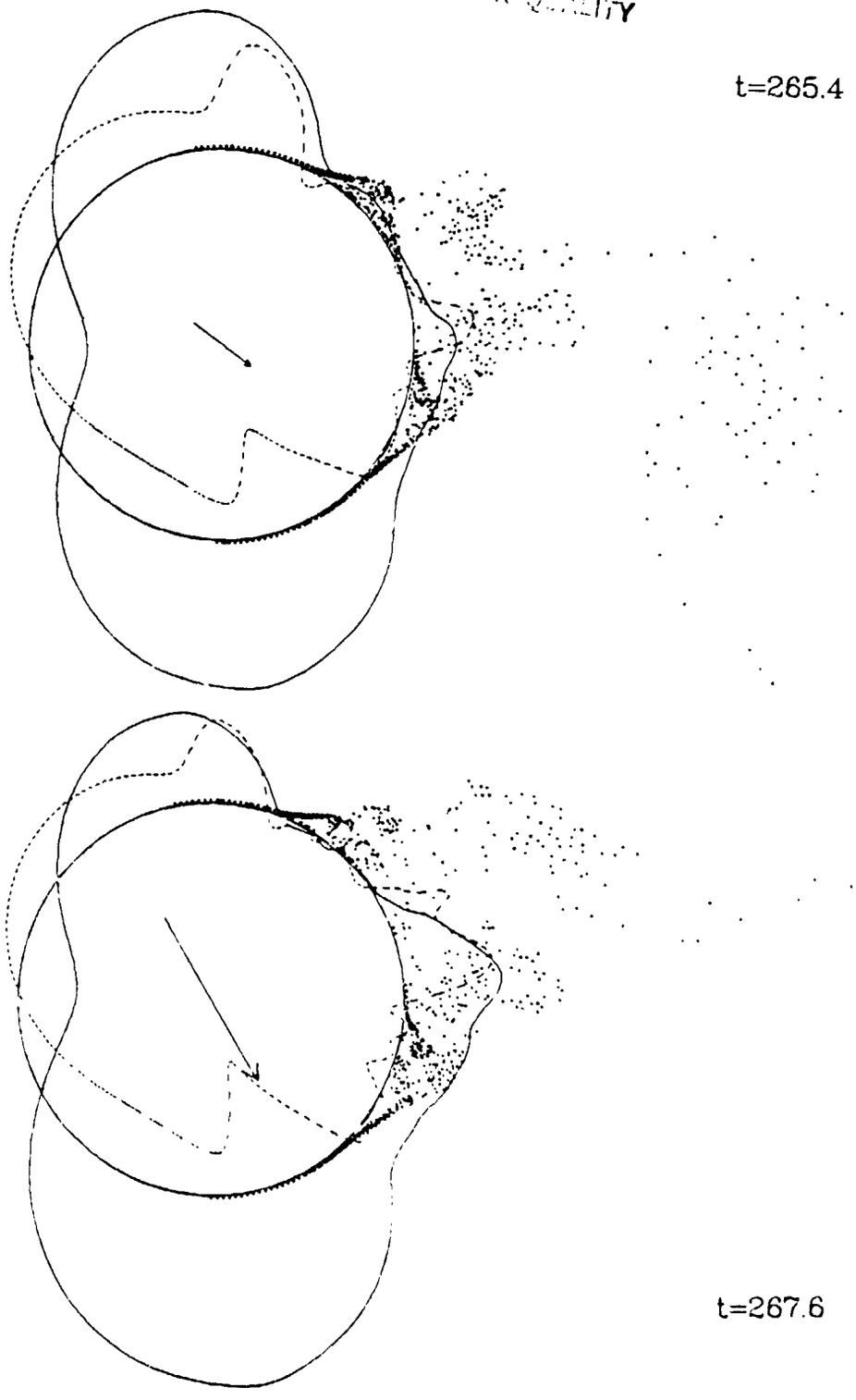

Fig. 43. Stills of the Simulation at Re=10^6

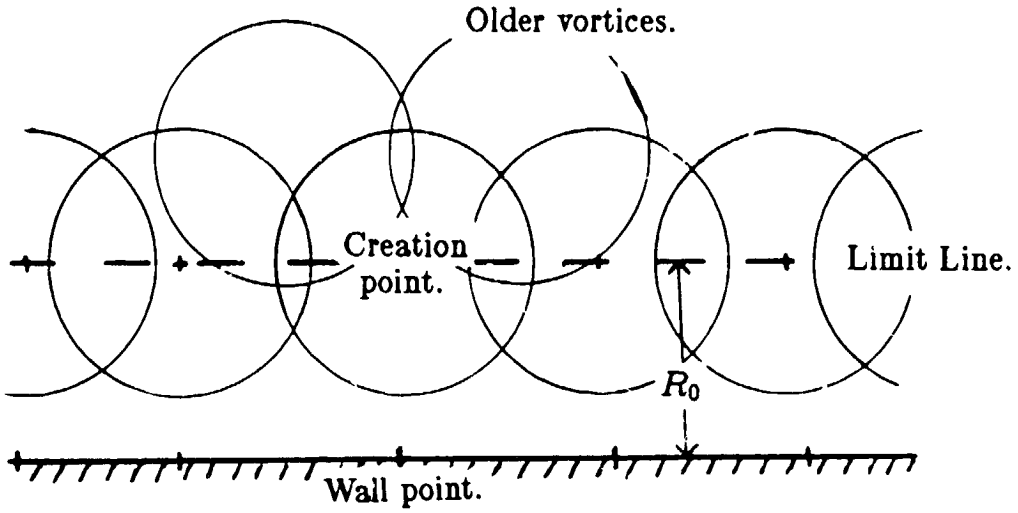

Fig. 44. Detail near wall in programs $KPD1$ and $KPD2$.

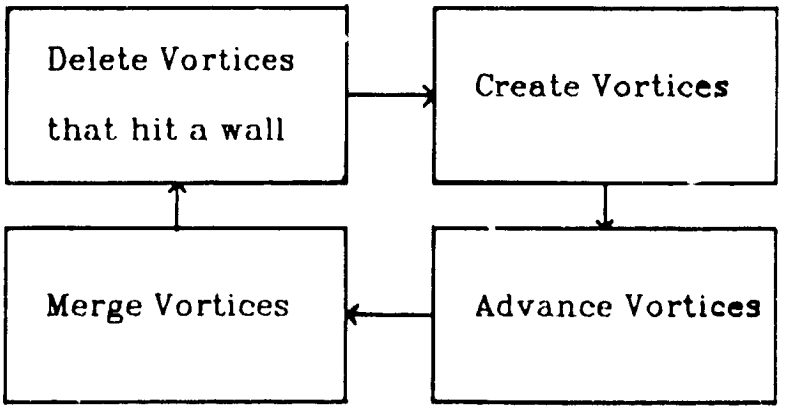

Fig. 45. Flow Chart of Program KPD1

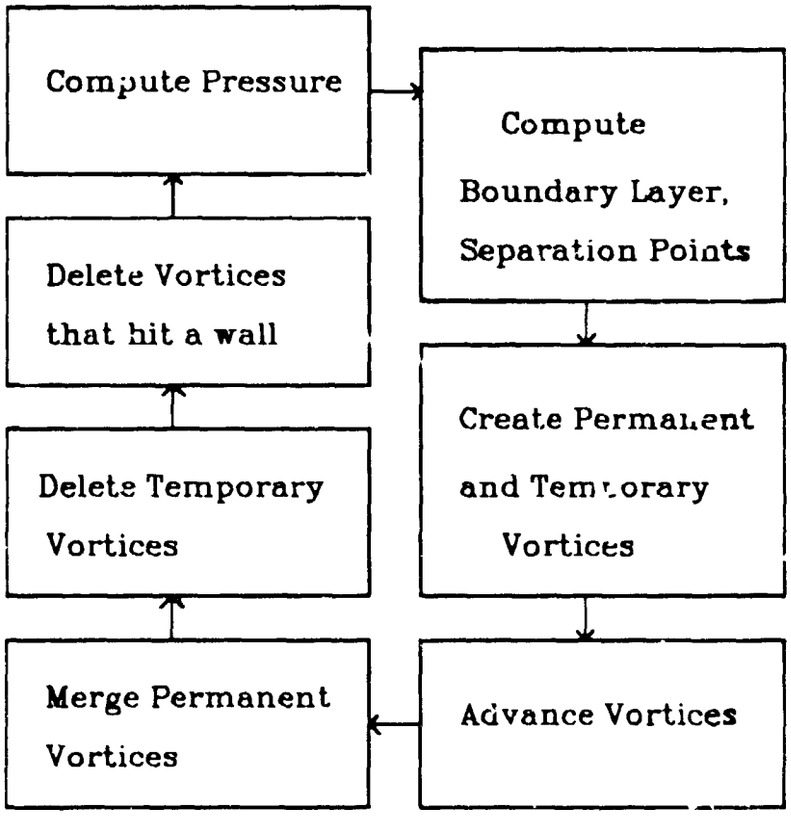

Fig. 46. Flow Chart of Program KPD2

REFERENCES

[1] Prandtl, L. and Tietjens, O. G., Applied hydro- and aeromechanics, Dover Publications, New York (1934).

[2] McCroskey, W. J., "Unsteady airfoils", Ann. Rev. Fluid Mech. 1982, Vol. 14, pp. 285-311 (1982).

[3] Favier, D.,Maresca, C. and Rebont, J., "Dynamic stall due to fluctuations of velocity and incidence", AIAA Journal, Vol. 20, No. 7, pp. 865-871 (1982).

[4] Szecheryi, E., "Supercritical reynolds number simulation for two-dimensional flow over circular cylinders", J. Fluid Mech., vol. 70, part 3, pp. 529-542 (1975).

[5] Roshko, A., "On the drag and shedding frequency of two dimensional bluff bodies", NACA T. N. 3169 (1954).

[6] Maskew, B. and Dvorak, F. A., "The prediction of Clmax using a separated flow model", Journal of the American Helicopter Society, Vol. 23, No. 2, pp. 2-8 (1977).

[7] Holst, T. and Thomas, S., "Numerical solution of transonic wing flow fields", AIAA paper 82-105, (1982).

[8] Metha, U. B., "Dynamic stall of an oscillating airfoil", presented at

the AGARD Fluid Dynamics Panel Symposium on Unsteady Aerodynamics, Ottawa, Canada, Sept. 1977.

[9] Leonard, A. "Vortex methods for flow simulations", Journal of Comp. Physics, Vol. 37, p. 289 (1980).

[10] McCormack, R. W. and Lomax, H., "Numerical solution of compressible viscous flow", Ann. Rev. Fluid Mech. 1979, Vol.11, pp.289-316.

[11] Thoman, D. C. and Szewczyk, A. A., "Time dependent viscous flow over a circular cylinder", The Physics of Fluids Supplement II, pp 76-86 (1961).

[12] Jordan, S. K. and Fromm, J. E., "Oscillatory drag, lift, and torque on a circular cylinder in a unifrom flow", The Physics of Fluids, Vol. 15, No. 3, pp 371-376 (1972).

[13] Wu, J. C., and J. F. Thompson, "Numerical solutions of time dependent incompressible Navier-Stokes equations using an integro-differential formulation", Computers and Fluids, 1, 197-215 (1973).

[14] Wu, J. C., "Aerodynamic force and moment in steady and time dependent viscous flows", AIAA paper 81-0011 (1980).

[15] Wu, J. C. and Gulcat, U., "Separate treatment of attached and detached flow regions in general viscous flows", AIAA Journal, Vol. 19, No. 1, pp. 20-27 (1980).

[16] Tassa, Y., and N. L. Sankar, "Dynamic stall of NACA 0012 airfoil in turbulent flow - numerical study", AIAA Paper 81-1289 (1981).

[17] Shang, J. S. [1982], "Oscillatory compressible flow around a cylinder",

AIAA Paper 82-0098 (1981).

[18] Davis, R. W., and Moore, E. F., "A numerical study of vortex shedding from rectangles", J. Fluid Mech., vol 116, pp. 475-506 (1982).

[19] Hald, O. H., "Convergence of vortex methods for Euler's equations", SIAM Journal of Numerical Analysis, Vol. 16, No. 5, pp.726-755 (1979).

[20] Bryson, A. E., "Symmetric vortex separation on circular cylinders and cones", Journal of Applied Mechanics, Vol. 26, March 1959, pp. 643-648.

[21] Clements, R. R., "An inviscid model of two dimensional vortex shedding", Journal of Fluid Mechanics 57, 321 (1973).

[22] Sarpkaya, T. and Shoaff, R. L., "An inviscid model of two dimensional vortex shedding for transient and asymptotically steady separated flow over a cylinder", AIAA Paper 79-0281 (1979).

[23] Katz, J., "A discrete vortex method for the non-steady separated flow over an airfoil", J. Fluid Mech., Vol. 102, pp. 315-328 (1981).

[24] Kiya, M., Sasaki, K. and Arie, M., "Discrete-vortex simulation of a turbulent separation bubble", J. Fluid Mech., Vol. 120, pp.219-244 (1982).

[25] Fink, P. T. and Soh, W. K. Proc. Roy. Soc. A 362, 195 (1978).

[26] Deffenbaugh, F. D. and Shivananda, T. P. , "Discrete vortex wake modeling of separated flow phenomena", TRW Report No. 33945-6001-UT-00 (1980).

[27] Stansby, P. K. and Dixon, A. G., "The importance of secondary shedding in two-dimensional wake formation at very high Reynolds numbers",

Aero. Quarterly, Vol. 33, part 2, pp. 105-123 (1982).

[28] Deffenbaugh, F. D. and Marshall, F. J., "Time development of the flow about an impulsively started cylinder", AIAA Journal 14, pp 908-913 (1976).

[29] Chorin, A. J., "Numerical study of slightly viscous flow", J. Fluid Mech., 57, Part 4, 785-796 (1973).

[30] Milinazzo, F., and P. G. Saffman, "The calculation of large Reynolds number two dimensional flow using discrete vortices with random walk", J. Computational Physics, 23, 380-392 (1977).

[31] Delcourt, B. A. G., and G. L. Brown, "The evolution and emerging structure of a vortex sheet in an inviscid and viscous fluid modelled by a point vortex method", Proceedings of the Second Symposium on Turbulent Shear Flows, July 2-4, 1979, Imperial College, London.

[32] Chorin, A. J., "Vortex sheet approximation of boundary layers", J. Computational Physics, 27, 428-442 (1978).

[33] Cheer, A. Y., "A study of incompressible 2-D vortex flow past smooth surfaces", Lawrence Berkeley Lab. Rep. LBL 9950, July 1979.

[34] Lewis, R. I., "Surface vorticity modelling of separated flows from two dimensional bluff bodies of arbitrary shape", Journal of Mechanical Engineering Science Vol. 23, No. 1, Feb. 1981, pp 1-12.

[35] Porthouse, D. T. C. and Lewis, R. I., "Simulation of viscous diffusion for extension of the surface vorticity method to boundary layer and separated flows", Journal of Mechanical Engineering Science Vol. 23, No. 3, June 1981, pp. 157-167.

[36] Pulliam, T. H., and J. L. Steger , "Implicit finite difference simulations of three dimensional compressible flow", AIAA Paper 78-10R, AIAA Journal, Vol. 18, N0. 2, Feb. 1980, pp. 159-167 (1978).

[37] Thompson, J. F., Thames, F. C. and Mastin, C. M.,"Automatic numerical generation of body-fitted curvilinear coordinate systems for field containing any number of arbitrary two-dimensional bodies", J. Computational Physics, Vol. 15, pp. 299-319 (1974).

[38] Hessenius, K. E. and Pulliam, T. H., "A zonal approach to solution of the Euler equations", AIAA paper 82-0969 (1982).

[39] Lasinski, T. A., Andrews, A. E., Sorenson, R. L., Chaussee, D. L., Pulliam, T. H. and Kutler, P., "Computation of the steady viscous flow over a tri-element "augmentor wing" airfoil", AIAA paper 82-0021 (1981).

[40] Spalart, P. R. and Leonard, A., "Computation of separated flows by a vortex tracing algorithm", AIAA paper 81-1246 (1981).

[41] Couet, B. and Spalart, P. R., "Simulation of the vortex emission behind a pair of bluff bodies by a vortex tracing algorithm", Proceedings of the international AMSE conference "Modeling and Simulation", Paris-Sud, July 1-3, 1982.

[42] Van Dyke, M., Perturbation methods in fluid mechanics (1975), The Parabolic Press, Stanford, California.

[43] Lighthill, M. J., in Laminar Boundary Layers, edited by L. Rosenhead, Oxford University Press, Oxford, p. 54 (1963).

[44] Shestakov, A. I., "A hybrid vortex-ADI solution for flows of low viscosity", J. Comp. Physics, Vol. 31, pp. 313-334 (1979).

[45] Nakamura, Y., Leonard, A. and Spalart, P. R., "Vortex simulation of an inviscid shear layer", AIAA paper 82-0948 (1982).

[46] Lomax, H., "An operational unification of finite difference methods for the numerical integration of ordinary differential equations," NASA TR R-262 (1967).

[47] Lamb, H., Hydrodynamics, (1945), Dover Publications, New York.

[48] Ting, L., "Integral invariants and decay laws of vorticity distributions", Courant Institute of Mathematical Sciences, New York University, N. Y., N. Y. 10012.

[49] Steger, J. L., "Implicit finite difference simulation of flow about arbitrary geometries with application to airfoils", AIAA Paper 77-665 (1977).

[50] Baldwin, B. S. and Lomax, H., "Thin layer approximation and algebraic model for separated turbulent flows", AIAA paper 78-257 (1978).

[51] Schlichting, H., Boundary Layer Theory, (1979), McGraw-Hill Book Company, New York.

[52] Goldstein, S., "On laminar boundary layer flow near a position of separation", Quarterly Journal of Mechanics and Applied Mathematics, Vol. 1, Feb. 1948, p. 43.

[53] Le Balleur, J. C., "Couplage visqueux-non visqueux: analyse du probleme incluant decollements et ondes de choc", Recherche Aerospatiale, No. 1977-6, pp. 349-358 (1977).

[54] Klineberg, J. M., and J. L. Steger, "On laminar boundary layer separation", AIAA paper 74-94 (1974).

[55] Briley, W. R. and Mc Donald, H., "Numerical prediction of incompressible separation bubbles", J. Fluid mech., Vol.69, part 4, pp. 631-656 (1975).

[56] Bradshaw, P., "Singularities in unsteady boundary layers", AIAA Journal, Vol. 17, No. 7, pp. 790-793 (1979).

[57] Delany, N. K., and Sorensen, N. E., "Low-speed drag of cylinders of simple shapes", NACA T. N. 3038 (1953).

[58] Pullin, D. I. and Perry, A. E., "Some flow visualization experiments on the starting vortex", J. Fluid Mech., vol. 97, part 2, pp. 23-255 (1980).

[59] Jones, R. T., "The unsteady lift of a wing of finite aspect ratio", NACA Report No. 681 (1940).

[60] McCroskey, W. J., McAlister, K. W., Carr, L. W. and Pucci, S. L.,"An experimental study of dynamic stall on advanced airfoil sections. Vol. 1 Summary of the experiment", NASA T. M. 84245 (1982).

[61] Kamiya, N., Suzuki, S. and Nishi, T., "On the aerodynamic force acting on a circular cylinder in the critical range of Reynolds number", AIAA Paper 79-1475 (1979).

[62] Kline, S., Cantwell, B. J. and Lilley, Proceedings of the 1980-1981 AFOSR-HTTM-Stanford Conference on Complex Turbulent Flows, Vol. 1, pp. 229.

[63] Achenbach, E., "Distribution of local pressure and skin friction around a circular cylinder in cross-flow up to $Re = 5. \times 10^6$", J. Fluid Mech., Vol. 34, part 4, pp. 625-639 (1968).

[64] Roshko, A., "Experiments on the flow past a circular cylinder at very high Reynolds number", J. Fluid Mech., Vol. 10, part 3, pp345-356 (1961).

[65] Roshko, A. and Fiszdon, W., "On the persistence of transition in the near-wake", Problems of Hydrodynamics and Continuum Mechanics, S.I.A.M. (1969).

[66] Dwyer, H. A. and McCroskey, W. J., "Oscillating flow over a cylinder at large Reynolds number", J. Fluid Mech., Vol. 63, part 4, pp. 753-767 (1973).

[67] Humphreys, J. S.,"On a circular cylinder in a steady wind at transition Reynolds numbers", J. Fluid Mech., Vol. 9, part 4, pp. 603-612 (1960).

[68] Cebeci, T. and P. Bradshaw, Momentum transfer in boundary layers, (1977), McGraw-Hill Book Company, New York.